CRANFIELD UNIVERSITY

Yang Wang

Virtual testing of post-buckling behaviour of metallic stiffened panel

School of Engineering
MSc thesis

MSc by research
Academic Year: 2010 - 2011

Supervisor: Dr James Campbell
December 2011

CRANFIELD UNIVERSITY

School of Engineering
MSc thesis

MSc

Academic Year 2010 - 2011

Yang Wang

Virtual testing of post-buckling behaviour of metallic stiffened panel

Supervisor: James Campbell
December 2011

© Cranfield University 2011. All rights reserved. No part of this publication may be reproduced without the written permission of the copyright owner.

ABSTRACT

The aim of the project presented in this thesis is to demonstrate a modelling method for predicting the variability in the ultimate load of stiffened panel under axial compression due to manufacturing variability.

Bulking is sensitive to imperfections. In the case of a post-buckled panel, manufacturing variability produces a scatter in the ultimate load. Thus, reasonable leeway for imperfections and inherent variability must be allowed in their design.

Firstly, a finite element model of a particular stiffened panel was developed, and all nonlinearities within the material, boundary condition and geometry were considered. Verification and validation were performed to examine the accuracy of the buckling behaviour prediction, especially ultimate load.

Experiments on 5 identical panels in design were performed to determine the level of panel-panel variation in geometry and collapse load. A data reduction programme based on the practical geometry scanning was developed, in addition to which, the procedure of importing measured imperfection into Finite Element model was introduced.

To identify and apply representative imperfections to the panel model, a double Fourier series representation of the random geometric distributions is attempted, and was used thereby to derive a series of shapes representing random geometry scatters.

With these newly generated geometric imperfections, the variation in collapse load was determined, using the validated FE analysis. And also, the probability of these predicted loads was generalized.

Keywords:

Buckling and Postbuckling, Stiffened panel, Initial Geometric Imperfection, FE method, ABAQUS, FE modelling, Compression

ACKNOWLEDGEMENTS

I would like to take this opportunity to express my gratitude to my supervisor Dr. James Campbell for his valuable guidance and great help during the period of my research.

I am very grateful to COMAC and the Chinese Scholarship Council for funding the project. Without them, I could not have the opportunity to study here in Cranfield for my further education after having worked for four years.

Also, I would say thank you to Dr Al Savvaris and Dr Xiang Zhang from School of Engineering, Dr Paul Baguley and Dr Yuchun Xu from School of Applied Science. And Mr Tony Lawrence, the Principal CAE Consultant in IT department, who introduced me to the national conference of Altair in UK, which is the top CAE engineers' communication.

Many thanks to all my friends and colleagues at Cranfield for all the discussion, especially Omkar Gulavani for his help in ABAQUS learning, Barry Walker for help with the panel tests, and Daqing Yang for his kindly help in proofreading.

Finally, I would give my thanks to my dear fiancée Linlin An for her love, understanding and support throughout the past 13 months. To my parents, who are always supporting and encouraging me.

TABLE OF CONTENTS

LIST OF FIGURES

LIST OF TABLES

LIST OF EQUATIONS

NOTATION AND ABBREVIATIONS

P_a	allowable applied load
P_{crit}	lowest buckling load of perfect structure;
γ	knockdown factor
FS	Safety Factor
σ	true stress
ε	true strain
E	Young's Modulus
n	strain hardening exponent
σ_y	Yield stress
v	Poisson's ratio
ε^{pl}	true plastic strain
ε^{t}	true total strain
ε^{el}	true elastic strain

CU	Cranfield University
FE	Finite Element
FEA	Finite Element Analysis
CAD	Computer Aided Design
CAE	Computer Aided Engineering
ESDU	Engineering Service Data Unit
ASCII	American Standard Code for International Interchange
ABAQUS	Software of Finite Element Analysis
MATLAB	MATrix LABoratory
SP-80	A label of rivet
L-D	Load-Displacement
DFS	double Fourier series

1 Introduction

1.1 Motivation of this research

Safety, economics, comfort and environmental friendly are the four main requirements for a new aircraft design. However, each aircraft handles somewhat differently due to its own particular feature and application. In the design of the C919 (Figure 1-1), one of the newest civil aircraft, the biggest advantage is stated into the Economics aspect: “fuel consumption and direct operating cost per seat per kilometre are lower than those of similar existing airplanes.”

For the economic reason, fuel cost is probably the biggest proportion of the total cost of the ownership of the aircraft. Thus, there is a big drive to reduce fuel consumption, to which a big contribution is from the weight of the aircraft. Weight has always been critical in aircraft designs. Designers have been making more and more effective use of structures, as well as the use of new design tools that results highly accurate prediction of structural strength.

Figure 1-1 One of the newest civil commercial aircraft - C919

Due to their superior strength over weight ratio, thin-walled structures, especially, stiffened metallic panels are widely used in the field of aerospace engineering, particularly as parts of aircraft fuselage, which can provide great weight saving potential.

Figure 1-2 A typical semi-monocoque fuselage in B787

In the case of semi-monocoque fuselage (Figure 1-2), which is really most popular in modern aircraft design, it is commonly required to design a structure component that can carry a certain ultimate compressive load in either end. Those fuselages will typically consist of a skin stiffened by longitudinal stringers. Due to the compressions, these thin-walled shells are very prone to instability failures, which include the well-known buckling.

Uncertainties in deterministic design

In practical structure design, a deterministic analysis is based on the perfect structure. Many design codes and other mechanical engineering text books [2][3] have been developed to explore the load carrying capability of stiffened panels.

However, in reality, the structure component is not perfect. On account of various conditions, such as ease of manufacturing, the initial deviation from the manufacture tolerance is widely existent. Besides, those uncertainties can also include variables such as emergency situations, unexpected loads, misuse, degradation, or any other unknown influences.

To account for the uncertainties many systems are designed deliberately much stronger than the actual applied load requirement. Hence, the safety factor was introduced. The safety factor is a term describing the structural capability of a system beyond the expected loads or actual loads, which can be expressed as following:

$$Safety\ Factor = \frac{Failure\ Load}{Design\ Load} \quad \textbf{(1-1)}$$

This term must never be smaller than 1. It can also be a measure of the reliability of a particular design, by means of margin of safety, which is defined as safety factor subtracted by 1.

Appropriate design factors are based on several considerations, one of which is the accuracy of prediction on the imposed loads. Aircraft and spacecraft use various safety factors from 1.2 to 3.0 depending on the application and materials. The field of aerospace engineering uses generally lower design factors because of the costs associated with structural weight are particularly high. The usually applied Safety Factor is 1.5, while for pressurized fuselage it is 2.0, to ensure reliability.

In addition to the concept of safety factor, a deterministic buckling procedure is performed by using an empirical knockdown factor, which specifies the reduction of the buckling load of the perfect shell in order to account for the inherent uncertainties.

$$P_a \leq \frac{\gamma \times P_{crit}}{FS} \quad \textbf{(1-2)}$$

Where

P_a is allowable applied load;
P_{crit} is lowest buckling load of perfect structure;
γ is the so-called ‘knockdown factor’;
FS is Safety Factor.

The so-called knockdown factor γ is based on a ‘Lower Bound Design Philosophy [4] to all the existing result of experimental data obtained. This philosophy has provided designers with a useful tool in shell stability design during the past

80 years.[5] However, this approach accounted for the uncertainties by using such ‘knockdown factor’ has been proved to be too conservative [6].

Probabilistic design

Currently, however, with the development of advanced computers technology, there are many nonlinear codes, such as ABAQUS, NASTRAN, ANSYS, STAGS, etc., that have the capability to deal with the complex effect of buckling, by means of advanced finite element analysis. An alternative design approach is required to take advantage of these currently advanced computer codes, based on high accuracy of which, the precise prediction can be obtained, so that one can get the scattering of the ultimate load on given initial imperfections.

Turning to the standpoint of reliability and probability, it is believed that quantifying and understanding the ‘problem uncertainties’ and their influence on the design variables can provide an approach which will ultimately lead to a better designed, better engineered and safer structure.[5]

Buckling is sensitive to uncertainties, which is embodied in the significant reduction of the critical load when structure buckles. Geometric imperfection is considered as a main resource of these uncertainties. With the increasing use of thin-walled structures, there is a need for a method to determine the probability that whether a structure having random initial geometric imperfections will fail at a load (see Figure 1-3).

If one can obtain the distribution of the ultimate collapse load on the global buckling of an imperfectly stiffened panel, and which can be normalized just like the normal distribution as shown in Figure 1-3, a lower bound of the load carrying capability is obtained by choosing the probability of the failure. In addition, the reliability of the structure can also be defined, as well as an improved safety factor.

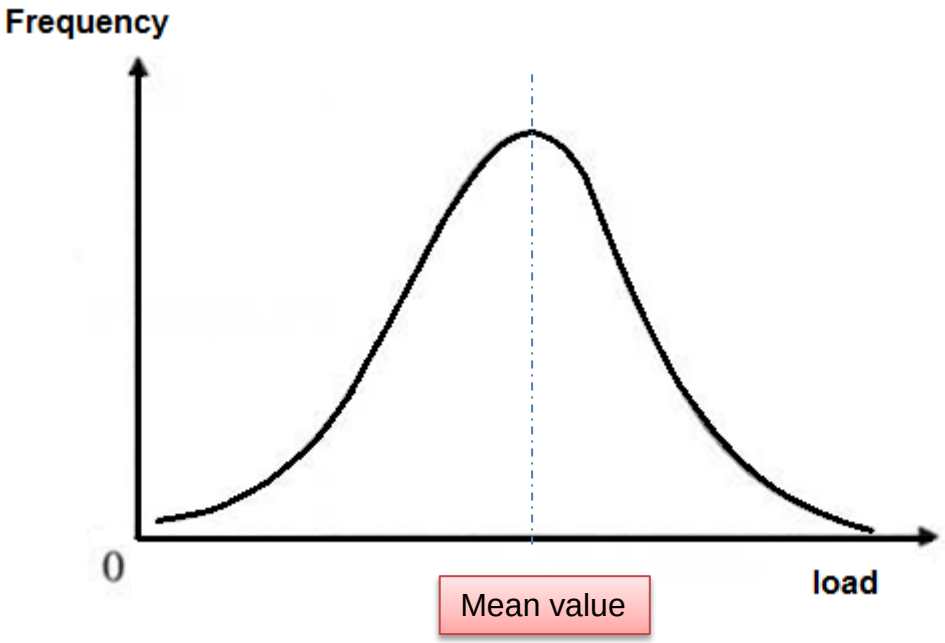

Figure 1-3 A typical Normal distribution of the load

1.2 Statement of objective

Buckling is a typical structural failure mode. It is well understood that buckling is sensitive to imperfection. In the case of a post-buckled collapse of a panel, manufacturing variability produces a variation in the ultimate load.

The overall aim of this project is to demonstrate a modelling method for predicting the variability in the ultimate load of stiffened panel under axial compression due to manufacturing variability. In order to achieve this aim the following objectives were identified:

1. To develop an efficient and reliable finite element model for the prediction of the post-buckled collapse of the stiffened panel design considered in this project.
2. To perform experiments on several panels to determine the level of panel-panel variation in geometry and collapse load.
3. To identify and apply representative imperfections to the panel model and determine the variation in collapse load due to these imperfections.

1.3 Methodology

In order to get a general knowledge of the relevant research field, a literature review is carried out. The review will also ensure that the research is abreast with recent study of the other scientists worldwide.

The second phase is devoted to software knowledge and skills acquisition, as ABAQUS software will be utilized to build a reference model. Building a basic and simple model without any other complexity is feasible at the beginning. In addition, to get ready to accomplish the simulation, all the nonlinearities including material plasticity, boundary conditions and contacts are included in the model.

A suitable software tool for adding geometry imperfections into the “perfect” model must be developed. These imperfections are measured by scanning the shape of real panels. To generalize the characteristic distribution of the measured imperfect shape of the panel, a surface fitting method must be developed to allow the imperfections to be parameterised.

Subsequently, comparison between the experiment results and the virtual FE analysis is performed. Experimental data will be acquired through panel tests. To compare with the numerical analysis, a small numbers of tests are necessary to be carried on the panels, generating the experimental data on the actual variation in the panel behaviour. With the comparison, it is practicable to assess the accuracy of the virtual simulation.

After the validation of the FE model, the virtual simulations will be executed as many simulations as the time allows, with different imperfect shapes of the panel, randomly picked out from the newly generated imperfections based on the method of surface fitting.

The result predicted by the simulations is plotted, as a scatter of the ultimate load of panels. Variations and an acceptable scope of the ultimate collapse load can be acquired.

1.4 Thesis structure

The initial chapter of this thesis is about the project general background, object and methodology.

Chapter 2 describes the literature review which has been carried all through the whole research period.

Chapter 3 presents the ABAQUS software and the development of the FE model for the buckling and postbuckling behaviour of the stiffened panel.

Chapter 4 describes the baseline establishment and numbers of nonlinearities are included to verify the virtual model.

In addition to chapter 4, chapter 5 introduces the geometric imperfections in reality and the approach to add those imperfections into the FE model.

Chapter 6 deal with the results from the imperfect model which was validated by the measured imperfection, and further predict a scatter of the ultimate load based on the correlated manufacturing process.

In the end, Chapter 7 gives the conclusion and points out the further work need to do in the future.

The appendix provides the ABAQUS input and MATLAB source code, as well as the experiment result data are recorded.

2 Literature review

This chapter contains some reviews of the reference that are beneficial with carrying out the above objective.

The first section consists of some theoretical fundamentals of buckling and postbuckling which are expounded in Classic theory books; and also different postbuckling behaviours during the load carrying course are described.

The second section gives some practical applications of thin-walled shell especially stiffened panel. The superiority of such panel is explained.

The third part of this review deals with the solution of nonlinear finite element analysis of buckling problems. Previous experiences in the similar field are reported, some of them are very interesting and of great reference value to the current project.

In the next coming section, a brief review of initial imperfections due to the manufacturing tolerance is introduced. The approach of modelling these imperfections into the above finite element analysis has been sought. Imperfection sensitivity was examined by lots of researchers. Large amount of references are centred in determine the effects of initial imperfections.

The last section concerns the reliability and probability design of buckling in those thin-walled structures.

2.1 Buckling and postbuckling

Fundamental of buckling and postbuckling is expounded in Classic theory books

In theory, buckling is due to a bifurcation in the solution to the equation of static equilibrium. Practically, in a structure which is subjected to certain constant compression, where the compressive stress at the point of failure is less than the ultimate compressive stress of the material, buckling occurs as a sudden failure of the structure.

The fundamental of buckling of shells is expounded in detail in Timoshenko [16], which is considered as the most classic theory book. Other books such as J. Thompson [17] presented a general nonlinear mathematical theory of elastic stability for conservative systems, as well as J.J. Stoker [18], which concentrated in the practical nonlinear problems in thin plates and shells.

Postbuckling behaviour

Based on Campbell [7], the buckling modes of a cold-formed stiffened panel can be subdivided into the following five main buckled failure modes:

the skin local buckling,
the inter-rivet buckling,
the stringer crippling,
the flexural failure and
the torsional failure.

All those modes that occur after local buckling in the skin are termed as post-buckled modes.

For stringer dominated designs, the first point of instability is usually reached when the skin between the stringers starts to buckle. Local buckling does not necessarily mean collapse of the panel since it can generally withstand load increase after buckling. The structural stiffness is reduced slightly, but the load still can be increased.

The post-buckling modes usually occur when one of the stiffeners buckles. Stiffeners with thin-walled open sections may, due to their low torsional stiffness, lead to twisting failures at loads well below the Euler flexural load. The mode of buckling will be pure torsion or a combination of torsion and flexure depending on whether or not the shear centre and centroidal axes of the section are coincident.

With the onset of global buckling, which often corresponds to a combination of torsional and flexural failure of the stringers, the sudden reduction of load is encountered, meaning the whole panel loses the capability of load carrying, thus the panel collapses.

2.2 Stiffened panel

The thin-walled structures are specified as those whose thickness is much less than the other dimensions such as length, width and so on.

Thin-walled shells are widely used in the field of many applications including aerospace, civil engineering, naval architecture and so on, due to their superior strength over weight ratio. But unfortunately, these thin-walled shells are very prone to buckling instabilities.

Particularly, in those cold-formed sections which are generally manufactured from very light-gauge sheet material, the design should be considered as against different types of buckling.

Stiffened panels are widely applied in fields of mechanics, as well as aircraft and shipbuilding industry. Generally, such a panel is only part of a large assembly in aircraft structure. Stiffened panels as part of aircraft fuselage provide great weight saving potential.

The Z-stringer and J-stringer are the most popular configurations utilized in recent transport structural design, especially the Z-stringer due to its high structural efficiency.[3] Panel stiffened with Z-stiffeners are introduced in [8], [7], [1], and [3]. These researches [9], [10], [11], [12] and [13] discussed such stiffened panel in various fields, including either metallic or composite of aircraft fuselage, ships and underwater vehicles. An analysis procedure for practical use in preliminary sizing was presented byNiu [3].

2.3 Buckling analysis with Nonlinear Finite Element Method

Previous research done by others all over the world who use FEA to simulate the behaviours of buckling in different areas

Using Nonlinear Finite Element Method to perform a buckling and postbuckling analysis has become more and more popular since last few decades. Currently, with the development of advanced computers technology, there are many nonlinear codes such as ANSYS, ABAQUS, NASTRAN and STAGS, all have the

strong capability to provide the numerical predictions for most buckling problems.

Paik et al [13] use nonlinear finite element analysis (FEA) with ANSYS to assess the ultimate limit state of stiffened plate of ship structures. A few similar analyses using ANSYS can refer to Cao et al [14] and Ghorbanpour et al [15]. Another powerful nonlinear code is STAGS, with which the stable and unstable postbuckling responses of the shell were predicted, see Arbocz and Starnes [16].

But more cases are using ABAQUS. Tao et al[17; 18], developed a three-dimensional nonlinear finite element model using ABAQUS, with nonlinear material behaviour, initial geometric imperfections included, to predict the buckling behaviour of concrete-filled steel tubes., where close agreement is achieved between the test and FE results in terms of load-deformation response and ultimate strength.

The group in Queen's University of Belfast focuses on investigating the post-buckling of metallic stiffened panels in aircraft fuselage. A number of project have been carried on the idealisation aspect of finite element modelling, including geometrical imperfection, material variance, joint, contact and so on. Some of their theses which are beneficial to this work are Murphy, Quinn and Lynch [10; 19-22].They investigated the efficient failure simulation for the design of low weight structures, using ABAQUS. In addition, some of their identified concerns were studied here in more detail in Chapter 4.

ABAQUS is believed to give fairly accurate solutions, as it provides modelling techniques adequate enough to representing actual structural behaviours, including concerns with geometrical and material nonlinearity, boundary condition, loading condition, mesh size, and imperfections [13].

2.4 Buckling with Initial Imperfections

The influence of initial imperfections on the buckling of thin-walled structures has been widely studied during the past 70 years. The statement that unavoid-

able small imperfections in actual structures were to blame for the large discrepancies between theoretical and experimental results was initially pointed out by Koiter [23], early in 1945.

Nowadays, all the designers know that the initial imperfections play an important role in buckling problems [5] [37]. If one wants to achieve a good correlation between test data and the corresponding theoretical buckling load predictions, then one must account for the effects of the unavoidable initial imperfections.[24] The initial imperfections include geometric imperfections, load eccentricities in columns, residual stress in welded assemblies and delamination in layered composite structures, etc.

In the past few decades, it has been firmly established that the largest reduction of the predicted buckling load of the perfect structure is due to the imperfection in geometry, with smaller percentages due to the others. [24] The so-called geometric imperfection is stated as the deviations from the perfect shape.

Some research found that the role of initial imperfection is very dramatic, especially in columns or unstiffened cylindrical shells under axial compression, such as Hutchinson et al [25], Byskov [26], and Su et al [27].

The influence of initial imperfections has been extensively studied. Most of the work pertaining to stability analysis with random imperfections deals with the modelling of imperfections which are known at discrete points on the structure, or with finding a critical imperfection shape that causes the largest reduction in the critical load for the structure. A theoretical study on random initial imperfections of structures was carried by Ikeda Kiyohiro [34]. In his paper, the explicit form of probability density function of the critical load of structures is derived for random initial imperfection. Tight bounds on the range of load-bearing capacity are presented for various types of simple critical points. By means of the asymptotic theory of statistics, he showed the inefficiency of a conventional random method that approximates the minimum load-bearing capacity by the minimum load for a number of random initial imperfections.

In many instances, details of imperfections caused in a manufacturing process are generally unknown, and only the maximum magnitude of an imperfection is known. Therefore, maximum imperfections may be used to provide a conservative estimation of imperfection magnitude in a particular eigenmode. It is basically assumed that the pattern of the plate initial deflection is equivalent to the plate buckling mode which may give the lowest resistance against the actions, but the effect of some different shapes of plate initial deflection is also studied in the present study. [27] In Tao et al [17; 18] the distribution of initial imperfection was assumed similar to the expected local buckling shape.

In some other cases, assuming the imperfections are linear combinations of the eigenmodes is a reasonable way to estimate the imperfect geometry. One popular way on introducing a geometric imperfection into the FE model is to combine the eigenvectors of the linear buckling analysis. [28] One can also refer in Graciano et al [29], where the imperfection shapes were obtained using a linear combination of the first three buckling modes.

However, all the aforementioned methods are proved too conservative if details of imperfections caused in a manufacturing process are unknown.

In contrast, if details of imperfections caused in a manufacturing process are known, it is normally more useful to use real geometry scatter as the imperfection. Nowadays, as the computer technology developed, the nonlinear analysis codes allow the buckling load solution without the necessity of the assumed shape of the imperfections.

In Hu and Jiang's research [30], the imperfections of FE model were directly mapped from the original measurement in the test, and a mapping process was presented, an evaluated extrapolation was adopted due to the edge of the panel not being directly measured. This approach was a beneficial reference, and will be adopted in the current work as well. Geometric imperfections are commonly defined as nodal displacements in the w-direction representing perturbations of the idealized shell geometry.

One approach is determining the limit load by means of analytical and semi-analytical procedures, e.g. [31] treated the Fourier coefficients of measured imperfections as random variables, and so that the histogram of the limit load can be obtained either by Monte Carlo simulation or approximate methods.

Some works using probabilistic approach were carried for reliable design of these thin-walled structures. Schenk and Schuëller carried a set of researches [32; 33] in buckling analysis of cylindrical shells with random geometric imperfections, where a representation of the geometric imperfections in terms of the Karhunen–Loéve expansion was applied, and also they proved that this K-L expansion is most instrumental for replacing the traditional Fourier series representation. The theory of stochastic processes, in particular the theory of random fields, can be applied most advantageously in order to capture the inherent randomness of imperfections of cylindrical shells and other types of shell structures [33].

However, discussions of the effect of these works above are most based on cylindrical shells; more focus should be contributed to other types of structures.

Ansourian [35] investigated the beneficial effects of a bulk solid content against buckling, reviewing the buckling behaviour and design of slender steel silos and tanks. Kiyohiro Ikedaa et al [38] investigated the imperfection sensitivity of ultimate buckling strength of simply supported elastic–plastic square plates subjected to uniform uniaxial compression, the Koiter power law is extended by implementing the quadratic law to describe the buckling in a synthetic manner.

The most concerned object here in this work is metallic stiffened panels. In Paik et al [13], the pattern of both column-type initial deflection and sideways initial deflection of stiffeners is supposed to be the buckling mode that results in the minimum buckling strength of stiffeners. The consideration of stiffener initial distortions is important, because the stiffener column-type initial distortion can significantly affect the beam-column-type collapse mode, while the stiffener sideways initial distortions can significantly affect the flexural-torsional buckling (or tripping) mode. Another application, bifurcation under axial compression of dis-

cretely stringer-stiffened cylinders in the elastic and plastic ranges is studied in Reddy [39].

This project will take the approach using real geometry scatter as the imperfection and also geometric imperfections will be defined as nodal displacements into the Finite Element model representing perturbations of the geometry. However, due to the few samples are measured, the Fourier coefficients of measured imperfections was not adequate to be treated as random variables, as well as the stochastic processes, which also needs sufficient numbers of samples. Thus, another approach by means of surface fitting should be developed, in order to parameterize the measured imperfections.

3 Finite Element Analysis

In the first stage, a simple model based on a perfect geometry was built, to perform a basic static buckling analysis. By means of this, a preliminary knowledge was understood on different buckling modes of a stiffened panel, as well as the use of the ABAQUS software.

This integrally stiffened panel aims to establish the accuracy of the latter riveted stiffened panel interface and idealizations. The effect of integrally stiffened panel was investigated in order to determine the different failure mode during the load carrying.

3.1 FEA process in ABAQUS

There are three primary manuals in the ABAQUS documentation: *Getting Started with ABAQUS: Interactive Edition* [42], *Abaqus/CAE User's Manual* [43], *ABAQUS Analysis User's Manual* [44]. Going through them costs lot of time, however, it is worthy to read these tutorials for a complete novice in CAE area.

A simple analysis procedure was introduced first in the tutorials. A complete ABAQUS analysis usually consists of three distinct stages: preprocessing, simulation, and postprocessing. These three stages are linked together by input and output files as shown in Figure 3-1.

In the first stage, the model of the physical problem is defined and thereby an ABAQUS input file is created.

In the following phase, the solver of Abaqus/Standard or Abaqus/Explicit will settle the numerical problem defined before. Normally, the simulation is carried as a background process. The process may cost a large amount of time due to the complexity of the problem.

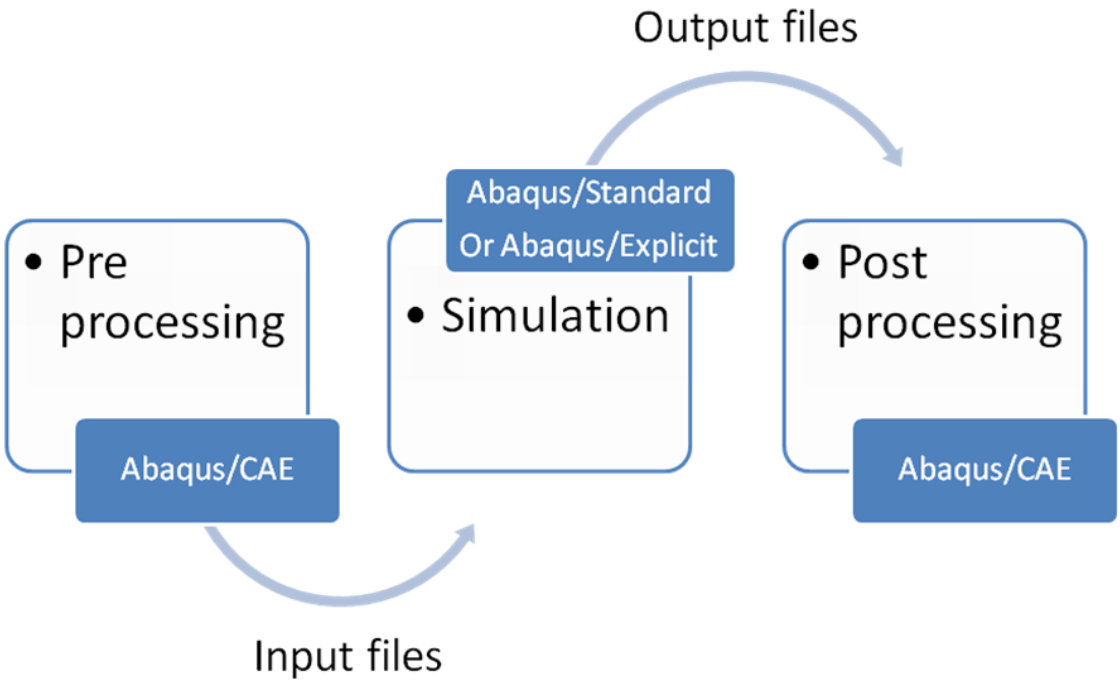

Figure 3-1 the process of ABAQUS analysis

After the simulation is completed, which means all the predefined variables have been calculated, the third step is to assess the results. The displacements, stresses and other variables can be shown in the postprocessor Abaqus/CAE, which is also a powerful pre-processor.

A number of very helpful examples are presented in <ABAQUS Analysis User's Manual> [44]. Particularly, the section 6.2 “Static stress/displacement analysis” demonstrates the procedure of buckling and post-buckling analysis in detail.

3.2 Panel description

The panel considered here is originally from the Structural Stability lecture module in Cranfield University presented by James Campbell [7]. It was designed as a class exercise in the lecture to help the students to understand the buckling calculation, and also was tested in the laboratory to reveal the actual behaviour of buckling and post-buckling.

It is a typical riveted skin-stringer panel, which consists of a rectangular flat skin 430mm long, 370mm wide, and 0.91mm thick, stiffened by six longitudinal stringers. The six stringers are identical in dimensions, with the height in 20mm, inner and outer flange width in 12mm and 8mm respectively, as well as a bend radius of 2.5mm and the same thickness with the skin. The overall length of the stiffeners is equivalent to the skin, and intervals between each stiffener are 70mm. All six stiffeners are fastened to the skin by 6 rows of 3/32” diameter snap-head rivet SP-80, with a pitch of 14mm. The Figure 3-2 supplies the geometry and all the dimensions of the panel.

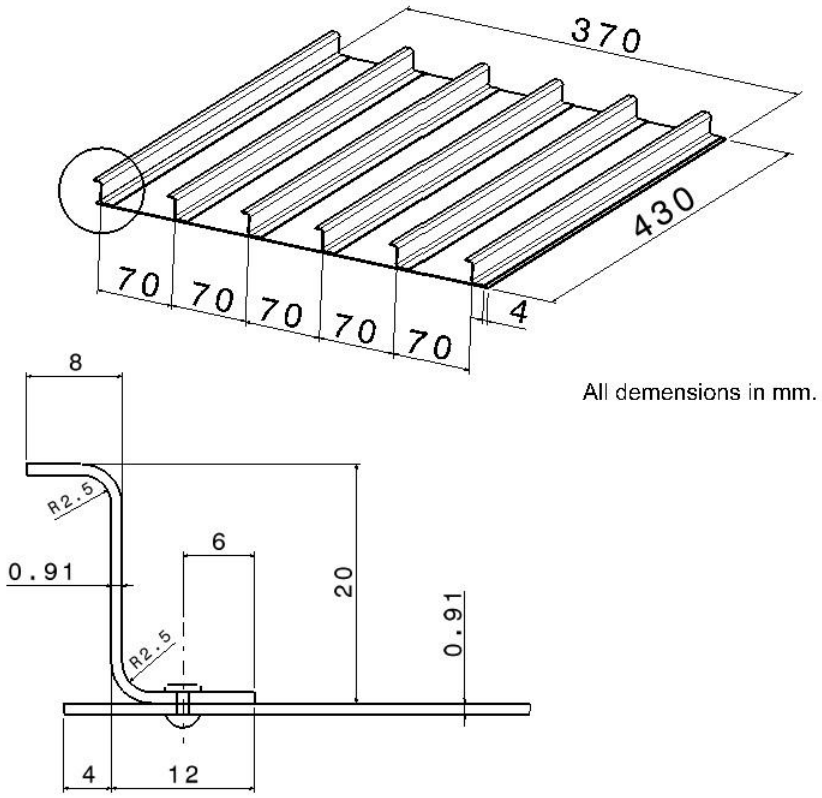

Figure 3-2 Dimensions of the baseline panel

Both of the stringer and skin are made of L165, a close-toleranced sheet of clad aluminium alloy, equivalent to the specification 2014A-T6, which is widely employed in aerospace fields.

The panel can represent a common part of large structures of the aircraft fuselage or upper wing frame, which are always subjected to compression in operation.

To demonstrate the buckling and postbuckling behaviour, this panel is tested in the laboratory in Cranfield University. The panel is subjected to an axial load from the top edge until it collapses. Therefore, two longitude sides of the panel have boundary conditions: the force is imposed from the top direction while the bottom edge is fixed.

In order to realize this, both top and bottom edges are cast into Cerrobend, so that the test rig can keep them from translation and rotation. The Cerrobend region has a width of 16.5mm in either end; therefore the actual panel length is shortened from 430 to 397mm.The following figure shows the Cerrobend area in the both ends of panel.

Figure 3-3 Cerrobend Cast in both ends of the panel

The load is enforced gradually by a hydraulic test machine, with a displacement control until the panel collapse. During the course, different modes of buckling and post-buckling behaviour can be investigated. The panel under testing is shown in Figure 3-4.

Figure 3-4 Panel under testing

3.3 Integral panel building

At the beginning, to help to get familiar with the FE modelling procedure in ABAQUS, an integrally-stiffened panel (hereinafter referred to as “integral panel”) was established.

As a simple reference, some assumptions were adopted, in order to reduce the complexities both in modelling and simulation. For instance, the panel stiffened by longitudinal stringers were treated as a combined component so that there is no interaction between the skin and stringer; stiffeners were modelled rectangular, with no real curved shapes due to the bending in reality; the material was

treated as absolute elastic; the boundary conditions of Cerrobend cast areas in both ends were not modelled as well. The dimensions can be seen in Figure 3-5.

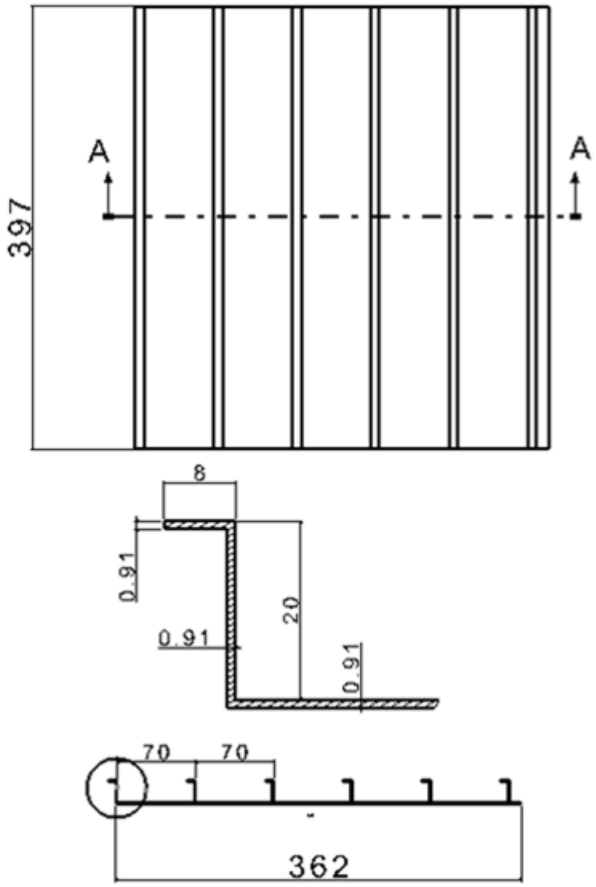

Figure 3-5 Dimensions of integral panel

Apart from the geometry, a basic static buckling analysis was performed. Four node shell elements with reduced integration were used, and a pure elastic material property was assumed. The mesh design was based on 4×4 mm size elements, and a displacement driven loading method was adopted to apply the axial shortening of the top edge, with an artificial constant damping. The following Table 3-1 lists all the modelling parameters in detail.

Table 3-1 the parameters setting in integrally-stiffened panel

Material	Aluminium; Elastic, Modulus of Elasticity E=68000N/mm^2; Poisson's ratio u=0.33.
Sections	Type: Shell Continuum Shell, Homogeneous; Thickness: 0.91 (with all the other default setting).
Step	Type: Static, General; With nonlinear geometry: Automatic stabilization, allsdtol=0; Increment size: 0.05, 1.,1E-005, 0.05.
Boundary condition	Bottom edge: all degrees of freedom of nodes are fixed; Top edge: restrict all the degrees of freedom of nodes except the displacement of 5mm in the positive axial direction.
Mesh	Element type: S4R5; Size: 5mm(mainly); Numbers of elements: 9288

Moreover, the simulation results were acquired. Abaqus/CAE can deal with these data into a variety of displaying, such as colour contour plots, deformed shape plots, and X–Y plots, see Figure 3-6, Figure 3-7 and Table 3-2.

This simple model will be referred and compared in the later paragraphs.

Benefits from the integral panel establishment:

1) Get familiar with the ABAQUS interface;

This simple reference panel could be a beneficial practise to train up with the Abaqus/standard interface.

2) Complete an FE analysis in ABAQUS.

The step by step procedure in preprocessing of FE model building was challenging for a newcomer to the subject.

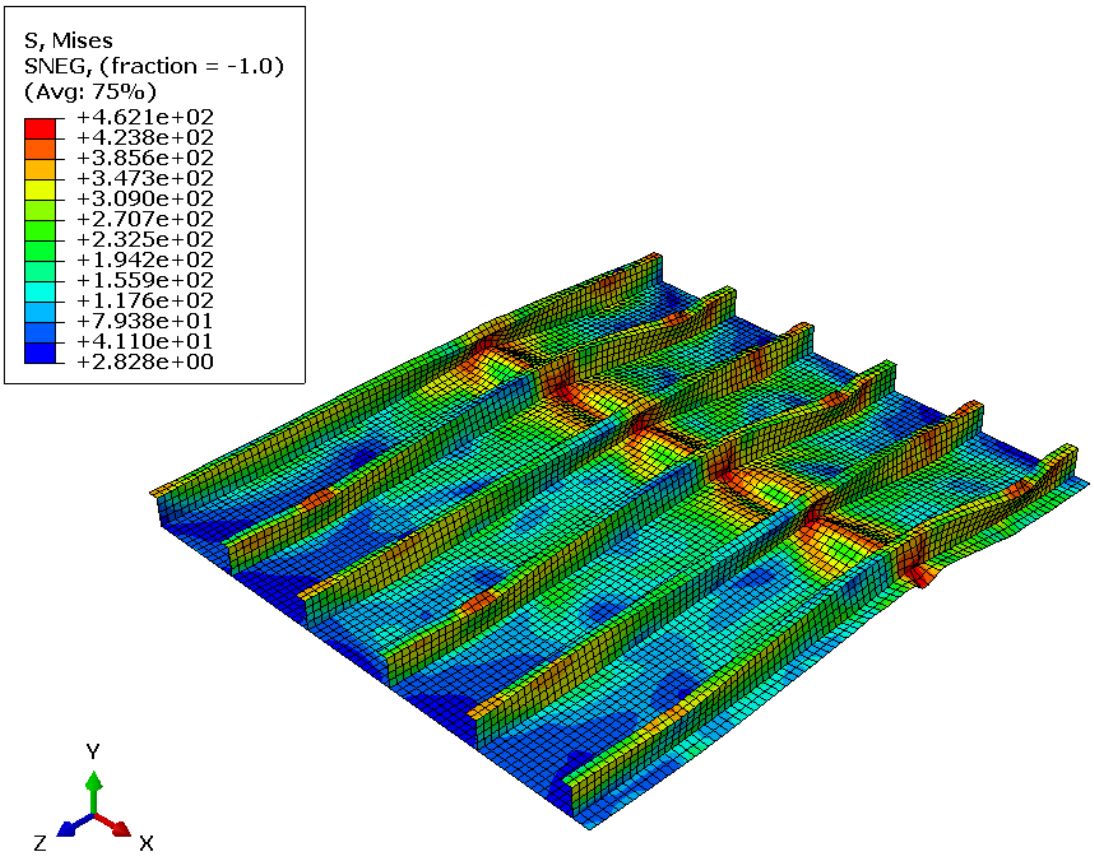

Figure 3-6 Stress contours of the buckling of integrally-stiffened panel

3.4 Buckling and postbuckling analysis

Another benefit from the integral panel simulation result is to investigate the buckling and postbuckling mode of this particular panel.

The load-displacement curve in Figure 3-7 reveals two main buckling modes:

-Local buckling- and -Global buckling-

The first “snap through” in the curve indicates that the initial buckling occurs when the skin between stiffeners starts to buckle. At the time, the first point of

instability is reached, which is termed as local buckling. The local buckling make the stiffness decrease slightly, while the load carrying capability still exits, which means the load can be increased.

Following the local skin buckling, there are 4 main post-buckled failure modes that may occur during the load carrying course: the inter-rivet buckling, the stringer crippling, the flexural failure and the torsional failure. All those occurring after local buckling in the skin are termed as post-buckled modes.

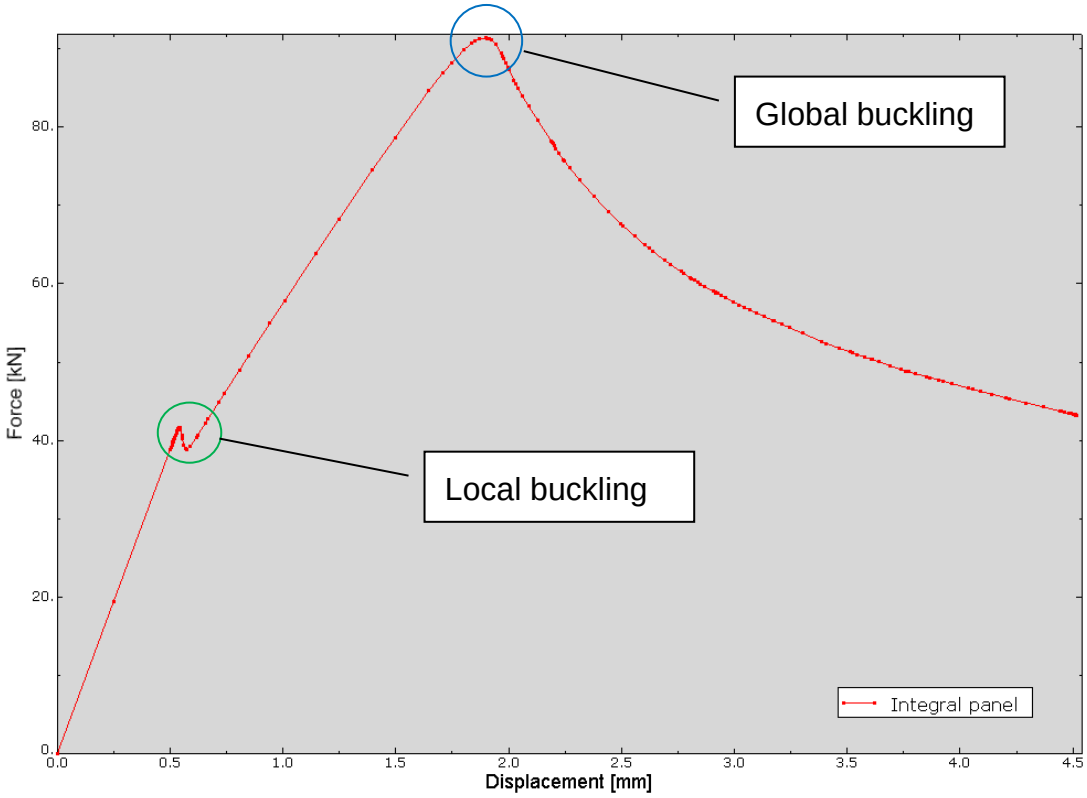

Figure 3-7 Load-displacement curve of integral panel

Table 3-2 Ultimate load of integral panel

panel	Displacement (mm)	Ultimate load (kN)
Integral panel	1.89904	91.3715

In addition, the global buckling in the term of collapse of panel reveals the loss of load capability. Commonly, this kind of buckling is due to local flexural or torsional buckling in the stiffeners, depending on different situations. The global buckling can be identified easily when the load displacement curve drops, after which the stiffness reduces significantly so that the panel cannot resist any more load.

3.5 Summary

In this chapter, for the aim of learning the ABAQUS software, a simple model based on a perfect geometry was built and used to perform a simple buckling analysis.

In addition, a preliminary knowledge was developed on different buckling modes of a stiffened panel.

This integrally stiffened panel model will also act as a reference panel for the later more complex panel models and help establish the accuracy riveted stiffened panel interface and idealizations.

4 Baseline model verification

The purpose of this chapter is to describe the development and verification of the baseline model of the panel. A geometrically non-linear finite element model is be developed using the commercial code ABAQUS, to determine the buckling load of this panel.

The previous simple model is not adequate for this study due to too many simplifications in the model that differ from reality.

Rather than an integral panel, this FE model must simulate a riveted skin-stringer panel, representative of the real situation. The skin and stiffeners are modelled separately, and the interaction among them will be also simulated.

In addition, with both geometric and material non-linearity included in the model, a non-linear analysis was then performed using the general static step in ABAQUS to obtain the ultimate load and failure modes of the panel. This final model can be compared with the real panel tested, as a reference, called baseline model.

Other than the baseline FE modelling, the results from the model will be discussed, to explain the effect of the various nonlinear uncertainties in the modelling. For example, what element is best to be adopted, how many elements are sufficient, what material model should be performed, how to make the rivet and contact modelling, and what boundary conditions should be applied. By investigating the response of the model, and comparing with different settings, observing how response changes as the setting changes, the verification is performed.

4.1 Material properties

To develop a suitable model for material can be very crucial in FE analysis, since the material behaviour of aluminium adopted here is not ideally elastic. In fact, the aluminium alloy can never be absolutely elastic. In this model, the nonlinearity of the material should be considered. It is also important to add the nonlinear behaviour into the material properties. The significant influence of the

nonlinearity of materials has already been demonstrated in L. Hetey's PhD thesis [9].

To describe this nonlinear stress-strain behaviour, the Ramberg-Osgood formula [45] has been developed and widely adopted for aluminium.

$$\varepsilon = \frac{\sigma}{E} + K[\frac{\sigma}{E}]^n \tag{4-1}$$

Herein, σ, ε are true stress and true strain respectively, E is the Young's Modulus and n refers to strain hardening exponent. This equation has been widely applied by Tao et al[17; 18],Rasmussen[46] and Quach et al[47], and is also given in ABAQUS Theory Manual [43].

When defining plasticity data in ABAQUS, one must use true stress and true strain; ABAQUS requires these values to interpret the data correctly [42]. Generally in engineering, material test data are supplied with values of nominal stress and strain. In such situations, the nominal values need to be converted into the true stress and strain values.

The Ramberg-Osgood formula gives a direct way to calculate the true stress-strain relation. In the formula, the constants K and n can be found in ESDU data sheet [48] for various materials. While in ESDU, the formula is presented in another form as following:

$$\varepsilon = \frac{\sigma}{E} + \frac{f_n}{Em}[\frac{\sigma}{f_n}]^m \tag{4-2}$$

Due to the lack of coupon test of this specific material used in the specimen of panel, either published material parameters in ESDU [48] or the former similar test result will be adopted in the simulation.

The parameters of L165 aluminium alloy adopted here from a tabulated material sheet in Cranfield University [49] are:

- Modulus of Elasticity $E = 68000N/mm^2$;
- Poisson's ratio υ=0.33;
- Yield stress $\sigma_y = 340N/mm^2$;

- $f_n = 296\ N/mm^2$;
- $m = 17$.

The true stress-strain curve can then be calculated, which is shown in Figure 4-1.

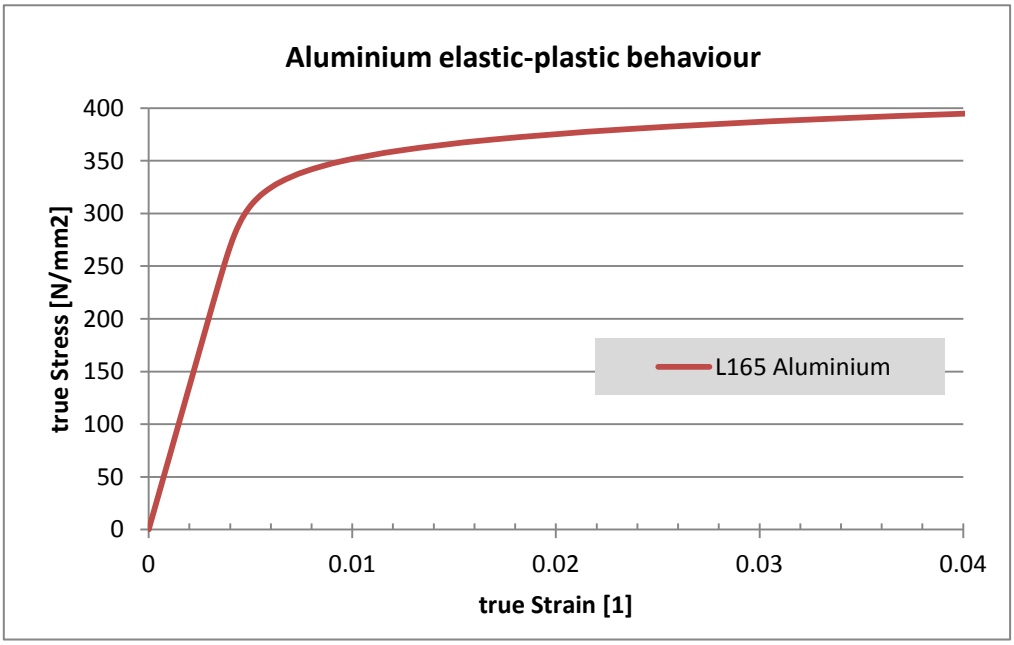

Figure 4-1 the Elastic-plastic material behaviour of L165

However, in the ABAQUS material definition format, it is required to enter the true plastic strain. Therefore, the true stress-strain curve derived by Ramberg-Osgood formula should be transformed using the following equation:

$$\varepsilon^{pl} = \varepsilon^{t} - \varepsilon^{el} = \varepsilon^{t} - \frac{\sigma}{E} \tag{4-3}$$

Here, ε^{pl} is true plastic strain, ε^{t} is true total strain, ε^{el} is true elastic strain, σ is true stress, and E is Young's modulus.

4.2 Shell elements investigation and mesh refinement study

In this section, the selection of shell elements from the element libraries in ABAQUS will be firstly stated. After that, the mesh refinement study is demanded to investigate which density of the mesh is sufficient for this research.

There are mainly two kinds of elements that can be used in finite element analysis for this case: continuum element and shell element.

Due to their high efficiency, shell elements are widely employed in finite element analysis. But the limit is that shell elements can only be recommended to apply in those cases where one dimension (the thickness, say) of a structure is significantly smaller than the other dimensions and the stresses in the thickness direction are negligible [42].

In this case, the skin thickness is significantly smaller than any other global dimensions, as well as the thickness in stiffeners. Therefore shell elements can be adopted to model the panel in the analysis.

4.2.1 Shell element selection

For the shell elements selecting, ABAQUS gives some advice in the tutorial. According to previous experience [17; 18][20][10][9][50], there are mainly three types of elements that can be the candidate: S4, S4R and S4R5.

S4: 4-node shell elements with full integration, can be used when greater solution accuracy is desired, for problems where in-plane bending is expected.

S4R: 4-node shell elements with reduced integration. It uses reduced (lower-order) integration to form the element stiffness. The mass matrix and distributed loadings are still integrated exactly. Reduced integration can provides more accurate results where elements are not distorted or loaded in in-plane bending, and significantly reduces running time, especially in three dimensions.

S4R5: 4-node shell elements with reduced integration and using 5 degrees of freedom (one in-surface rotation component is reduced). For very large models which will experience only geometrically linear behaviour, the element S4R5 can be can be more economical. However, they are available only as “thin” shells.

A tabular comparison of these distinct types of shell elements is shown in Table 4-1.

Table 4-1 three types of Shell elements

Shell type	Description	Application
S4	4-noded shell element, first order, full integration	General purpose; Great solution accuracy; High computational cost.
S4R	4-noded shell element, first order, reduced integration,	General purpose; Robust accuracy; Suitable for a wide range of applications.
S4R5	4-noded shell element, first order, reduced integration, thin-shell	Only experience geometry linear behaviour; Most cost-effective for very large models.

In order to get an idea of these three elements and investigate which one is most suitable, a numbers of models were built, and the responses were compared as Table 4-2 and Table 4-3.

Theoretically, the element type S4 is the most powerful one that predicts the greatest accuracy in solution, mentioned at the beginning of this subchapter. Thus, the comparison is based on the result calculated by S4 elements. From both tables, compared with the result of S4, one can easily see that S4R can predict as similar accuracy in terms of the ultimate load, less than 0.70%. While the difference between S4 and S4R5 is generally larger than 1%. From the side of collapse mode, all three elements did not show big disparities.

However, the shortcoming of S4 elements is that it requires great cost in computer resource as it behaviours in high accuracy. Both S4R and S4R5 significantly reduce the CPU time, with an average percentage of 20%.

The same investigation can also be found in Hetey [9], where a research based on which a comparison was presented.

The conclusion is that S4R was chosen as the appropriate element type because it more economic than S4, while S4R5 seems not showing sufficient accuracy.

Table 4-2 Comparison in shell element selection: collapse load

Elements' number	Elements' type			Ultimate load Comparison	Computational cost Comparison
	S4	S4R	S4R5		
17696	**Model-1**	Model-4	/	-0.70%	-23.90%
27777	**Model-2**	Model-5	/	-0.36%	-25.37%
23072	**Model-3**	Model-6	/	0.25%	-25.60%
17696	**Model-1**	/	Model-7	-1.66%	-19.88%
27777	**Model-2**	/	Model-8	-1.00%	-8.59%
23072	**Model-3**	/	Model-9	-1.36%	-23.7%

Table 4-3 Comparison in shell element selection: collapse mode

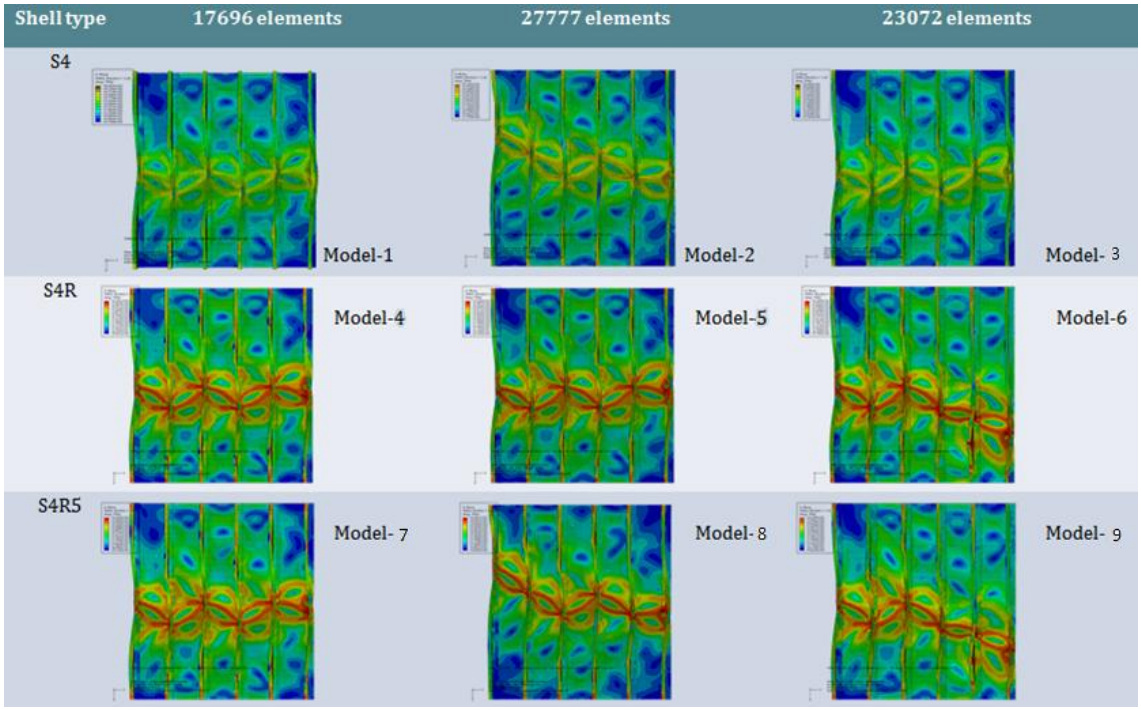

4.2.2 Mesh refinement

Based on the conclusion of previous element selection process, the mesh refinement uses S4R as the default element, as it can be more effective due to the great time-saving advantage.

The mesh convergence study will be executed to determine the necessary mesh refinement.

4.2.2.1 Mesh density study

The convergence of the mesh density is based on the relative change of the response of buckling load as the mesh is refined.

The so-called buckling load is actually the “Ultimate collapse load” in which the global buckling occurs and the whole panel automatically collapses without any continuous force implement.

The mesh must have enough numbers of elements along the inter-rivet areas, which is between the two rivets, to simulate such inter-rivet buckling model mentioned in chapter 3. The area where the stiffeners contact skin is more important due to this is the mainly stiffness originated and needs finer mesh, while in the patch other than the contact region, the mesh can be coarser.

Therefore, the level of mesh refinement depends on the size of elements assigned in the panel, especially in the stiffeners, which carry most of the load of buckling in axial direction.

The coarsest model-10 is based on an 8mm×8mm size mesh, which has the fewest elements, with the number of only 5684. Obviously, this kind of mesh will lead to the incorrect prediction of the ultimate load.

The finest model-15 is based on a 2mm×2mm size mesh, which is considered as the most accurate as the real result of such an assumed panel cannot be obtained. The comparison of different mesh density can be found in Table 4-4. And the Load-Displacement plots are in Figure 4-2.

Table 4-4 Comparison in mesh density study: collapse load

Model class	Elements numbers	Model	Total CPU time (s)	Comparison in Ultimate load
Coarse	5684	Model-10	455.1	-3.75%
Medium	17696	Model-11	2024.1	1.79%
Medium fine	27777	Model-12	3300.9	0.56%
Refinement-1	**23072**	**Model-13**	**2664.2**	**0.53%**
Refinement-2	40851	Model-14	7484.6	0.42%
Finest	59899	Model-15	11942.0	0.00%

From the Load-Displacement plot, all the panels coincide roughly as the load increases, although there might exist slight difference when the slope of the curve first changes, which means the local buckling comes up.

As the curves keep rising, the model-10 starts to apart from the others before reaching the upper bound, and the ultimate load predicted by which differs greatly with the rest panels, where it also proves that the coarsest model is incorrect.

One can easily see that as the numbers of element increases, the model predicts closer load compared with the finest model-15.However, the mesh refinement also means the time consuming rises simultaneously.

Model-13 is a revision of model-12, to reduce the mesh numbers, which indicates sufficient accuracy in predicting the ultimate load. Meanwhile, the CPU time is dramatically reduced, from the highest 11942.0 second to 2664.2 second.

Another point that should be declared is that after global buckling, i.e. the whole panel collapse, the load-displacement paths diverge separately. This is because of the solution adopted in this analysis. Except for some simple cases, the displacement control static procedure cannot provide a very good solution after the

load-displacement response shows a negative stiffness, meaning the global buckling occurs.

It is argued that if one attempts to model the exact behaviour after the panel collapses, one can treat the buckling response dynamically, or using the Riks method. The dynamical solution actually models the response with inertia effects included as the structure snaps. The Riks method uses the “arc length” as the third quantity to measure the progress of the solution and solves simultaneously for loads and displacements. Both approaches can provide solutions regardless of whether the response is stable or unstable. However, the accuracy in predicting the critical load is sufficient by means of the current solution, which is exactly fit to the core aim of this project.

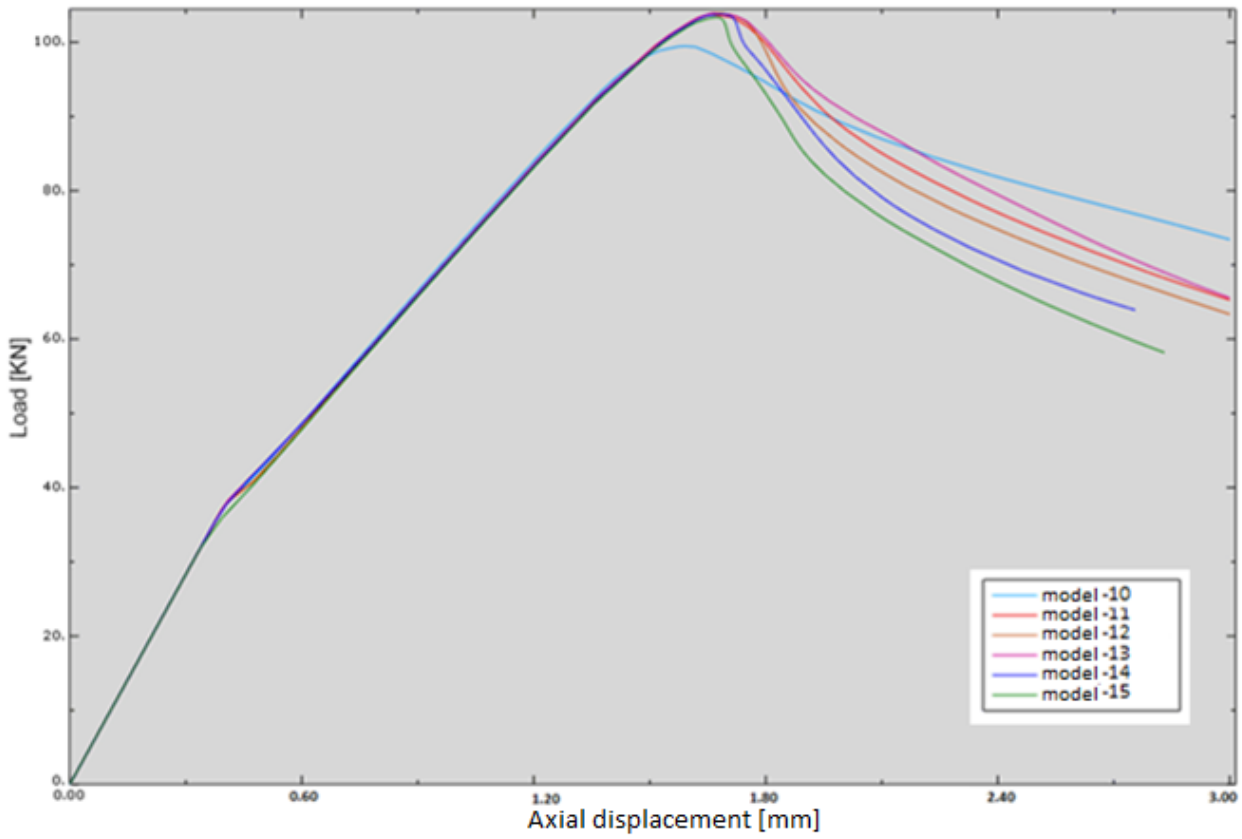

Figure 4-2 Comparison in mesh density study: Load-Displacement plot

In summary, the model with 23072 elements is the most economical model, which provides sufficient accuracy in prediction of the final collapse load.

4.2.2.2 Curvature in stiffeners

As described in chapter 3, for simplification, the stringer corner was modelled as rectangular shape in the simple model, which is also due to the flatness of shell element.

The rectangular simplification is not identical to the real shape in the panel. As described in Figure 3-2, the bend radii of stringers are 2.5mm, which will be investigated by a comparison in the model.

In fact, the FE model cannot delineate the exact curved feature because of the quad element shape. The practical way is to refine the mesh size in these curved edges, where a certain number of nods are seeded. The next job is to vary numbers of elements assigned in a curve, from 2 to 4 as shown in Figure 13, then by comparing the results to determine which refinement is most appropriate, accurate enough while not so much time costly.

From the comparison in Figure 4-4, compared with model-13, the reference model with 0 elements in the curve, one can see that as the numbers of element increased, the predicted ultimate load drops. L.Hetey [9] believed that the decrease in collapse load is caused by shortening the contact area, which has the biggest thickness and therefore is the most stabilising part of the whole panel.

Model18 with 4 elements in the curve of the stiffener is selected to be the favourite, as it is most close to the reality while the time consumption is relatively less.

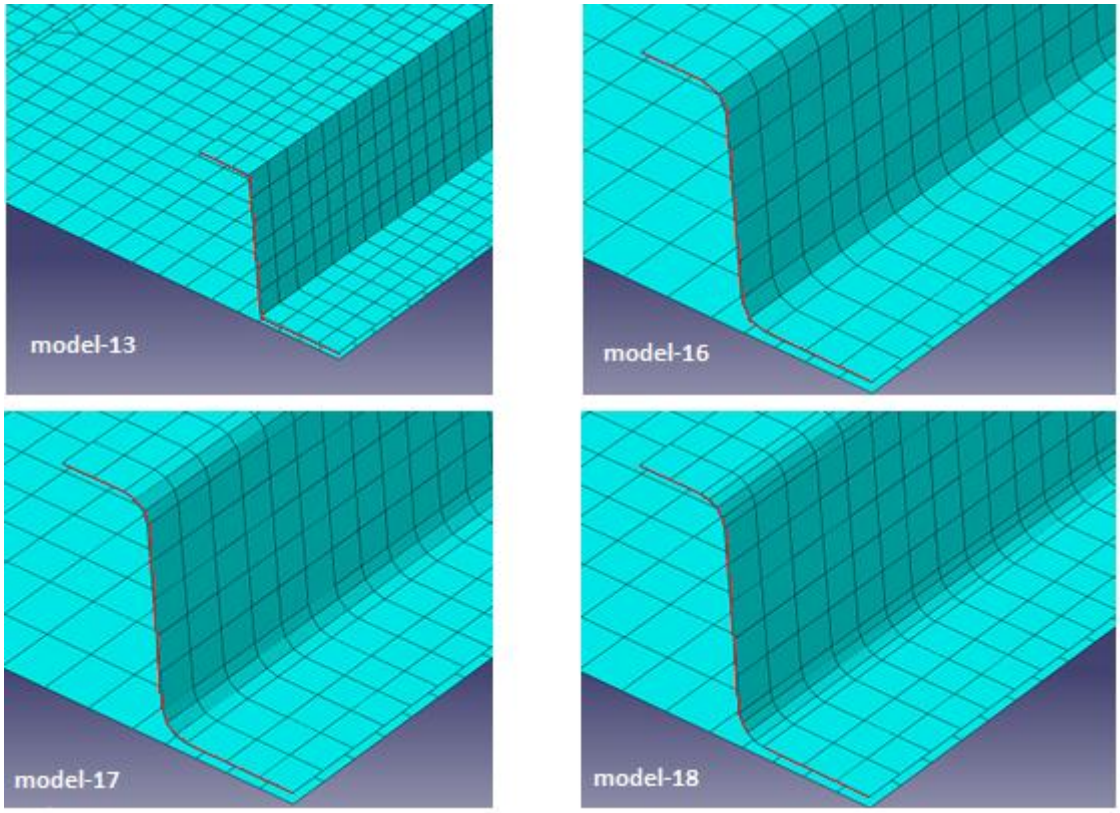

Figure 4-3 Curve modelling

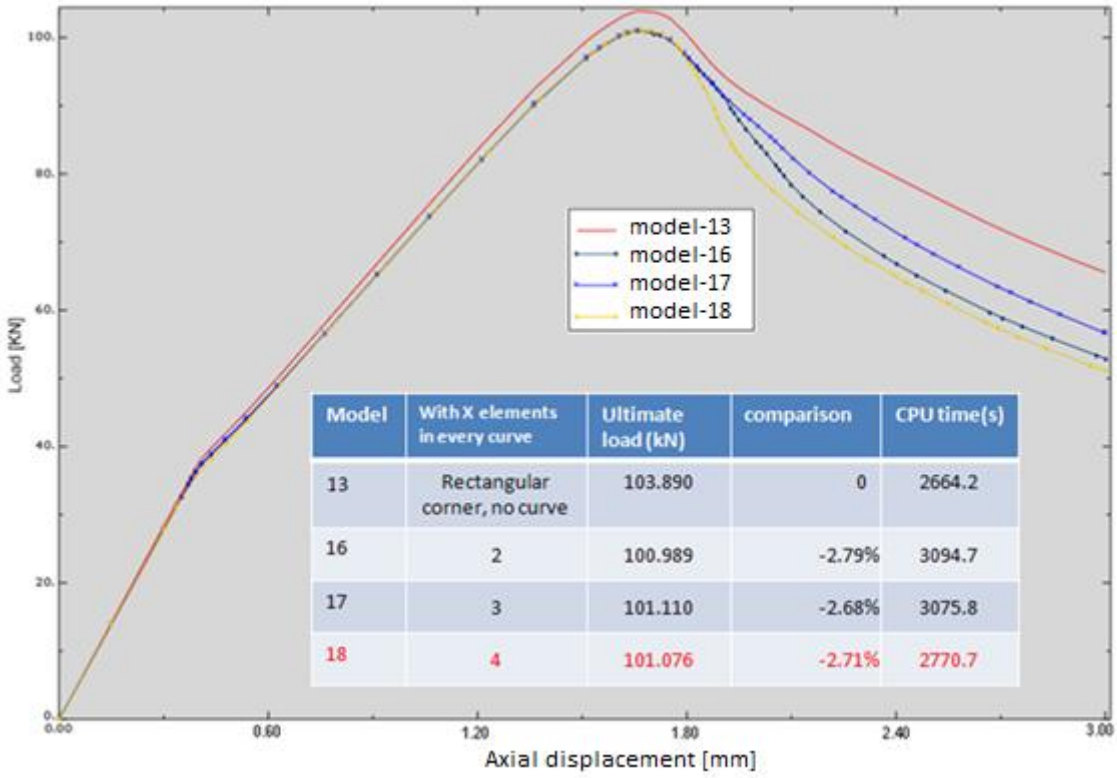

Model	With X elements in every curve	Ultimate load (kN)	comparison	CPU time(s)
13	Rectangular corner, no curve	103.890	0	2664.2
16	2	100.989	-2.79%	3094.7
17	3	101.110	-2.68%	3075.8
18	4	101.076	-2.71%	2770.7

Figure 4-4 Comparison with different curve modelling

4.2.2.3 Mesh design

A fine mesh, based on the results of the above refinement study, is thereby determined.

The mesh in this model is based on the design shown in Figure 4-5, which is mainly consisting of 25668 elements with the size of 3.5mm×3.5mm in both stiffeners and skin. It provides moderate accuracy while keeping the solution time to a minimum.

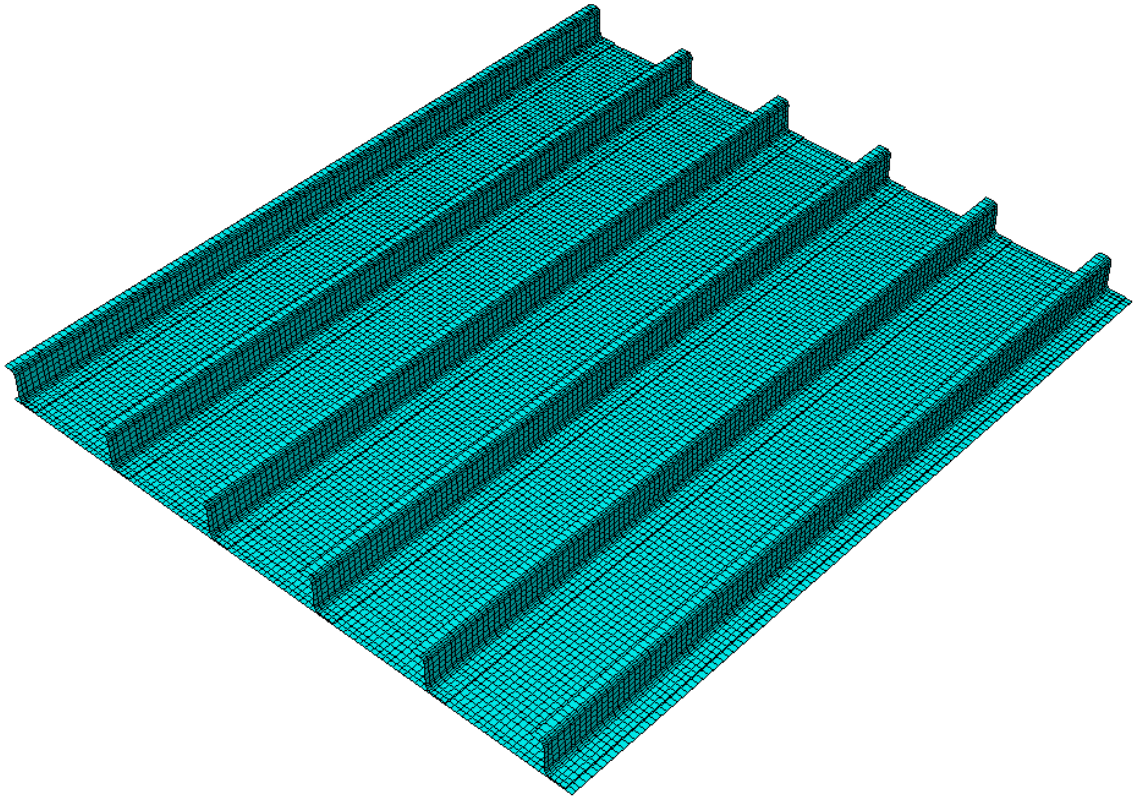

Figure 4-5 Mesh design for baseline model

This mesh corresponds to the input files.

Moreover, it is notable that the mesh must have sufficient elements along each rivet position, in order to satisfy the constraint region of the independent fasteners which will be introduced subsequently.

And also, the level of mesh refinement depends on the optical scan density.

4.3 Skin-Stringer Interaction

The interaction module in ABAQUS is used to model the Mechanical interactions in a region or between different parts in the model, as well as the Analysis constraints, interface region.

For this model, there are two main aspects of interactions: contact between the skin and stiffeners; rivets which restrain the skin and stiffeners together.

4.3.1 Contact between skin and stiffeners

The first problem comes from the contact between skin and stringers. ABAQUS provides more than one approach for defining contact. In Abaqus/Standard, the following approaches for defining contact are included:

- *General contact;*
- *Contact pairs; and*
- *Contact elements.*

The third option, contact elements, is based on some idealization assumptions, as has been investigated by Lynch et al [51].Lynch presented four different FE idealizations of the skin/stiffener interface including rigid beam, dummy layer, gap element and spring element, and examined them one by one. However, the result proved that they were not representative of the actual structure.

In ABAQUS, there is one type of contact named surface-to-surface contact, which describes contact between two deformable surfaces or between a deformable surface and a rigid surface [42]. The Surface-to-surface contact was selected to model the interaction as it is most close to the reality.

This surface-to-surface contact consists of a master and a slave surface forming a contact pair, by default. Contact pairs use a pure master-slave contact algorithm: nodes on one surface (the slave) cannot penetrate the segments that make up the other surface (the master). In this case, the skin is treated as the master and the surface on the stiffeners is considered as slaves.

After the surfaces are specified, the next step is to define the mechanical property models that govern the behaviour of the surfaces when they are in contact.

The finite sliding and “hard” contact normal to the surfaces are adopted by default. Moreover, the friction model must be included, since the static coefficient of friction of Aluminium on aluminium is 1.05 (dry), given by *Marks’ standard handbook for mechanical engineers, 11th edition* [52].

4.3.2 Rivet modelling

The next important concern is the modelling of rivets. The whole panel was combined by a sheet of skin stiffened by six identical Z sections stiffeners in longitude direction. As mentioned before, all six stiffeners are fastened to the skin by 6 rows of 3/32” diameter snap-head rivet SP-80, with a pitch of 14mm. The rivets were also presented in Figure 3-2.

There are in total 6 lines of rivets and with 31 per line. Due to the number of rivets, it is too costly to model each rivet as a real shape with a 3D model. Otherwise, the mesh size would be too large and it is not realistic as well. Therefore, a rivet idealisation is necessary.

The previous work conducted by Murphy et al [19] in 2001 investigated the spring elements technique used to model this kind of rivets at a low fraction of the cost of above detail 3D shell modelling. However, it was required at least 3 spring elements to model a single rivet: one representing the axial stiffness and two representing the shear stiffness, still too elaborate.

Alternatively, to model the rivets, it is advised to use the mesh-independent Fastener in ABAQUS. The Mesh-independent Fastener is considered as a convenient method to define a point-to-point connection between two or more surfaces such as a spot weld or rivet connection. However, the fastener should combine connector elements with distributing coupling constraints. In addition, one should define the connector section and assign it so that the fastener can play its role.

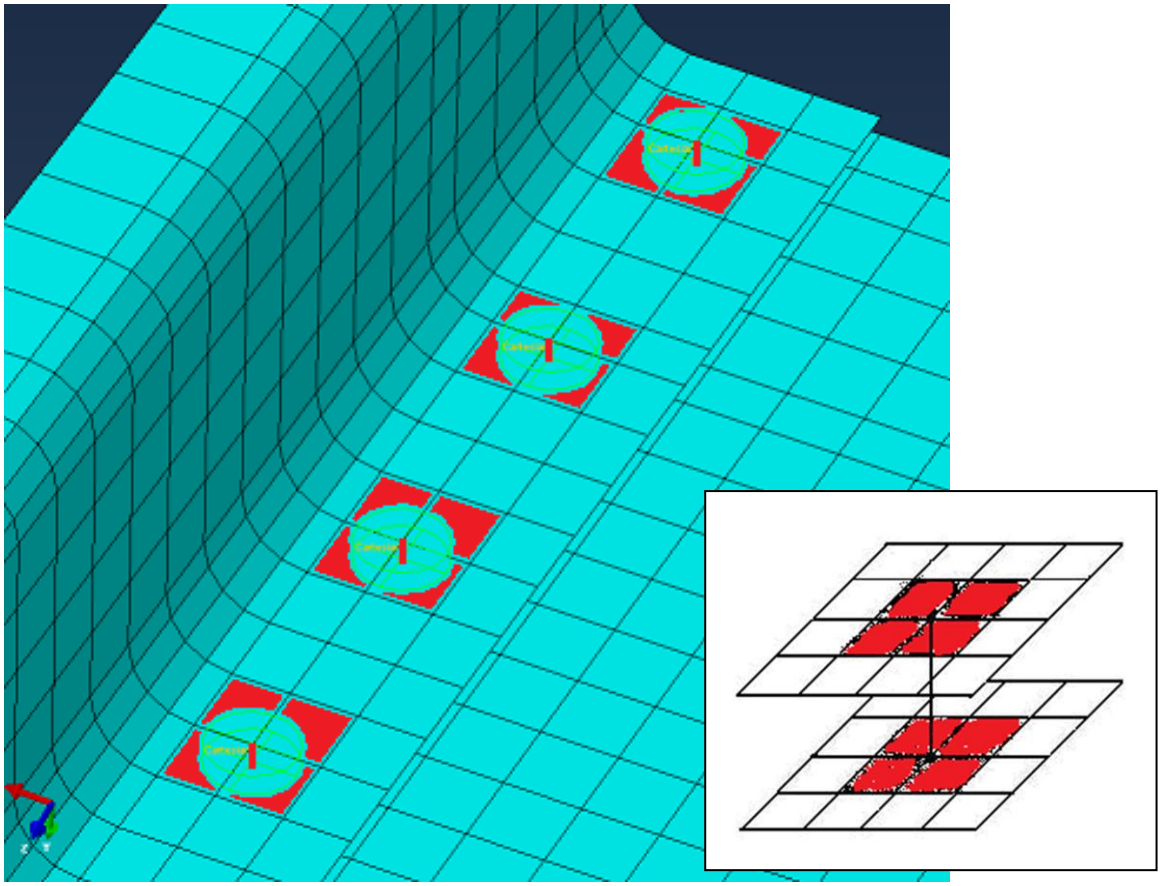

Figure 4-6 the radius of influence of rivets

The mesh-independent fastener can be used to connect both deformable and rigid element-based surfaces. Elastic and inelastic connections with failure can also be modelled by using the generality of connector behaviour definitions. The last point, it is available only in three dimensions.

One should notice that the rivet radius of influence must be defined. Each fastening point is associated with a group of nodes on the surface in the immediate neighbourhood of the fastening point called a region of influence. The motion of the fastening point is then coupled in a weighted sense to the motion of the nodes in this region by a distributed coupling constraint. From the point of view of accuracy, this influence region should be consistent with the real geometry (diameter, say) of the rivet itself. However, due to the mesh design, for simplification consideration, such radius is artificially specified equivalent to the area of nearest 4 nodes, illustrated in Figure 4-6; otherwise it will disturb the regular size of mesh,

According to the experience in L. Hetey [9], none of the rivets failed in ten compression tests, so the failure of rivets can be ignored. In contrast, the ductile behaviour of rivets should be taken into account.

As far as the connector behaviour, the Cartesian connector element is recommended in ABAQUS. The plasticity attribution in connectors is similar to general metallic plasticity, as described in section 4.2.

4.4 Boundary conditions

The whole panel, as mentioned in Chapter 3.1, is subjected to an axial compressive load until it collapses. The load is applied at the top edge of the panel.

To connect to the test machine, both ends are cast in Cerrobend. Cerrobend is a low melting point alloy which can be easily reshaped flatly. By means of this cast, the displacement move and especially the rotations in both ends of the panel can be restrained. This technology was also adopted by Lynch C.J. et al [51].

There are some methods to simulate this kind of boundary conditions. In his PhD thesis, Hetey [9] discussed the sensitivity to boundary conditions, where two boundary condition idealisations were illustrated:

One is “End cast + constraint band”, which casts the ends nodes and allows only an axial displacement of the nodes in the constraint band. The other way is to model the Cerrobend explicitly using solid elements, named “Cerrobend modelled”.

A comparison was also carried with the effect, which indicated that the former was decided as the most realistic variant and therefore adopted in the improved model.

This approach is inherited in the current modelling. In this project, a displacement control method was used here. Axial compressive load was applied by specifying a displacement to the nodes at the top end of the panel. By iteration,

a displacement of 3 mm specified was sufficient, which is equivalent to the axial shortening of the panel.

Due to the cast region in Cerrobend, the actual panel length is shortened to 397 mm, with a 16.5 mm width in each end. In the FE model, the loaded edge is clamped. For the edges which were termed as “End cast”, the degree of freedom of these nodes are strictly restrained. Since the load is implemented from the top, in the top edge, a line of the nodes are set to be prevented all the rotations and displacement, with only the axial displacement is defined as 3mm (blue nodes in the right of Figure 4-7). In the bottom edge, all the degrees are set as zero (left blue nodes in Figure 4-7).

For the potted regions other than edges at the ends, so-called “constraint band”, those nodes in these areas only the axial translation has a degree of freedom (red nodes in Figure 4-7).

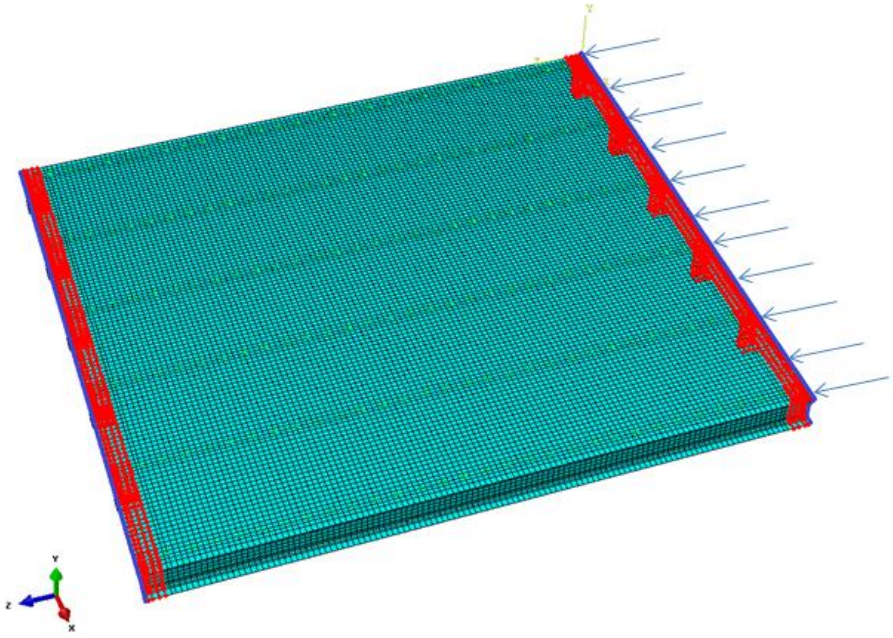

Figure 4-7 Boundary conditions of baseline model

As indicated in Figure 4-7, the Red and Blue spots illustrate the Cerrobend regions which are mounted in a test rig. In the simple model referred in chapter 3.3, these “constraint band” areas were neglected; only the nodes of “End cast”

were restrained from rotation and displacement. Nevertheless, these areas must be restrained as well.

An additional investigation was performed in this project in order to examine the influence of such “End cast + constraint band” modelling. In Figure 4-8, the model in the right side is modelled in such way described before, which was compared to another model (shown in the left side in Figure 4-8) where the end and constraint band were combined as an integral part, and the constraints assigned on the “End Cast” were enforced. The predicted load in Table 4-5 shows no distinct difference, only 0.81%. However, the deformation contour shown in Figure 4-8 reveals that in the left one the stress in the combined area was zero, while the right figure shows reasonable stress in those areas. This comparison supports that the conclusions from Hetey [9].

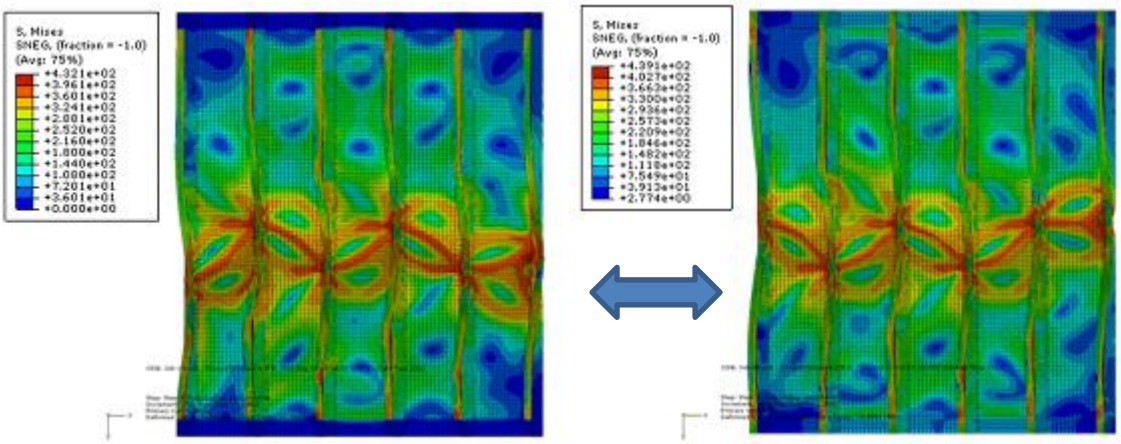

(Mises stress is shown in MPa)

Figure 4-8 Comparison of different boundary modelling

Table 4-5 Prediction in different boundary modelling

model	Ultimate load (kN)	Comparison
19	103.309	0
24	102.469	-0.81%

In summary, the boundary conditions adopted in this research can be stated as follows:

- *For the nodes at the bottom edge, all the degrees of freedom are restrained*
- *For the nodes at the top edge, the unique difference from the bottom edge is that the displacement in the axial direction is given with 4mm, due to the load applied at the top end of the panel.*
- *For the other nodes in the cast area, the translational degree of freedom is released; all the other five degrees of freedom are fixed.*
- *For the nodes other than the area, the translations and rotations are all free in any directions.*

4.5 Geometric nonlinearity

Herein the nonlinearity means in the problem the structure's stiffness changes as it deforms. In practice, all physical structures are nonlinear, as the linear analysis is based on a convenient approximation in order to make design process easier. However, it is obviously that not all can be treated as linear for many structural simulations, such as manufacturing processes. A simple example is the elastic plastic properties of an aluminium material (see Figure 4-1).

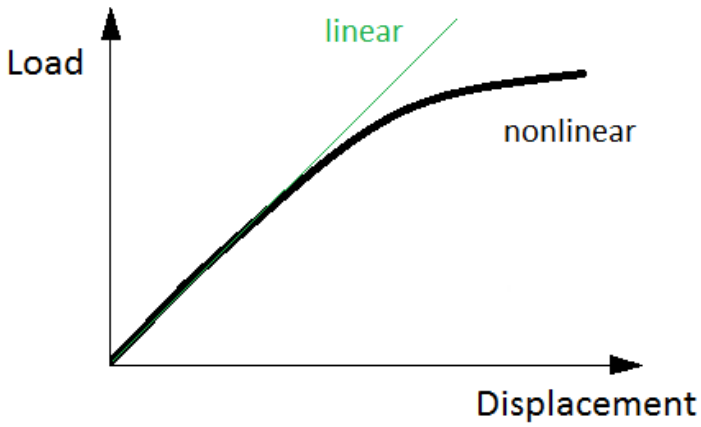

Figure 4-9 Linear and Nonlinear curves

The three main sources of nonlinearity in structural mechanics simulations are Material Nonlinearity, Boundary Nonlinearity and Geometric Nonlinearity. As the first two have been already discussed in previous paragraphs (see 4.1 and 4.4), this chapter will only introduce the nonlinearity in geometry.

During the analysis, the geometry of the structure changes due to many reasons such as Large deflections or rotations, or the dramatic change in the stiffness-the so called “Snap through”, which can be seen in Figure 3-7. As the load increases, “snaps through” occurs in the panel when the local buckling appears and the stiffness becomes negative. Therefore, although the magnitude of the displacement is very small, there can still be a significant geometric nonlinearity in the simulation, which must be taken into consideration.

This chapter will discuss how to account for geometric nonlinearity in FE analysis within ABAQUS. In a general static analysis, to incorporate the effects of geometric nonlinearity one must include the NLGEOM parameter in the *STEP setting. Nevertheless, it is far from enough. One should also suggest the size of the increment in each step of the simulation. However, due to the automatic incrementation control in Abaqus/Standard, the default of automatically adjusting the size of the load increments is sufficient and can solve most of the problem effectively.

Apart from those basic setting, another and the most important statement comes to the automatic stabilization of unstable problems. Nonlinear static problems become unstable when buckling occurs during the analysis.

Although Arc length methods such as the Riks method are powerful in solving global and postbuckling analyses, however, before expanding the discussion, the analysis procedure of this project should be introduced first. In this project, we are more interested in investigating the structure's additional load carrying capacity after it starts to buckle, rather than the postbuckling behaviour after global buckling of the panel.

Before the global buckling, equivalent to whole collapse of the panel, the instability is localized. The global control solution methods may not do function well, since during the local instability there will be a local transfer of strain energy from one part of the model to neighbouring parts.

Alternatively, either the dynamical solution or introducing damping is available in ABAQUS. However, solving a static problem dynamically is generally too ex-

pensive. In this project, the automatic stabilization is adopted, which applies volume proportional damping to the structure, to provide stability to the numerical solution.

In the damping case, the strain energy released locally from buckling is dissipated. There are two forms of automatic stabilization supplied in ABAQUS, one with a constant damping factor that is chosen by default, and one with an adaptive damping factor. Both of them are considered in the following comparison.

By comparing the viscous damping energy (ALLSD) with the total strain energy (ALLIE), the ratio of the method “Stabilization with a constant damping factor” exceeds the 5%, see Figure 4-10. However, the percentage of 5% is considered as a reasonable amount, by default in ABAQUS. This means the damping factor calculated from the first increment of the step is not sufficient which can lead the structure goes to a distortion of the solution, see Figure 4-11.

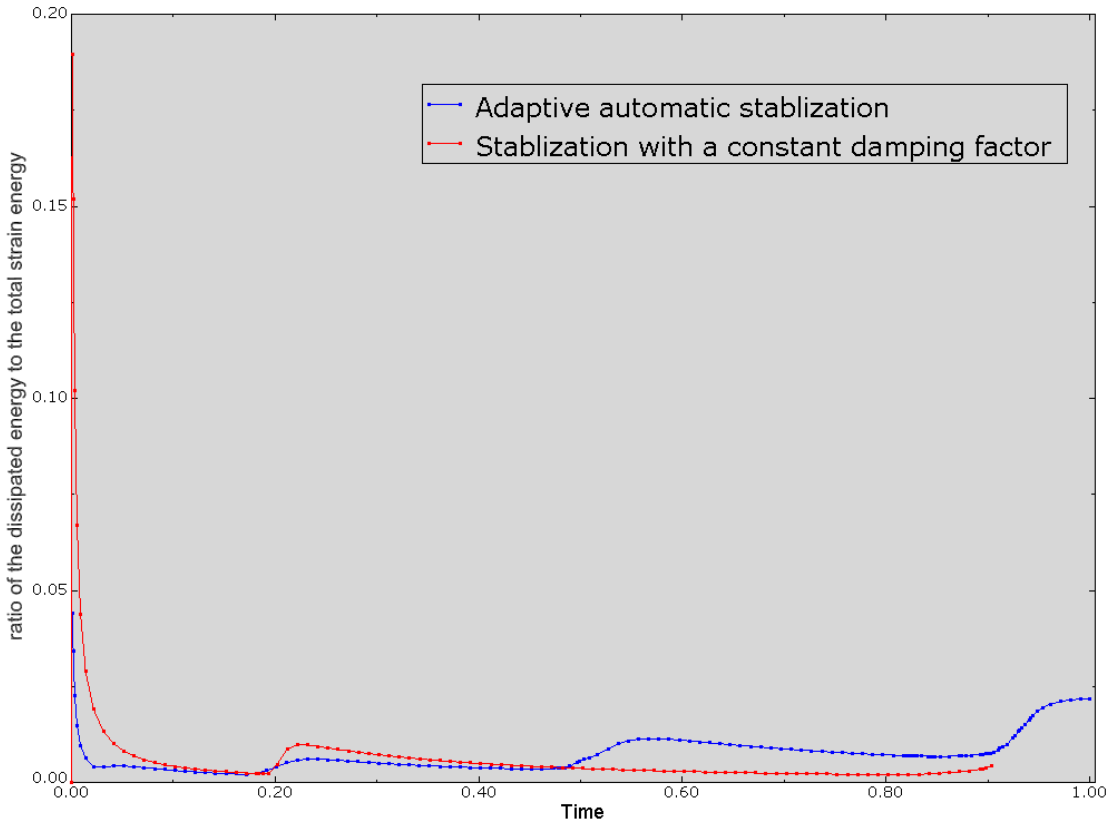

Figure 4-10 Ratio of dissipated energy to total strain energy using a constant damping factor and adaptive stabilization

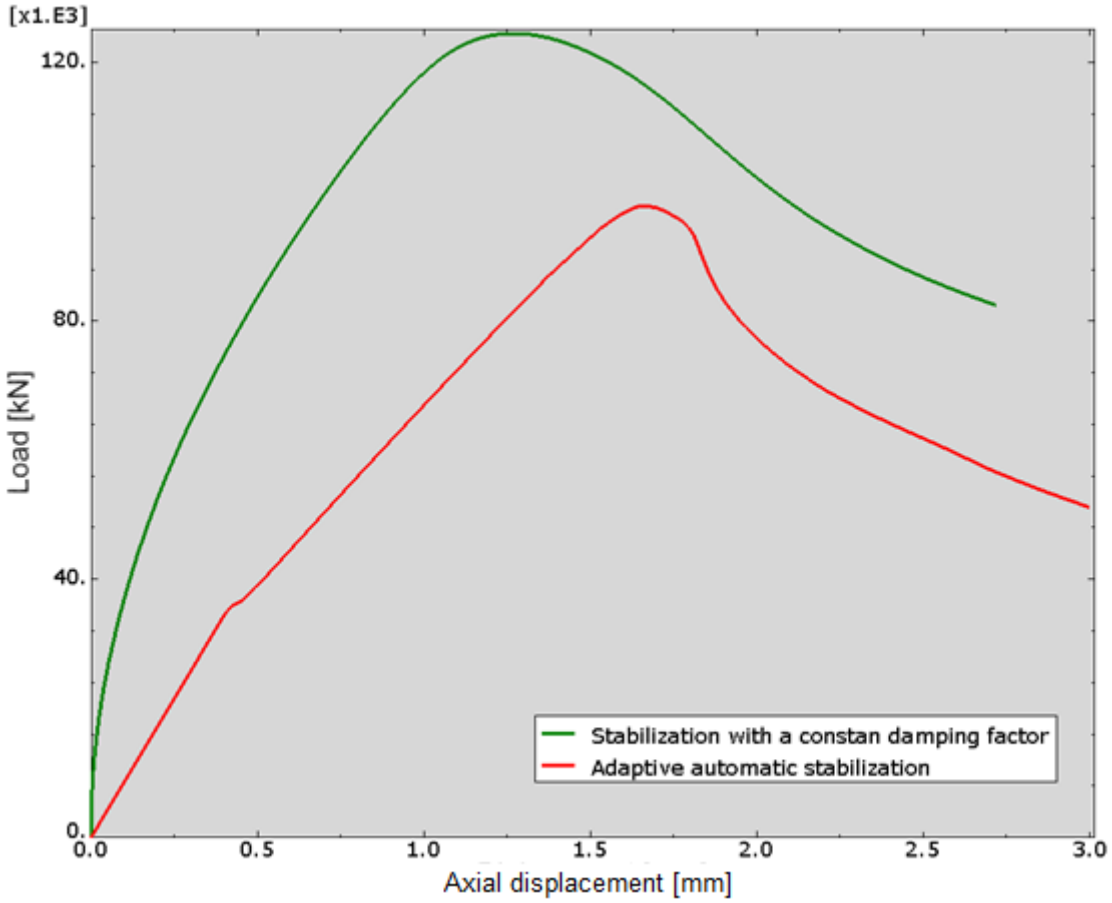

Figure 4-11 Predicted collapse load using a constant damping factor and adaptive stabilization

From Figure 4-11, there is an obviously significant divergence between the two different setting. One can easily make the decision that the Adaptive automatic stabilization is demanded to be included in the coming FE model.

4.6 Summary

In this chapter, some important parameters in the Finite Element analysis were described, and the influences of those inputs were discussed. Thus, the baseline model was established and verified.

As the objective is to establish the global buckling collapse load rather than capturing the exact post-collapse behaviour, a general static analysis was per-

formed. A displacement driven simulation with adaptive damping included was adopted. Thus, the buckling load and corresponding mode can be determined.

The panel model includes material and geometric nonlinear behaviour. The job of choosing a best model that is most suitable for the later simulation carried with the geometric imperfection has been completed.

5 Geometric imperfection

This chapter will discuss the geometric imperfection, as the FE model has been verified and is ready to simulate the more complex problems.

First, for all the real structures, there are permanent unavoidable imperfections coming from the manufacture process, no matter how carefully they are fabricated. The statement that unavoidable small imperfections in actual structures were to blame for the large discrepancies between theoretical and experimental results has initially been pointed out by Koiter [23], early in 1945.

In addition, in order to get the geometric imperfection, a geometry scanning was carried in Cranfield University before the panel buckling experiment. Thus, the real imperfection can be acquired from the measurement and introduced into the FE analysis.

And later the scanned imperfection will be calculated with a surface fitting via MALTLAB. The surface fitting toolbox was adopted to obtain a mathematical expression of the surface. Two approaches were tried, and the coefficients were acquired from the equation.

Then by changing the values, the fitted coefficients were used to derive new shapes of imperfection, which can be used in the later large amount of simulations and a series of collapse load will be predicted in chapter 6.

5.1 Introduce imperfections into FE model

It has been pointed out that no matter how careful manufacturing is, the initial imperfections exist in all structures.

In ABAQUS, imperfections are usually introduced by perturbations in the geometry. ABAQUS offers three ways to define an imperfection:

- As a linear superposition of buckling eigenmodes,
- From the displacements of a static analysis,
- By specifying the node number and imperfection values directly.

Ignoring the second option listed above, the remaining are the two common methods of introducing geometric imperfections into a Finite Element analysis. Most of the works deal with the modelling of imperfections either by finding a critical imperfection shape that arouses the largest reduction in the critical load for the structure, or from known displacement at discrete points on the structure.

Eigenvalue buckling analysis

For some cases, the real initial geometric imperfections are generally unknown. The most unfavourable shape of the imperfections was thereby taken into account with the amplitudes specified by manufacturing tolerances; such way of carrying can be seen in Pavlovčič et al [53] and Stull et al [36]. The guideline can refer to Eurocode, which allows modelling the geometric imperfection within the given tolerance, depending on the characteristic dimensions.

One has to decide which mode need to be defined, either global imperfections or local imperfections. Pavlovčič et al [53] studied the influence of different shape and amplitudes of initial imperfection on the panel from which the combined equivalent geometric imperfection can be determined. This method is very simple when doing the deterministic calculation and is set as default and recommended in ABAQUS. The imperfection pattern is obtained from a buckling mode shape of an eigenvalue buckling analysis. And then a scaling factor is added by some specifications of empirical equations. The first stage in the simulation is a linear eigenvalue buckling analysis. The second stage involves introducing the imperfection into the structure using the *IMPERFECTION option.

However, due to the most unfavourable imperfection model, the predictions can lead to the lowest collapse load. Although in the comparison carried by Tao et al [18] good agreement of calculated load-deformation curves is achieved in both assumed imperfections and realistic measured imperfections. However, most of the researchers have demonstrated that such an assumption is too conservative in predicting the buckling load, see [53][54].

Defining imperfection directly

Another suggested method of including geometric imperfections is explicitly changing the coordinates of each node in the FE model. The imperfections are interpolated as the displacements and so that the stiffness matrices can be derived directly.

This method is very convenient because most of the realistically measured imperfection data are obtained by taking measurements at discrete points. Also, with the explicit appearance of the imperfections, the probabilistic analyses can thus be carried out.

An external computer programme is demanded so that the measured data can be transformed into what can be read in FE code. The linkage from the real scanning to the FE analysis is essential.

The imperfection was then written into a table of node numbers and coordinate perturbations in the global coordinate system.

5.2 Measured imperfections

A scanning device that can pick up and record the imperfections was used here in this project. The scanning device used in this work is a Cyclone Series 2 scanning machine from Renishaw Corp.

This is a Contact scanning system with a 3-axis SP620 analogue scanning probe that has the repeatability of 5 μm and axial resolution of 1 μm. For most applications, the Renishaw contact sensors can acquire very high accuracy and quality of a surface. Figure 5-1 demonstrates the device in scanning.

Figure 5-1 scanning geometric imperfection

This Renishaw Cyclone is a very powerful tool for reverse engineering which enable one to capture 3D information about an object. This information enables us to reproduce anything we can physically scan. It can also produce an accurate 3D model. Capture and manipulation will be automatically done by the software and output to CAD. In this project, the machine outputs the data to CAD using IGES format.

The measure of the imperfection size used in this problem is the out-of-plane in the skin of the stringer stiffened panel. The shapes of the stringer were not planned to be scanned. This information is then computed as nodal displacement from their initial position in the global coordinate system.

The scanning was carried with the interval of 5mm both in x direction and y direction. This means every 5mm one point's coordinate value will be recorded.

The output is here is an IGES file including a set of point cloud (see Figure 5-2) which can be read and manipulated by CATIA.

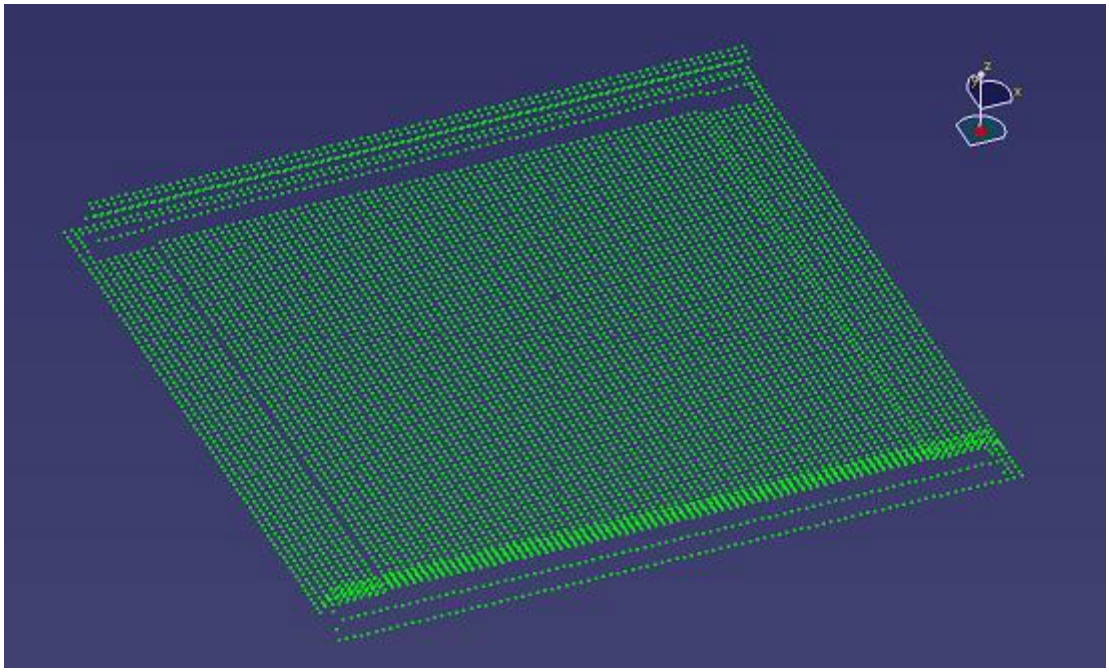

Figure 5-2 Point Cloud from the scanning of Panel 2

The scanning was carried along the transverse direction(X direction in Figure 5-2). One point should mention here is due to the Cerrobend casting, the panel was reduced by 16.5mm in each end, so the overall scanning length of this panel in axial direction (Y direction in Figure 5-2) was reduced from 430 to 397mm.

The coordinate matrix was recorded for each panel, see Appendix B.

5.3 Import real geometry into ABAQUS/CAE

DATA REDUCTION PROGRAMME

In total, five panels (named from panel2 to panel6 respectively) were scanned to get the geometric imperfections, from the machine mentioned above. From Figure 5-2, it can be seen that the point cloud is not well-organized and needs

to be processed. Therefore the data reduction programme based on MATLAB is introduced.

This data reduction programme is developed upon the powerful calculation capability of MATLAB. MATLAB (matrix laboratory) is a numerical computing environment developed by MathWorks. It is very robust in matrix manipulations, plotting of functions and data, implementation of algorithms, creation of user interfaces, and interfacing with programs written in other languages.

By scanning the real shape of the panel, with 5 mm intervals, the point cloud of each stiffened panel has been obtained. The first step is to remove those part of the point cloud where the area other than the panel was scanned, including the operating floor in both side of the panel, as well as the Cerrobend in both end, using the embedded Digitized Shape Editor in CATIA. These points are unprofitable for the research and should not be picked out. After that, CATIA can export the selected points as an ASCII file that consists of the matrix of coordinates of each point. The matrix can be transformed as an excel file, since MATLAB can read the data from an excel file.

5.3.1 Noise points removing

The scan was carried as the contact probe of the machine going along the surface of the panel. However, when the probe goes through the rivets, there will be a significant displacement out of the plane (see Figure 5-3). These points are the noise point, or so called outlier in MATLAB, and should be smoothed as the normal deformation as nearby.

Outliers are defined as data values that are dramatically different from patterns in the rest of the data. They may due to the measurement error, or they may represent significant features in the data. In this case, the outliers are because of the existence of rivet. One cannot include those significant values as common imperfection of the geometry shape, or it will lead to unexpected errors.

The deflection is shown in Figure 5-3, with the out-of-plane data matrix in each point, in the form of scanning lines along the transverse direction, in which the real scan was carried.

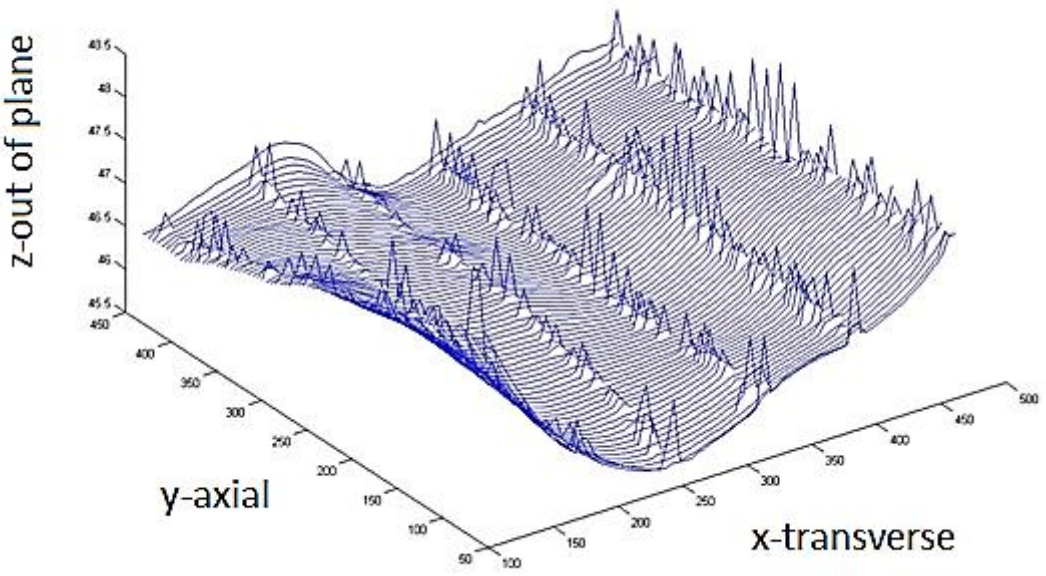

Figure 5-3 Scanning lines plot along the X direction- in Panel 2

The noise point process was performed by deleting outliers. First, one must build certain criteria so that the data matrix can be included if they meet the criteria.

As it is necessary to identify the noise points, based the criterion as follows:

$$\text{if } \mathrm{z(i,j)} > z(\mathrm{i}-1,\mathrm{j}) + 0.06, \mathrm{z(i,j)}, \text{ or} \tag{5-1}$$

$$\text{if } \mathrm{z(i,j)} > z(\mathrm{i}+1,\mathrm{j}) + 0.06, \mathrm{z(i,j)} \tag{5-2}$$

then delete the value at $\mathrm{z(i,j)}$, where $\mathrm{z(i,j)}$ is the out-of-plane value of each point. In other word, for any point when it is significantly higher than their neighbours (>0.06mm) it should be considered as an outlier and delete this value in the data matrix.

Alternatively, one can delete the outliers manually, as following codes in MATLAB.

$$\mathrm{z(i,j)} = \mathrm{NaN} \tag{5-3}$$

$$\mathrm{z(i,:)} = \mathrm{NaN} \tag{5-4}$$

$$\mathrm{z(:,j)} = \mathrm{NaN} \tag{5-5}$$

where the term ‘NaN’ means “not a number”. One can either use (5-3) to delete the value of certain individual point, or delete a certain row (column) of points

using (5-4) or (5-5) when they are obviously not in the reasonable range, especially for four edges of the panel. The points after outlier processing are meshed in Figure 5-4.

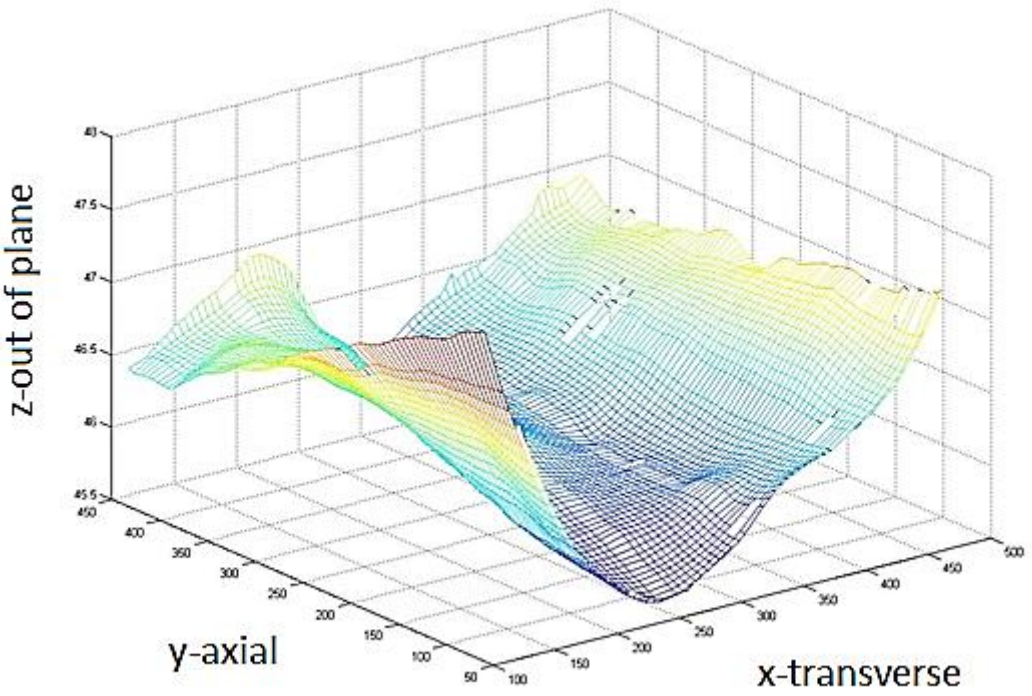

Figure 5-4 Points after outlier processing-in Panel2

5.3.2 Coordinate system transform

After deleting the noise points, the data is getting prepared. Then the following step is to convert these values to the coordinates of each node in FE model.

Before the data conversion, one should have noticed that there is a disparity between the two coordinate systems. By convenience, the data from scanning is recorded yielding to the default system of the scan machine, where the X-Y plane was set as the base panel plane. However, from the FE model, the built-up assembly panel is based on the X-Z plane. Hence, there is a demand to transform the coordinates system from measurement to that in FE model.

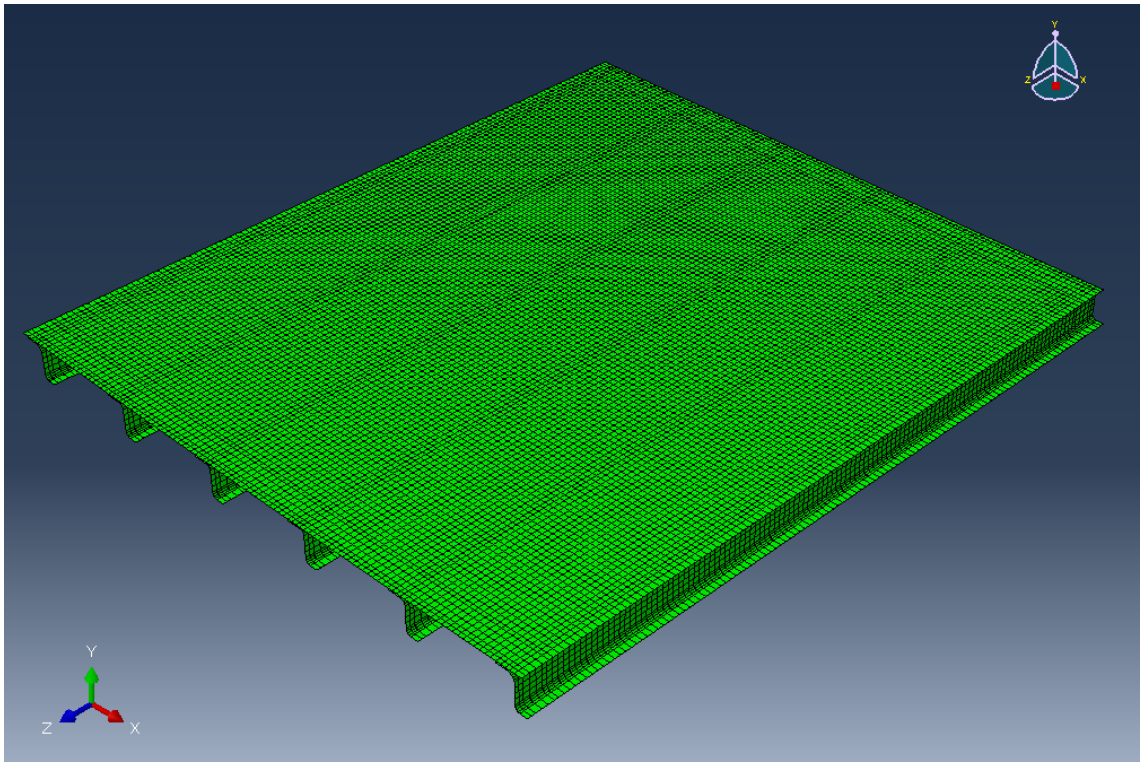

Figure 5-5 coordinates system in FE model

For the aim of distinction, the coordinates system from real scanning is defined as x-y-z; while the coordinates system in FE model is X-Z-Y. For transformation of the two systems, one can try the following equations:

$$X(i,j) = x(i,j) - a \tag{5-6}$$

$$Y(i,j) = z(i,j) \tag{5-7}$$

$$Z(i,j) = b - y(i,j) \tag{5-8}$$

The two variables ‘a’ and ‘b’ depend on different case; there are no constant values for all the panels, since in measurement the initial starting point is not exactly the same for every scan attempt.

The variables ‘a’ and ‘b’ dependent to different panels can refer to Appendix C, where all the codes in the form of MATLAB are recorded, as well as the way of reading coordinate from perfect FE model from excel files.

5.3.3 Interpolation and extrapolation

Due to the randomness in measurement stated above, the measured initial imperfections are not at positions that correspond exactly to the finite element mesh. As mentioned in section 5.2, the scanning was carried with the interval of 5mm both in x direction and y direction, which means every 5mm there would be one point's coordinate value recorded. However, as the mesh density defined that the normal size of the each element will be within 3.5-4mm. Therefore, the interpolation is demanded.

Meanwhile, because of the significant deviation in the edge area of the panel, which is determined as unreasonable and has been deleted in the noise points removal, extrapolation is also required. Another reason calling for the extrapolation is that the edges cast into Cerrobend are not measured directly, which need to be smoothed as well.

The interpolation and extrapolation can be performed simultaneously thanks to the 'Gridfit' function in MATLAB. The Gridfit is developed by John D'Errico and shared in the forum of MathWorks website 'file exchange' zone.

By default, for modelling a surface from 2D data from scattered data it has few options in MATLAB - mainly griddata. Griddata is a useful tool for interpolation. However, the 'griddata' function has some shortcuts, for example, it fails when there are replicates or when the data has many collinear points, and cannot extrapolate beyond the convex hull of the data satisfactorily.

Gridfit is developed to solve all of these problems. It builds a surface over a complete lattice, extrapolating smoothly into the corners. One can also control the amount of smoothing done, interpolation methods, as well as which solver to use, etc.

Basically, Gridfit is based on 'interp2' algorithm integrated in MATLAB. The goal of Gridfit is a smooth surface that approximates the original scattered data. Gridfit uses all methods to extrapolate to the grid boundaries, such as a modified ridge estimator to generate the surface, where the bias is toward smooth-

ness. By default, the smoothing parameter is 1, a value which will yield relatively little smoothing.

Using Gridfit, the following code (equation) is adopted:

$$\mathrm{Z} = \mathrm{gridfit}(\mathrm{x}, \mathrm{y}, \mathrm{z}, \mathrm{X}, \mathrm{Y}) \tag{5-9}$$

Where x, y, z are the vectors of scattered data (real measurement data after reduction in this case). 'X', 'Y' are the vector defining the nodes in the grid in the independent variables. The independent variables do not have to be equally spaced, but they should completely cover all the data of the grid, meaning the min and max of the data included. 'Z' is the smooth surface nodal value generated, corresponding to each value of 'X' and 'Y'.

So far, the Z value of each point on the imperfect surface has been obtained. However, what is the so-called geometric imperfection? What is required to export to the perfect FE model?

The answer was given in ABAQUS, since this commercial code was adopted in this work. ABAQUS requires the imperfection as a table of node numbers and coordinate perturbations, if the directly specified option is determined. Coordinate perturbations is defined as the d-value of each node between the imperfect surface and the perfect surface. So the question is:

What is considered as the perfect surface?

The perfect surface is done by finding the best-fit plane to the measured data of the initial scan surface. Based on the method of least squares, by computing the sum of the squares of the normal distance in space to the surface of the assumed best-fit plane, one can get the unknown coefficients by minimizing the sum. This method is related a lot of mathematical calculation. Another convenient approach is using the surface fitting toolbox. In MATLAB, one should only enter the X-input, Y-input and Z-input respectively, and then select the polynomial fitting with the degree of 1,1. The linear equation is shown as following:

$$\mathrm{f}(\mathrm{x}, \mathrm{y}) = \mathrm{a} + \mathrm{b} * \mathrm{x} + \mathrm{c} * \mathrm{y} \tag{5-10}$$

One can obtain the coefficients a, b, c of the best fit plane from surface fitting toolbox very easily and conveniently. With the obtained coefficients, one can also recalculate each nodal value in the best fit plane:

$$\mathrm{Yfit}(i,j) = a + b * X(i,j) + c * Z(i;j) \quad (5\text{-}11)$$

$$\Delta Y = \mathrm{Ygrid} - \mathrm{Yfit} \quad (5\text{-}12)$$

ΔY is the D-value from the curve and best-fit plane. It is this value defined as the imperfection in the form of a sheet of nodal data, importing to the perfect FE model. Figure 5-6 and Figure 5-7 demonstrate the normalized deformation of panel2 and panel4, in the form of X-Z- ΔY.

ΔY is exported using the 'dlmwrite' function in MATLAB.

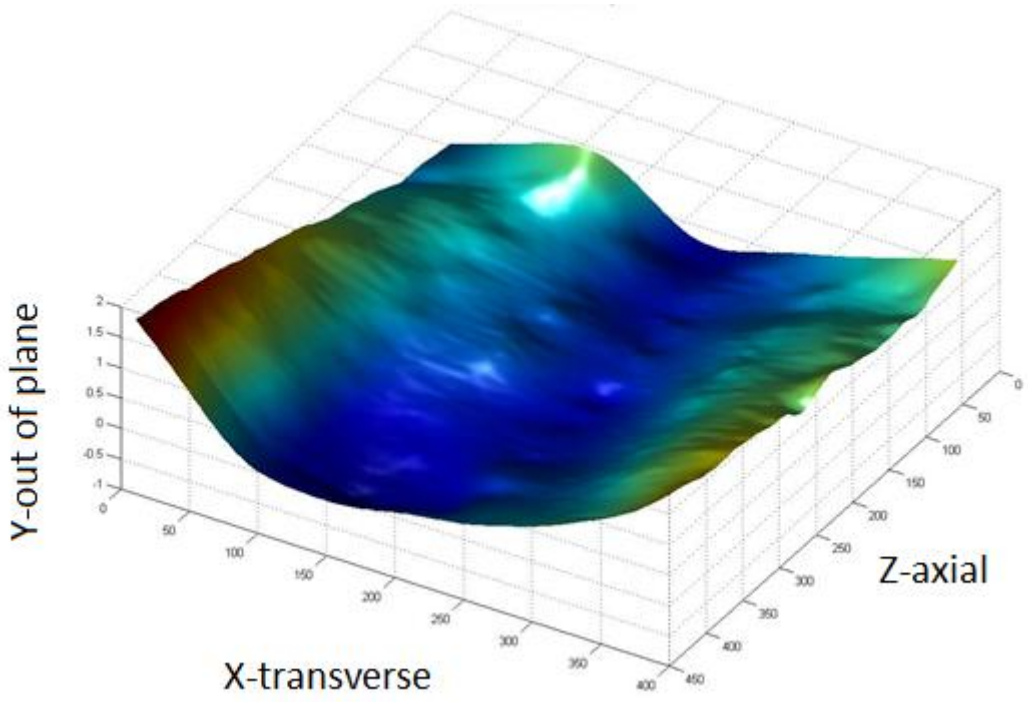

Figure 5-6 Normalized deformation-Panel2

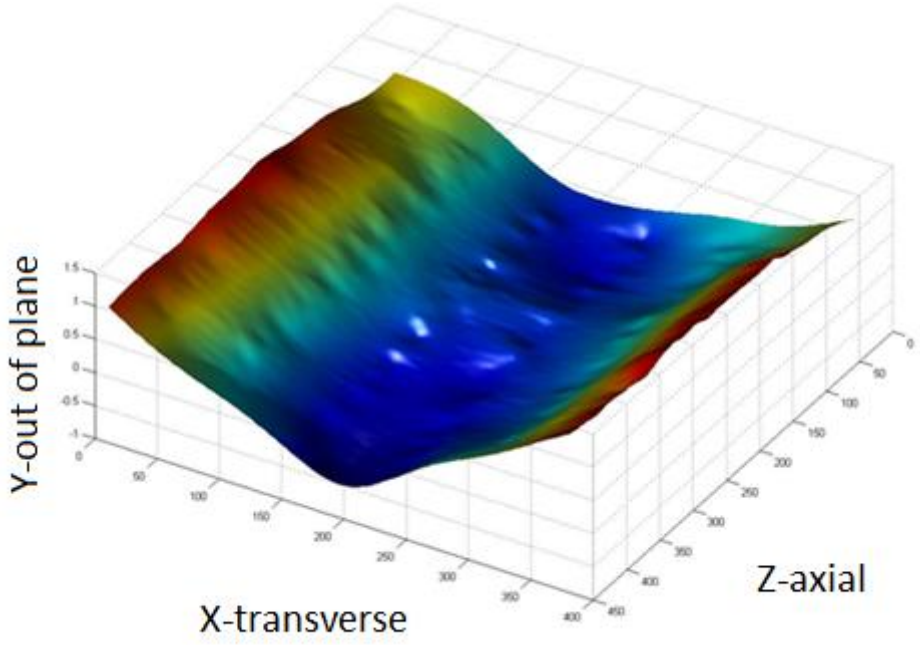

Figure 5-7 Normalized deformation-Panel4

5.3.4 Map the imperfections onto the mesh

ABAQUS import the imperfection file by means of the *IMPERFECTION keyword. Directly specifying the imperfection requires imperfection data from a separate input file in the form of a table, including node numbers and coordinate perturbations in the global coordinate system.

The output from MATLAB calculation is an '.inp' file. ABAQUS reads this file and modified the original nodal value as the new value, forming the new imperfect shape.

Overall, the goal of this Data Reduction Programme is to deal with the recorded data, and get prepared to read into FE model. Finding out the Best-fit plane based on the least squares fit, recalculating the measured data to be the actual deviation from best-fit plane, consistent with the perfect model. The imperfections were, finally, mapped onto the mesh. The whole process was based on the beneficial use of the MATLAB code. The whole programme codes refer to Appendix C.

5.4 Geometric imperfections prediction

As mentioned above, five actual geometry scans have been carried. However, one should always be aware of that due to the nature of the manufacturing process, the real shape of the geometric imperfection varies from one panel to another; they can never be exactly the same with the measured one.

The next coming problem that we have to face is: it is the different geometries that we are trying to simulate primarily because of the manufacturing tolerances. In other word, the primary sources of imperfections. From the view of statistics, the more samples the better distributions can be generalized. However, due to the reason of cost, it is impossible to measure too many real panels as expected. However, there are five real geometries of the stiffened panel obtained from the scanning. The coming question is:

Can one generalise a regular pattern from the five exist samples?

The answer is definitely yes and will be demonstrated as following sections.

5.4.1 Surface fitting

As the real measurement is scattered and arbitrary, maybe the only way to generalize is finding out a best fit surface that can be represented by a set of functions to these scattered x-y-z data points.

However, search for a good fit may be more of an art than a science. It is obvious that if a large set of basic functions are adopted one can get a surface passing closely through each point of the scatters, while it brings great complexities. This is a constant contradiction. The goal of getting an elementary function which is smooth and easily expressed, yet hits each data point exactly, may be unattainable.

Using few basic functions may yield a smoother, simpler surface which only approximates the original data. One should be aware of always choosing the basis according to the kinds of functions which are appropriate for the existing data,

whether trigonometric (if periodic), polynomial, rational, exponential, logarithmic, etc.

In the following two sections, two ways of surface best fit using either polynomial or double Fourier series will be stated. Both of them are accomplished by using a least square method to pick up calibration data.

5.4.1.1 Least Squares Method

Before the two surface fittings are demonstrated, a least squares method should be introduced first.

The method of least squares assumes that the best-fit curve of a given type is the curve that has the minimal sum of the deviations squared (*least square error*) from a given set of data.

Suppose that the data points are$(x_1, y_1), (x_2, y_2), \dots, (x_n, y_n)$, where x is the independent variable and y is the dependent variable. The fitting curve $f(x)$ has the deviation (error) d from each data point, i.e. $d_1 = y_1 - f(x_1), d_2 = y_2 - f(x_2), \dots, d_n = y_n - f(x_n)$. According to the method of least squares, the best fitting curve has the property that:

$$\mathrm{S} = {d_1}^2 + {d_2}^2 + \cdots + {d_n}^2 = \sum_{i=1}^{n} {d_i}^2 = \sum_{i=1}^{n} [y_i - f(x_i)]^2 = min. \quad \textbf{(5-13)}$$

Multiple Regressions

Multiple regressions estimate the dependent variables that are affected by more than one independent variables. For example, the two independent variables x and y and the dependent variable z are in the linear relationship case:

$$\mathrm{z} = a + bx + cy \quad \textbf{(5-14)}$$

For a given data set $(x_1, y_1, z_1), (x_2, y_2, z_2), \dots, (x_n, y_n, z_n)$, where $n \geq 3$, the best fitting curve $f(x)$ has the least square error, i.e.,

$$S = \sum_{i=1}^{n} {d_i}^2 = \sum_{i=1}^{n} [z_i - f(x_i, y_i)]^2 = \sum_{i=1}^{n} [z_i - (a + bx_i + cy_i)]^2 = min. \quad \textbf{(5-15)}$$

Please note that a, b and c are unknown coefficients while all x_i, y_i and z_i are given. To obtain the least square error, the unknown coefficients a, b and c must yield zero first derivatives.

$$\begin{cases} \dfrac{\partial S}{\partial a} = 2\sum_{i=1}^{n} [z_i - (a + bx_i + cy_i)] = 0; \\ \dfrac{\partial S}{\partial b} = 2\sum_{i=1}^{n} [z_i - (a + bx_i + cy_i)] = 0; \\ \dfrac{\partial S}{\partial c} = 2\sum_{i=1}^{n} [z_i - (a + bx_i + cy_i)] = 0. \end{cases} \quad \textbf{(5-16)}$$

The unknown coefficients a, b and c can hence be obtained by expanding the above equations with the above linear equations being solved.

The solving process for the least squares problem could be accomplished with the software MATLAB.

5.4.1.2 Polynomial fitting

The first approach which has been tried to search for the best fit surface is using polynomials. Polynomials are one of the most commonly used types of curves in regression.

$$f(x, y) = \sum_{i=0}^{m} \sum_{j=0}^{n} p_{ij} x^i y^j$$

In this work, the polynomial with 3th degree in x and 2rd degree in y was used to produce a surface fitting for both panel2 and panel3. The so-named linear model ***'Poly32'*** has the following equation:

$$f(x,y) = p_{00} + p_{10}x + p_{01}y + p_{20}x^2 + p_{11}xy + p_{02}y^2 + p_{30}x^3 + p_{21}x^2y + p_{12}xy^2 \quad \textbf{(5-17)}$$

The poly32 fitting can be easily performed in Surface Fitting Tool in MATLAB. One just needs to clicking the degrees of x and y as 3 and 2 in addition to selecting the three variables. After that, the tool will automatically calculate and validation statistics will be displayed in the result. Looking into the results of surface fitting, the values of the coefficients and the goodness-of-fit statistics are showing in Table 5-1.

Table 5-1 Results of Polynomial fitting of panel2 and panel3

Coefficients	Panel2	Panel3
$\mathbf{p_{00}}$	0.161	0.8531
$\mathbf{p_{10}}$	-0.003706	-0.01136
$\mathbf{p_{01}}$	0.003287	0.002151
$\mathbf{p_{20}}$	1.388e-005	6.341e-006
$\mathbf{p_{11}}$	-4.265e-005	-1.651e-005
$\mathbf{p_{02}}$	-2.286e-006	-4.45e-006
$\mathbf{p_{30}}$	-1.003e-008	6.976e-008
$\mathbf{p_{21}}$	1.064e-007	4.035e-008
$\mathbf{p_{12}}$	8.926e-009	1.216e-008
Goodness of fit:		
SSE:	192.6	165.3
R-square:	0.8887	0.9648

Herein, some validation statistics terms needs to be explained.

SSE is the Sum of Squares due to Error of the fit. This statistic measures the total deviation of the response values from the fit to the response values. It is also called the summed square of residuals which was mentioned in previous subsection to be minimized in the least square method.

R-square is the square of the correlation between the response values and the predicted response values. For simplified statement, a value closer to 1 indicates that a greater proportion of variance is accounted for by the model; a better surface fitting is obtained, in other word.

For example, the R-square value of panel2 is 0.8887means that the fit explains 88.87% of the total variation in the data about the average. In contrast, panel3 fits the R-square value of 0.9648, better than panel2. It seems that the polynomial is not a good fit for panel2. In fact, there is no guarantee that a polynomial is a good option for a surface fitting. One should always have tried other different expression such as trigonometric or exponentials instead, or in addition to, polynomials.

From Table 5-1, one can easily find that by comparing all the 9 coefficients, only $\mathbf{p_{00}}$ is significant. However, this does not mean that the character can be picked up only by $f(x,y) = p_{00}$, because the term such as x^2y and x^3 can be farley significant even the correlated coefficients are very small. This particular property will be compared with the double Fourier series expression, stated in the following subsection.

Figure 5-8 and Figure 5-9 give the result of fitting using poly32 respectively.

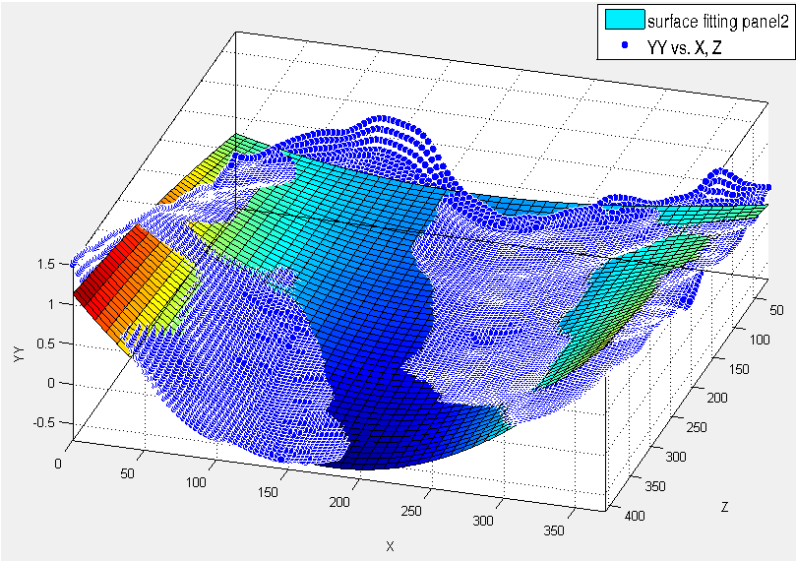

Figure 5-8 Surface fitting of panel2 using polynomials

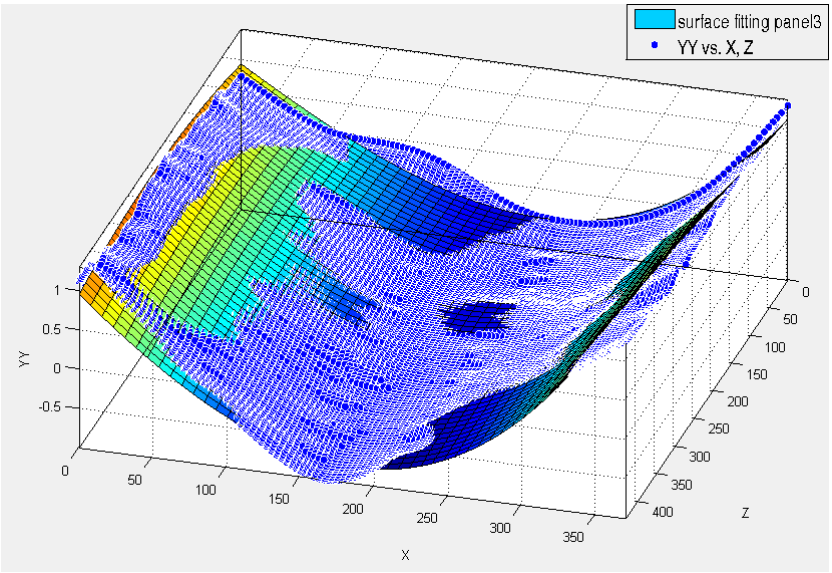

Figure 5-9 Surface fitting of panel3 using polynomials

5.4.1.3 Double Fourier series fitting

Another approach is using trigonometric polynomials.

One widely accepted representation of the measured initial imperfection data were Double Fourier series, introduced by Singer et al [24] and Teng et al [5].

The recommended double Fourier series have the following two forms:

$$w(x,y) = \sum_{k=0}^{n_1} \sum_{l=0}^{n_2} cos\frac{k\pi y}{L}\left(A_{kl}\cos\frac{l\pi x}{B} + B_{kl}\sin\frac{l\pi x}{B}\right) \tag{5-18}$$

named as half-wave cosine representation, and

$$w(x,y) = \sum_{k=1}^{n_1} \sum_{l=0}^{n_2} sin\frac{k\pi y}{L}\left(C_{kl}\cos\frac{l\pi x}{B} + D_{kl}\sin\frac{l\pi x}{B}\right) \tag{5-19}$$

referred to as the half-wave sine representation.

Where:

L, B--the length (in axial, y direction) and breadth (in transvers, x direction) of the panel, respectively;

x, y--axial coordinates, transverse coordinates;

k, l- -the number of axial half waves and transverse half waves;

$A_{kl}, B_{kl}, C_{kl}, D_{kl}$--coefficients of Fourier series.

The upper bound of k and l is $n_1$and n_2 respectively. To fit a surface perfectly, $n_1$and n_2 need to tend to infinite. However, due to the limit of calculation ability of computers, it is usually impossible to set too large upper bound in reality. In fact, good approximation can be reached with a rather low number depending on the level of accuracy required. A small number of hale waves can represent the scatter real geometry shape, which will be proved to be adequate as well.

By reducing $n_1$and n_2 to small numbers, the Double Fourier series can be decomposed to the expression to:

For half-wave cosine representation:

For $n_1 = 1, n_2 = 2$ (5-20)

$$w(x,y) = A00 + A10cos(1\pi y/\mathrm{L}) + A01cos(1\pi x/B) + B01sin(1\pi x/B) + A02cos(2\pi x/B) + B02sin(2\pi x/B) + A11cos(1\pi y/L)cos(1\pi x/B) + B11cos(1\pi y/L)sin(1\pi x/B) + A12cos(1\pi y/L)cos(2\pi x/B) + B12cos(1\pi y/L)sin(2\pi x/B).$$

For half-wave sine representation:

For $n_1 = 1, n_2 = 2$ (5-21)

$$w(x,y) = C10sin(1\pi y/L) + C11\sin(1\pi y/L)cos(1\pi x/B) + D11sin(1\pi y/L)sin(1\pi x/B) + C12sin(1\pi y/L)cos(2\pi x/B) + D12sin(1\pi y/L)sin(2\pi x/B).$$

or on the same analogy of this.

At first, half-wave sine and half-wave cosine representation were compared in the fitting of panel2, in order to determine which is more appropriate to represent the characteristic imperfection distribution.

As given in Table 5-2and Table 5-3, 7 types of double Fourier series equation and 13 different expressions were attempted for half-wave sine and half-wave cosine fitting, respectively. In the table, R-square and RMSE give the direct in-

formation of how successful the fit. Here the terms of R-square can refer in section 5.4.1.2, and RMSE is the abbreviation of Root mean squared error. RMSE is an estimate of the standard deviation of the random component in the data, and is defined as:

$$RMSE = \sqrt{MSE} = \sqrt{\frac{SSE}{n}}$$

where *n* is the number of observations, MSE is the mean square error, and for details of SSE one can see section 5.4.1.2. Just as with SSE, an RMSE value closer to 0 indicates a fit that is more useful for prediction.

With 18 coefficients, the best fit of half-wave sine fitting of Panel2 is when $n_1 = 2, n_2 = 4$, the R-square is 0.7326, meaning 73.26% of the total variation in the data is explained about the average. In contrast, the second row shows that the half-wave cosine fitting can get more accurate fits at the R-square of 0.9633, with only the requirement of 10 coefficients, see Table 5-3.

Table 5-2 half-wave sine fitting of Panel2

Fit name	SSE	R-square	RMSE	Coefficients
k=1,l=0:1	822.4533	0.5883	0.2424	3
k=1,l=0:2	822.2386	0.5884	0.2424	5
k=1,l=0:3	811.5982	0.5937	0.2408	7
k=1:2,l=0:1	658.1718	0.6705	0.2169	6
k=1:2,l=0:2	551.3473	0.7240	0.1985	10
k=1:2,l=0:3	536.2906	0.7315	0.1958	14
k=1:2,l=0:4	534.0346	0.7326	0.1954	18

Table 5-3 half-wave cosine fitting of Panel2

Fit name	SSE	R-square	RMSE	Coefficients
k=0:1,l=0:1)	264.7957	0.8674	0.1376	6
k=0:1,l=0:2)	73.2131	0.9633	0.0723	10
k=0:1,l=0:3)	61.4555	0.9692	0.0663	14
k=0:1,l=0:4)	59.5855	0.9702	0.0653	18
k=0:2,l=0:1)	261.1271	0.8693	0.1366	9
k=0:2,l=0:10)	114.5584	0.9426	0.0907	63
k=0:2,l=0:2)	68.9249	0.9655	0.0702	15

k=0:2,l=0:3)	46.0236	0.9770	0.0574	21
k=0:2,l=0:4)	41.4700	0.9792	0.0545	27
k=0:2,l=0:8)	39.7512	0.9801	0.0534	51
k=0:2,l=0:9)	51.4768	0.9742	0.0608	57
k=0:3,l=0:4)	33.5718	0.9832	0.0490	36
k=0:4,l=0:4)	25.3125	0.9873	0.0426	40

The same information can be obtained also from the comparison between Figure 5-10 and Figure 5-11. Thus, the conclusion is obviously that the half-wave cosine can represent more characters based on the fitting of panel2. This has also been proved on both panel3 and panel4, demonstrated in Table 5-4 and Table 5-5.

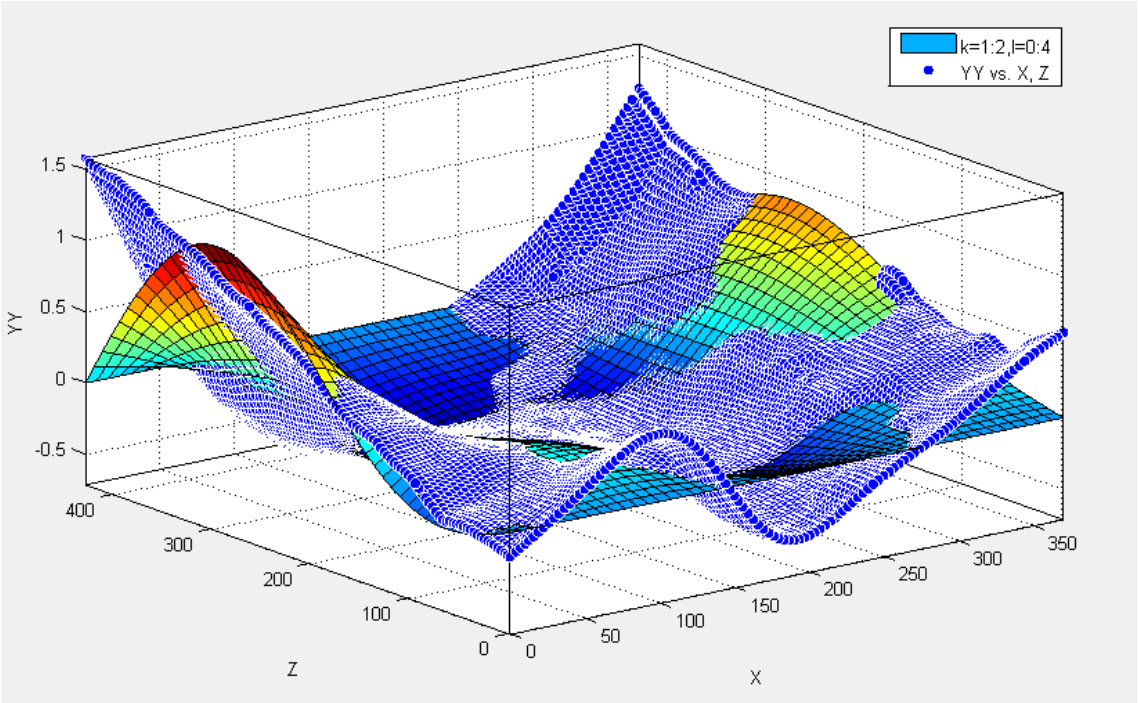

Figure 5-10 half-wave sine fitting of Panel2

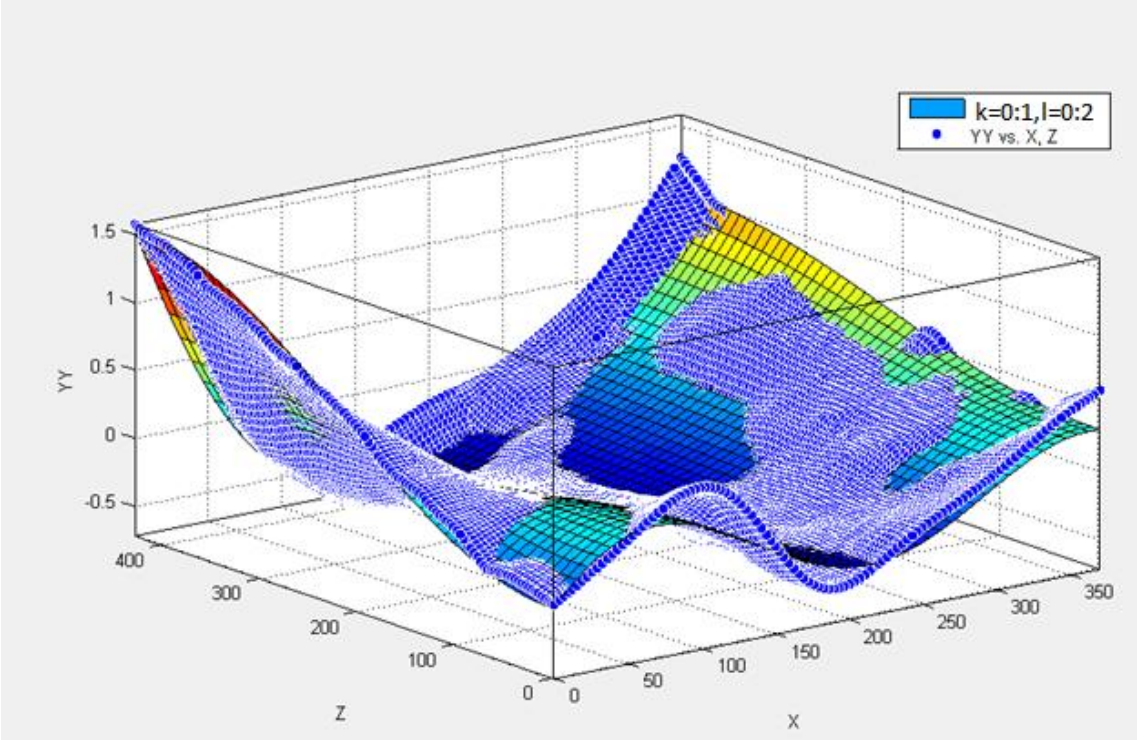

Figure 5-11 half-wave cosine fitting of Panel2

Table 5-4 half-wave cosine fitting of Panel3

Fit name	SSE	R-square	RMSE	Coefficients
k=0:1,l=0:1)	211.6346	0.9549	0.1230	6
k=0:1,l=0:2)	69.8378	0.9851	0.0707	10
k=0:1,l=0:3)	64.3524	0.9863	0.0678	14
k=0:2,l=0:1)	186.4649	0.9602	0.1154	9
k=0:2,l=0:2)	43.9058	0.9906	0.0560	15
k=0:2,l=0:3)	31.6813	0.9932	0.0476	21
k=0:2,l=0:4)	30.6389	0.9935	0.0468	27

Table 5-5 half-wave cosine fitting of Panel4

Fit name	SSE	R-square	RMSE	Coefficients
k=0:1,l=0:1	89.4542	0.9697	0.0800	6
k=0:1,l=0:2	75.7931	0.9743	0.0736	10
k=0:1,l=0:3	67.8816	0.9770	0.0697	14
k=0:2,l=0:1	69.9942	0.9763	0.0707	9
k=0:2,l=0:2	46.1929	0.9844	0.0575	15
k=0:2,l=0:3	32.0658	0.9891	0.0479	21

k=0:2,l=0:4	30.7574	0.9896	0.0469	27

Now, three tables of Table 5-3, Table 5-4 and Table 5-5 all indicate that with just 10 coefficients, one can generalise the characteristic of geometry imperfection with a reasonable accuracy. In other words, the more coefficients can definitely acquire much better fitting, but is not necessary.

Thus, the type of half-wave cosine fitting is determined as when $n_1 = 1, n_2 = 2$, which is written as the following equation:

$$w(x,y) = \sum_{k=0}^{1} \sum_{l=0}^{2} cos\frac{k\pi y}{L}\left(A_{kl}\cos\frac{l\pi x}{B} + B_{kl}\sin\frac{l\pi x}{B}\right) \tag{5-22}$$

The decomposed expression can refer to equation (5-20). This type of representation is adopted as the basic surface fitting, based on which the new imperfections will be derived.

Table 5-6 summarizes the result of surface fitting using the equation (5-22). One can see with the same expression, each panel can get the best-fit surface, with the similar Goodness. Panel3 has the best fitting goodness, with 73.26% of the total variation in the data is explained about the average; panel5 has the relatively worst fitting, but the value of 0.9592 in R-square means at least 95% of the total variation in the data is explained, which is still reasonable.

Figure 5-12, Figure 5-13, Figure 5-14 and Figure 5-15 illustrate the fitting from panel3 to panel6 respectively, using the recommend expression.

Table 5-6 Goodness of Surface fitting

panel	SSE	R-square	RMSE	Coefficients
panel2	73.2131	0.9633	0.0723	10
panel3	69.8378	0.9851	0.0707	10
panel4	75.7931	0.9743	0.0736	10
panel5	76.5162	0.9592	0.0740	10
Panel6	78.6781	0.9775	0.0750	10

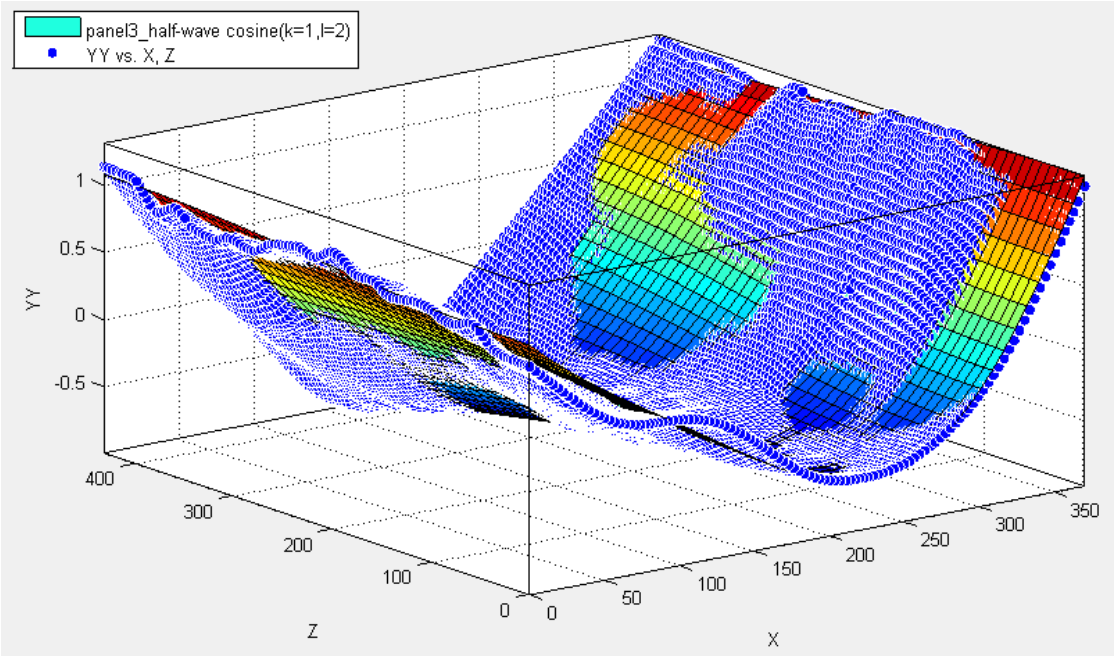

Figure 5-12 half-wave cosine fitting of Panel3

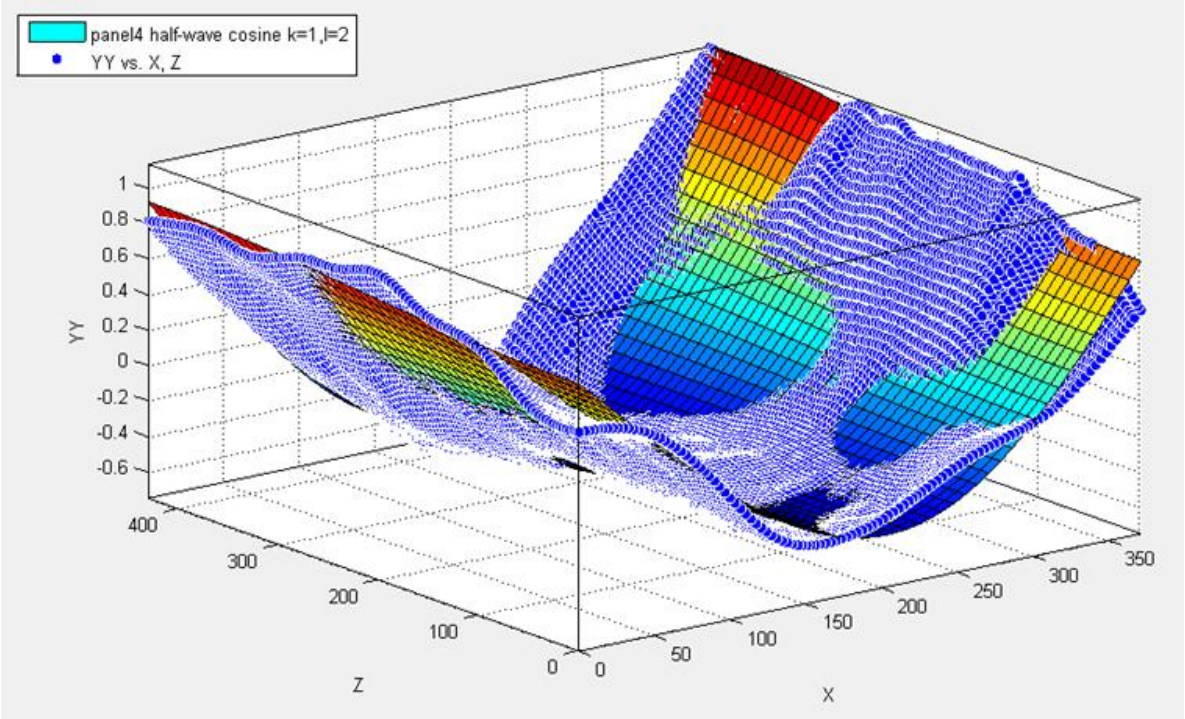

Figure 5-13 half-wave cosine fitting of Panel4

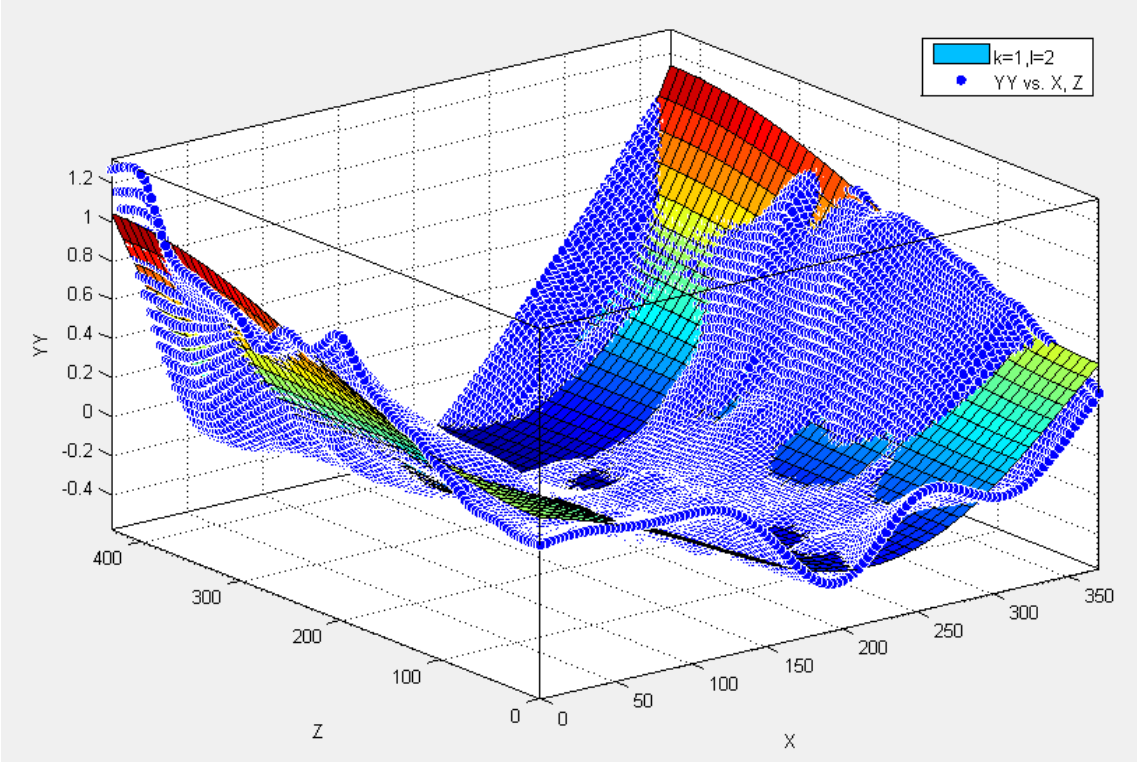

Figure 5-14 half-wave cosine fitting of Panel5

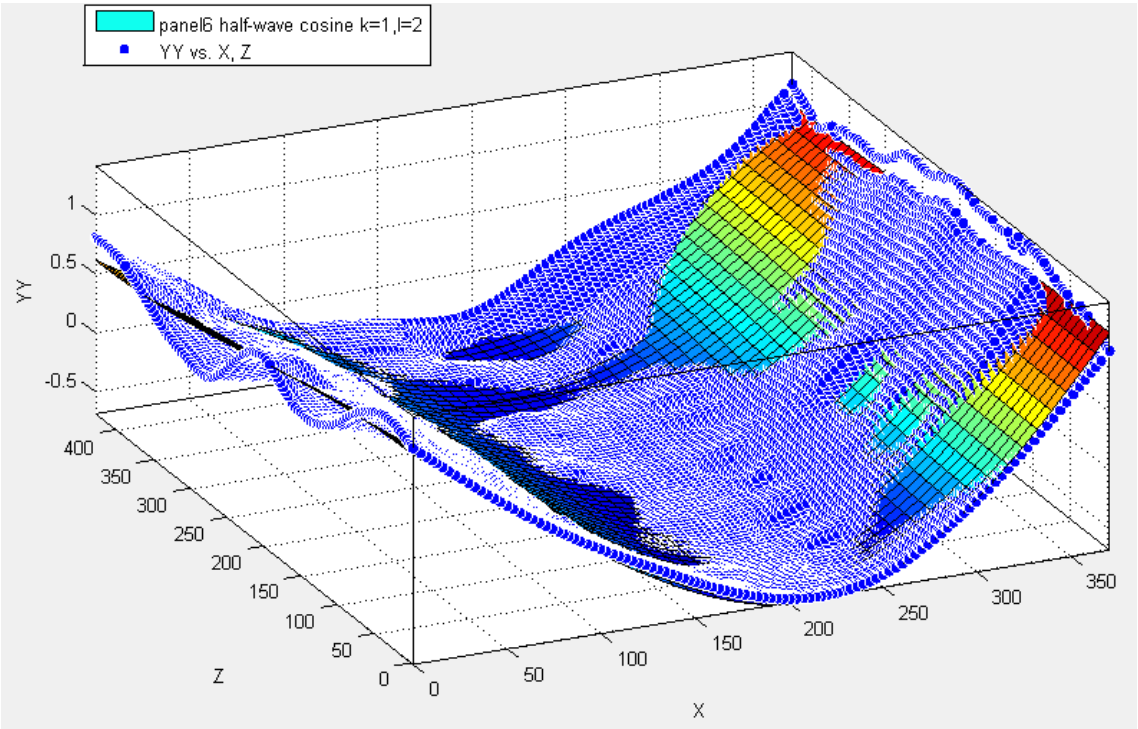

Figure 5-15 half-wave cosine fitting of Panel6

5.4.2 New imperfection derivation

This subsection discusses the parameterization of the geometry of the panels, for the aim of finite element modelling.

For one attempts to get the characteristic imperfection distributions associated with the different manufacturing processes, it is necessary to get a standard representation for the measured imperfections. It is assumed that all the panels are manufactured from the same process. Based on this assumption, finding the regular pattern of the imperfection in the test panel can only be meaningful.

The trigonometric equation of double Fourier series (5-22) was finally chosen to fit the surface. Indeed, it converges much faster than the polynomial and more efficient to simulate the symmetrical property of the surface.

With the recommended double Fourier series (DFS) expression given in (5-22), all the 10 coefficients of three panels were obtained, showing in Table 5-7.

Table 5-7 Coefficients of DFS fitting of three panels

coeff	panel2	panel3	panel4	mean	max	min	max-min
B_{01}	-1.015	-1.61	-1.383	-1.3360	-1.015	-1.61	0.5950
A_{00}	0.6525	1.014	0.8737	0.8467	1.014	0.6525	0.3615
B_{11}	1.86	-0.4612	0.1845	0.5278	1.86	-0.4612	2.3212
A_{10}	-1.191	0.2949	-0.1127	-0.3363	0.2949	-1.191	1.4859
B_{12}	0.3515	0.2366	0.02205	0.2034	0.3515	0.02205	0.3295
A_{11}	-0.2564	-0.08567	0.0477	-0.0981	0.0477	-0.2564	0.3041
A_{12}	0.5809	-0.3154	-0.01696	0.0828	0.5809	-0.3154	0.8963
B_{02}	-0.01308	0.1761	0.07956	0.0809	0.1761	-0.01308	0.1892
A_{01}	0.002309	-0.1376	-0.06298	0.0661	0.002309	-0.1376	0.1399
A_{02}	0.0137	0.08285	0.02309	0.0399	0.08285	0.0137	0.0692

In Table 5-7, those significant coefficients are marked in red. For panel2, there are at least five that are much bigger than the others, which are B_{01}, A_{00}, B_{11},

A_{10} and A_{12}. While for the other two panels, only two out of them are distinct; they are B_{01} and A_{00}.

Also, Figure 5-16 gives the combination of three panels fit with DFS. The regular pattern is that in all three panels, there is a dominant sine curvature in transverse (x) direction, while in axial (z) direction no obvious curve is significant. However, due to an unexpected external impact probably, there is a torsion in the axial (z) direction in panel2, while the rest two display normal. This torsion can be expressed by the coefficient A_{10} B_{11} and $A_{12,}$ which are significantly bigger than the others. The coefficient A_{00} form the offset from the original plane, $y=0$ in this coordinate system. The other large coefficient B_{01} corresponding to the term of $sin(\frac{1\pi x}{B})$, meaning the magnitude of the half sine wave in x direction.

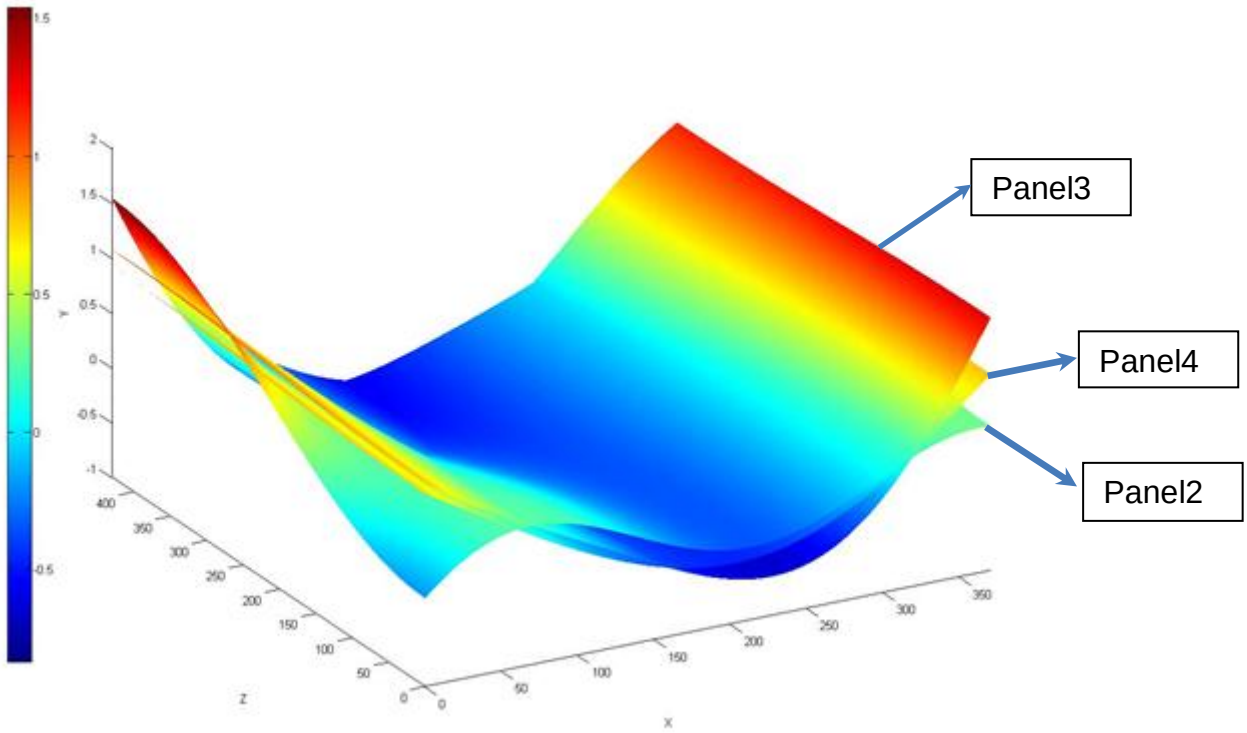

Figure 5-16 DFS fitting of three panels

From the side of mean value of these three panels, one may generalize the law in hiding. The top five coefficients are marked in red, however, in which the value of A_{12} is not included. But, the deviation of difference between maximum and

minimum indicates the scatter of this coefficient is quite big, which cannot be ignored.

A consensus that has been widely accepted is that in the DFS expression all the coefficients are assumed as independent with each other. With this basis, the generalization seems easier. By neglecting the minor coefficients both in itself magnitude and in the value of mean and deviation, B_{01}, A_{00}, B_{11}, A_{10}, B_{12}, A_{11} and A_{12} are picked out to present the main shape.

Each coefficient may have its own range of scatters. To model the imperfections in a realistic manner, one can treat the imperfections as random, scattered from the max to min. Specifically in this case, all the coefficients are treated as random in their ranges. One can pick up any out of its range randomly, while, the neglected coefficients B_{02}, A_{01} and A_{02} are assigned as in the mean value. These selected coefficients are then combined to form the new shape. For example, if one choose 5 different numbers out of the range, with 7 coefficients there are $5^7 = 78125$ different combinations.

Furthermore, the coefficients of panel5 and panel6 can be taken to examine the predicted ranges. From Table 5-8, one can see that the major coefficients generalized by DFS fitting are almost within the scatter ranges, which proves that the predicted range is correct and rational.

Table 5-8 Coefficients of Panel5 and the predicted ranges

coefficient	B01	A00	B11	A10	B12	A11	A12
max	-1.015	1.014	1.86	0.2949	0.3515	0.0477	0.5809
min	-1.61	0.6525	-0.4612	-1.191	0.02205	-0.2564	-0.3154
panel5	-1.4	0.8818	0.8484	-0.5358	0.08889	-0.007691	0.1971
panel6	-1.507	0.9472	-0.2894	0.1854	0.09054	0.07196	-0.02209

However, these combinations of coefficient cannot be uncontrolled and a limitation should be applied to restrict the shape variation. The claim is also supported by the algorithm of structure design. When a structure is designed, an allowed tolerance should be specified by a design code, in order to keep the

structure within a controllable variation. Usually, a maximum allowable limit on the imperfection on the structure is dictated by the manufacturing process.

However, due to little information is available from manufacture, the design code of British Standard is referred. Here in this work, the BS EN 485-4 gives some useful tolerances on shape for cold-rolled Aluminium and aluminium alloys.

For a sheet with the length (L) of 430mm, width (B) of 370mm and thickness of 091mm, the total deviation from flatness tolerance is the minor value from the two following specifications:

$$d_{max} = 0.5\% \times B = 1.85mm$$

$$d_{max} = 0.5\% \times L = 1.72mm$$

Therefore, if the maximum allowable is set as ±1.72mm, the above 78125 combinations can be sharply reduced. This hypothesis was backed from all the scanned panels, the maximum and minimum deviation from the perfect shape is listed in Table 5-9, all of which are within the range pre-established.

Table 5-9 Max and Min deviation based on measurement

Panel	Max(mm)	Min(mm)	Total(max-min)
Panel2	1.5760	-0.7152	2.2912
Panel3	1.2972	-0.9983	2.2955
Panel4	1.1275	-0.7503	1.8778
Panel5	1.3127	-0.5862	1.8989
Panel6	1.4195	-0.6804	2.0999

The variations of different type of geometry shapes are shown in Figure 5-17; only a few of them are listed.

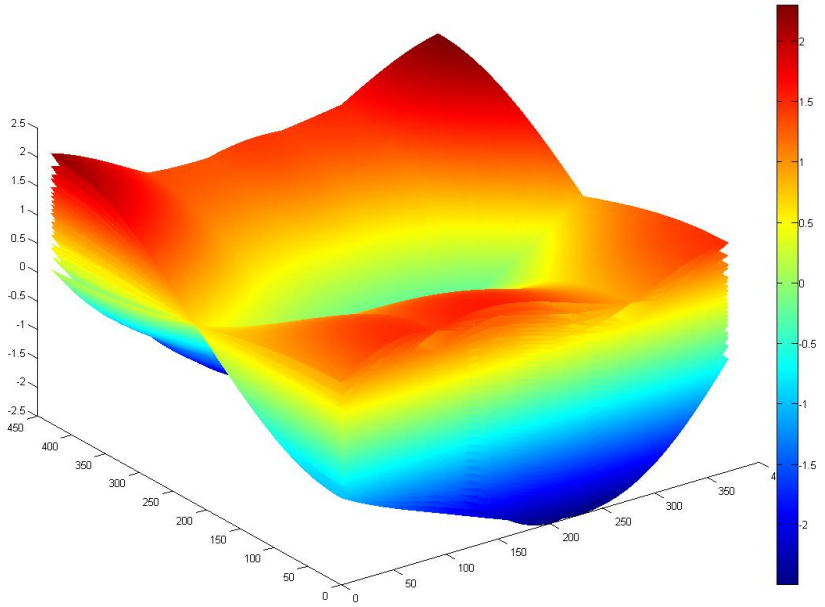

Figure 5-17 variations of different type of geometry shapes derived

5.5 Summary

This chapter discussed the geometric imperfection.

Firstly the imperfection was obtained by realistic measurement, and then was processed with a data reduction programme to be imported into FE analysis.

Later, the parameterization of the geometry of the panels was developed by means of the Double Fourier series surface fitting, for the aim of new imperfection derivation.

6 Experimental results and comparison with simulation

6.1 Panel experiments

This section will describe the real panel test carried in Cranfield University. The tests were carried in the laboratory of the School of Engineering at Cranfield University from September to the end of October, 2011. Five identical panels were ordered from manufacture, while the riveting and Cerrobend casting were done by hand. The test equipment is shown in Figure 3-4, in which the panel is in testing.

The panel was mounted in a vertical position with both ends cast into Cerrobend. The axial load was imposed on the Cerrobend from the top end of the panel, in order to give a compressive force. The both ends were rigged by means of the Cerrobend casting, while the two edges in the transverse side is left free. An INSTRON test machine was used to provide a uniform compressive displacement.

The signals of displacement and load data were recorded by transforming the electronic signals. All the data were recorded on a sheet, together with the time. And then the load-displacement curve can be potted as an X-Y plot, from which the ultimate load value can be easily identified. The test results in the form of load and displacement data can be looked up in Appendix B.

Meanwhile, during the load carrying, another optical system was set to capture the digital images of the deformed panel, called Correlation Instrument<Q-400>. The Q400 Correlation system was used to investigate the deformation on the panel as well as to extract the axial load and displacement. Although it can record the Applied Load, the precise of load recording is less than the test machine because of the larger time intervals during the recording course. With the use of two CCD cameras, see Figure 6-1, the 3D surface contour of the object can be determined.

The 3D image Correlation was only carried on panel2 and panel3 to support validation of the model.

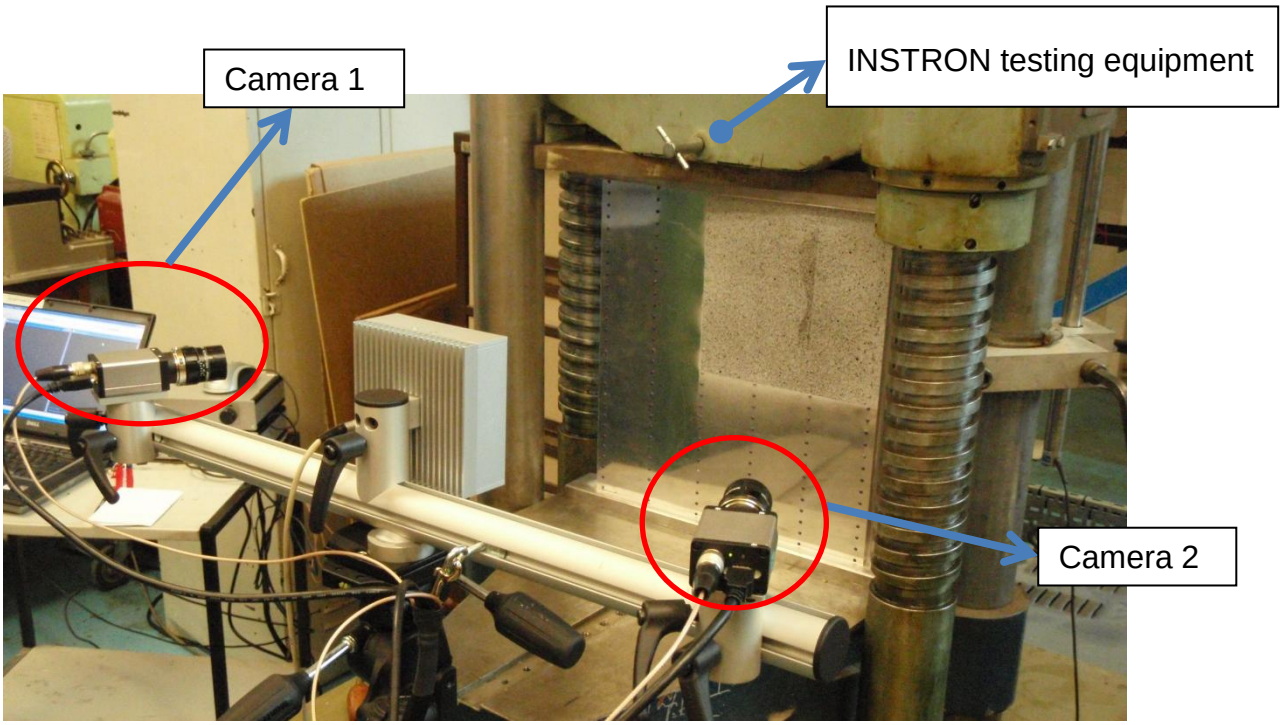

Figure 6-1 Panel test and Image Correlation

In the experiments, the following results were obtained:

1) A data sheet recorded by the INSTRON testing equipment, which includes the time, displacement and load values.

2) A set of capture pictures which were then processed in a software named Istra 4D. The output of Istra 4D is a contour of the deformation all through the panel testing.

These data were then collected to get comparison with the modelling simulation, for the purpose of validation, stated in the coming section.

6.2 Comparison of analysis with experiment

To validate the FE model, two main aspects are concerned:

1 buckling mode during the load carrying

2 Ultimate load prediction with the test results.

Buckling Mode

The validation from the buckling mode is accomplished by comparing the buckling pattern in FE-Analysis with that in physical test captured by the image correlation.

Figure 6-2 is the image correlation captured from the software Istra-4D, and Figure 6-3 gives the buckling pattern simulated in the FE analysis, both of which are based on panel3. By comparing the two figures, it can be observed that both indicate 3 waves in axial direction and one and a half wave from the transverse direction. In addition, from the comparison in terms of the half-wave length given in Table 6-1, one can see that the difference is controlled within the range of 5%. Thus, the conclusion can be made as:

The virtual simulation matches the experimentally result with a sufficient accuracy.

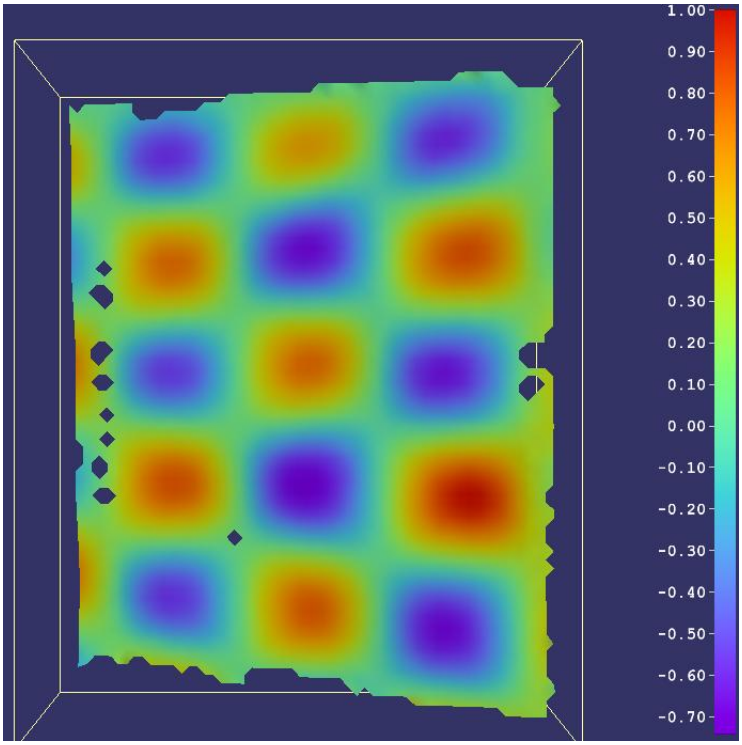

Figure 6-2 Measured Buckling Pattern in the Physical Test (Correlation Image)

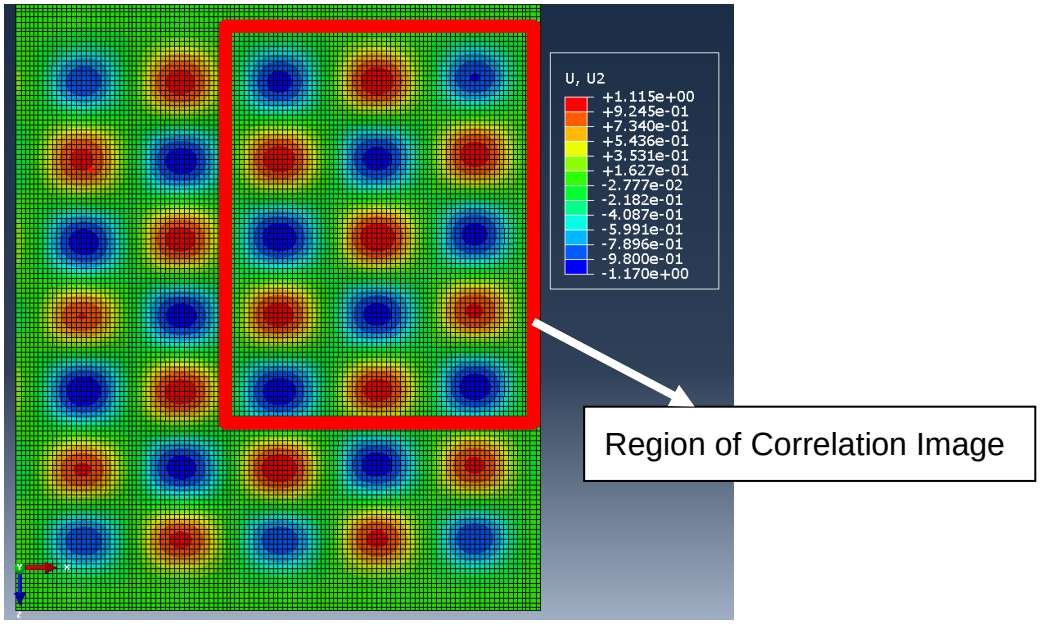

Figure 6-3 Buckling Pattern in FE-Analysis

Table 6-1 Comparison of the half-wave length

Typical half-Wave length	Image Correla-tion	FE-Analysis	Comparison
Longitude	56.72±0.22mm	54.20±0.16mm	≤4.75%
Transverse	71.18±0.18mm	70.00±0.12mm	≤1.86%

Ultimate load prediction

The next concern comes to investigating whether the FE model can predict the ultimate load accurately.

Table 6-2 above lists the ultimate load predicted by different models, compared with the real test results. It can be read that with no geometric imperfection the perfect panel predict the load at 98.9568kN. This perfect panel is the exact baseline model referred in chapter 4.

For panel2 and panel3, the recorded physical results of the test give the load at 97.1191kN and 97.7051kN, respectively. Through the Data reduction pro-

gramme mentioned in chapter 5.3, one can import the real geometry into the FE model, as which the so-called 'direct incorporation'. The 'direct incorporation' models can predict the ultimate load very close to the reality, with the difference in 0.52% and -0.21%. This means the FE model has a fantastic accuracy.

Later on, by comparing the loads with that of perfect panel, each of them is a little lower, within the percentage of 1.5%. This demonstrates that the geometric imperfection can slightly affect the ultimate load of this particular type of stiffened panels.

Table 6-2 Ultimate load record of five panels

Panel type		Ultimate load (kN)	Compared with perfect panel	Compared with test result	Compared with direct incorporation
Perfect panel		**98.9568**	0.00%	-	-
panel2	test	97.1191	-1.86%	0.00%	-
	direct incorporation	97.6234	-1.35%	0.52%	0.00%
	DFS fitting	98.5256	-0.44%	1.45%	0.92%
panel3	test	97.7051	-1.26%	0.00%	-
	direct incorporation	97.4955	-1.48%	-0.21%	0.00%
	DFS fitting	97.8614	-1.11%	0.16%	0.38%
panel4	test	106.2010	7.32%	0.00%	-
	direct incorporation	98.1731	-0.79%	-7.56%	0.00%
	DFS fitting	98.6890	-0.27%	-7.07%	0.53%
panel5	test	95.9473	-2.62%	0.00%	-
	direct incorporation	97.1518	-1.82%	1.26%	0.00%
	DFS fitting	98.8136	-0.14%	2.99%	1.71%
panel6	test	99.0234	1.19%	0.00%	-
	direct incorporation	97.2058	-1.34%	-1.84%	0.00%
	DFS fitting	98.8505	0.33%	-0.17%	1.69%

However, the argument cannot be supported on the test of the next panel-panel4. As in the experiment, the maximum load obtained was 106.2010kN, which is not only dramatically higher than the previous two panels, but also higher than that of the perfect model.

Nevertheless, fortunately, the FE simulation can still match the law generated from panel2 and panel3. The ‘direct incorporation’ model predicted the load at 98.1731kN, a little higher than panel3, which is proved to be reasonable judging from the geometric shape shown in Figure 5-16. Panel4 has a smaller imperfection upon the transverse half-sine curvature, compared with panel3. Thus, the fairly large divergence of panel4 in test may due to some other uncertainties which have not been included in this FE model, and this will be left for the discussion in the next chapter.

Another disparity comes from the result of panel5. The ultimate load from the experimental result displays 95.9473kN, while the predicted value of load from the ‘direct incorporation’ model is 97.1518kN, 1.26% higher than the former. However, such deviation on the value from prediction is reasonable and understandable, although it seems bigger than that of panel2 and panel3, 0.52% and -0.21% respectively.

In addition, double Fourier series (DFS) fitting brings a few errors but it is minor and could be neglected. The deviation from ‘DFS fitting’ model to ‘direct incorporation’ model is 0.92%, 0.38% and 0.53%, corresponding to panel2, panel3 and panel4, in terms of the final collapse load. The exception is panel5, but the disagreement of 1.17% is still insignificant. This also supports the premise that DFS fitting can be used in the geometric imperfection representation.

The conclusion can thereby be made that FE model acquires the ultimate load that is very close to the reality and can then be used to the further prediction.

6.3 Further prediction of the load

355 shapes were generated with the method of varying the coefficients using Double Fourier series surface fitting. As mentioned before, these shapes can predict a range of imperfections that cover the measured five testing panels, within the specified fabrication tolerances.

Due to the limit of time and cost, 80 models were randomly selected out of them, with different geometric imperfections from each other. These imperfect models are then analysed with the verified nonlinear FE method.

Each simulation calculates the buckling of imperfect panel with finite element analysis, and an ultimate load was finally predicted and recorded. The distribution of these loads was then plot as a histogram shown in Figure 6-5.

Among the 80 simulations, 25 out of them predicted the load between 98.5 and 98.7kN, by 31.25%. 75 simulations predict the load lower than 98.9568kN, the critical load of perfect panel, by the percentage of 93.75%.

In other word, the probability of failure load can be derived from the percentage. For a reliability of 0.9375, the Finite Element Analysis provides an ultimate load lower than that of the perfect panel, in terms of global buckling of the whole panel, including the geometric imperfections.

It can be observed from Figure 6-5, for some values of imperfections, the ultimate load may be even higher than the value of the model without imperfection (P_0=98.9568kN).

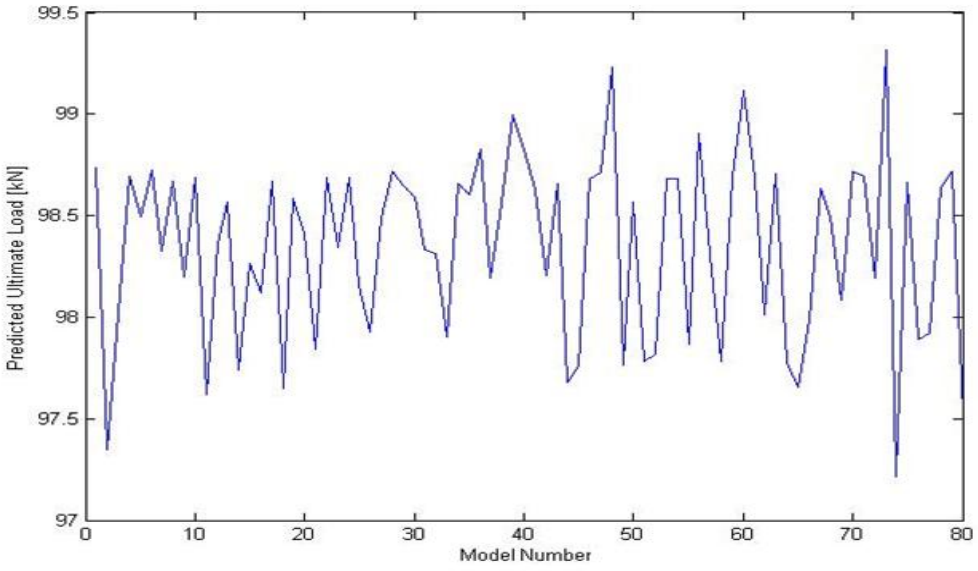

Figure 6-4 Ultimate loads predicted by 80 simulations

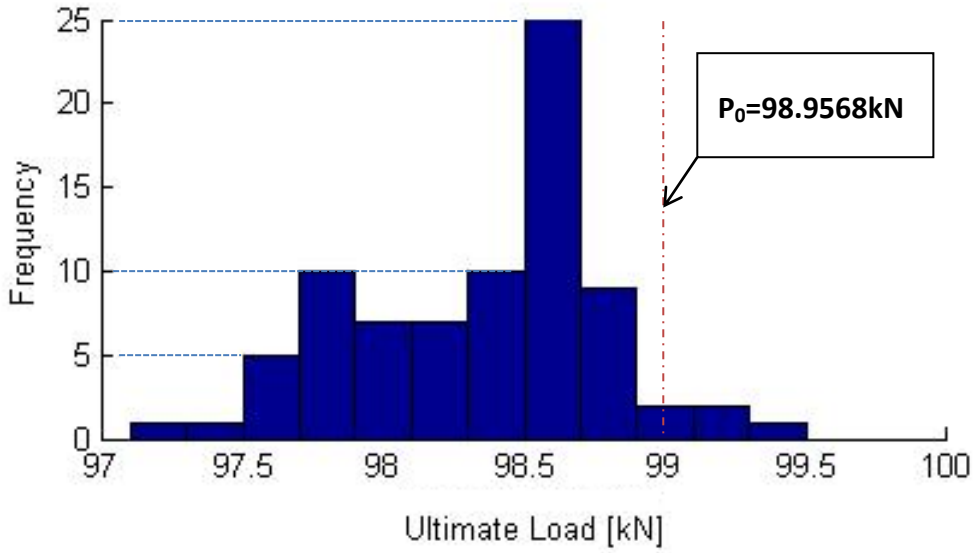

Figure 6-5 Histograms of the ultimate load (80 simulations)

Table 6-3 summarizes the results for the probabilistic analysis. In Table 6-3, a small variation within 7% is obtained between the real experiments and virtual simulations, in terms of the maximum value. It can also be observed that the variation between mean values of experiments and simulations is 0.91%, which means a very good match has been obtained. Because few samples are acquired from the real experiment, the standard deviation is quite big, much higher than that obtained from the simulations.

Table 6-3 Probabilistic results of ultimate load

	experiments	**simulations**	**Δ (%)**
Mean value (kN)	99.1992	98.3529	0.91%
Maximum value (kN)	106.2010	99.3140	6.93%
Minimum value (kN)	95.9473	97.2156	-1.30%
Most frequent value (kN)	-	98.6901	-
Standard deviation	4.0649	0.4491	-

Overall, a scatter of the ultimate load can be predicted numerically, while the accuracy of the scatter is left for discussion.

7 Discussion and Conclusion

7.1 Discussion

As mentioned before, the accuracy of predicting the ultimate load of stiffened panel was left for discussion. Also, this section will discuss those uncertainties that have not been considered in this project.

7.1.1 Model validation

The validation of FE model was performed by comparing the result of virtual prediction with those come from the reality.

In Table 6-2, the nonlinear analysis results indicate that the perfect panel buckled at a load value of 98.9568kN. The experimentally measured results scattered the load at a scatter from 95.9473kN to 106.2010kN, corresponding to panel5 and panel4, respectively.

The biggest difference in the analytical and experimental results is approximately 7%. However, one of the test results should be noticed. The problem comes from the real test of panel4 results a collapse load of 106.2010kN, which is even higher than that of the perfect panel, 98.9568kN.

One uncertainty is the imperfection in stiffeners. The geometry of stiffeners is not exactly measured in the scanning, instead of which the imperfection were assumed as the same geometry of the skin where they are corresponding to. However, in fact, the geometric imperfections cannot be exactly same as the skin. As mentioned in chapter 3, the global buckling, i.e. collapse of panel is commonly due to local flexural or torsional buckling in the stiffeners. Thus the real geometric imperfections in the stiffeners are significantly important. Unfortunately, such assumed geometry of stiffeners ignored the effect, which can be considered as the biggest uncertainty in terms of the ultimate load's scattering.

Another uncertainty comes from the boundary conditions, which is also very important in determining the critical load during the whole panel global buckling. The boundary condition is not absolutely rigid in reality. As one can see in Figure 7-1, there are obviously out-of-plain deformations in the edge of the panel

after global collapse in the real test, where the Cerrobend is casting and the rigid constraint was implemented. However, in FE simulation, it is modelled as totally rigid; the edge only has one displacement degree of freedom in axial direction. As the flexibility of the Cerrobend casting was not adequately modelled, such idealisation leads to the discrepancies of the critical load, which was stated by Hetey, with a estimation up to 3% .From this point of view, the uncertainties of the boundary conditions should be accounted for if possible.

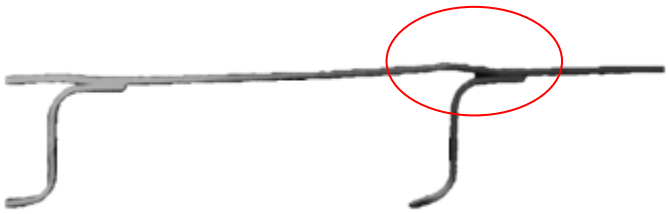

Figure 7-1 Out-of-plain deformation in the top edge of panel4 after real test

In addition, the third uncertainty which should not be ignored is scatters in material properties. A scattering of material properties in terms of elastic modulus or yield stress widely exists, due to the variation of temperature, thickness, manufacture process and so on. This will affect the final capacity of the panel sustaining axial compression. Thus, a specimen test on the material is necessary in order to characterise the material from batch to batch.

The fourth uncertainty may come from rivet modelling. In baseline model establishment, the elastic-plastic behaviour of rivets was included. However, in reality, each rivet may be pre-stressed when fabricated. The pre-stress can bring effect to the postbuckling behaviour and thus affect the ultimate load.

The last consideration is from the test machine. To concentrate on the investigation on the internal factors of the panel, the external factors were neglected. One of the external factors is test machine. In this investigation, the test machine was assumed rigid and perfect. Same as the boundary conditions, the in-

fluence on test machine can be one of the causes of the great difference between virtual simulation and real experiment.

The accuracy of the absolute value of the predicted load was not completely satisfied, but the approach revealed the effect of geometric imperfection, i.e. the initial geometric imperfections indeed changed the capability of the stiffened panel, in terms of global collapse.

7.1.2 Prediction

The histogram shown in Figure 6-5 indicated that, 25 out of 80 simulations predicted the load between 98.5 and 98.7kN, by 31.25%. For a reliability of 0.9375, the Finite Element Analysis provides an ultimate load lower than that of the perfect panel, in terms of global buckling of the whole panel, including the geometric imperfections.

From the comparison shown in Table 6-3, the mean value of the ultimate load predicted by virtual simulation is 98.3529kN, whereby for the five real experiments the corresponding value is 99.2431kN. From this point of view, the calculated mean value is obtained very close to the experimental results.

However, the simulations cannot predict the upper and lower bound of the load. This can be explained by the aforementioned fact that in addition to the geometric imperfections there are other uncertainties such as stiffener imperfection, non-perfect boundary conditions and test machine, varying material properties and pre-stressed rivets. All these unknown uncertainties can affect the prediction accuracy in terms of the ultimate load of global buckling of stiffened panel.

However, this project is aiming to focusing only on the geometric imperfections, omitting the other source of uncertainties. Nevertheless, they do have effects on the ultimate load, as discussed in chapter 6.3.

7.2 Conclusion

In this project, a finite element analysis of axial compressed metallic stiffened panel was performed taking into account geometric imperfections, in order to investigate the effect of manufacturing variability in terms of the ultimate load of the post-buckled panel.

1. An efficient and reliable FE model was established, with material, boundary and geometric nonlinearities included, as well as geometric imperfections. In addition, this model was used to investigate the effect of geometric imperfections on the ultimate load of a metallic stiffened panel under axial compression.
2. Geometry scanning and experiments were performed with 5 panels. Panel tests gave the scatters of 10.25kN in terms of the ultimate load, and the panel-to-panel variations in geometry were obtained by the realistic measurement.
3. Real geometry of each panel was identified and parameterised by means of surface fitting algorithm. In addition, the numerical representation of the geometric imperfection was adopted into the FE simulations and produced a scatter in collapse load.

However, numerical predicted scatter is less than that observed in experiments. This is due to some other uncertainties which have not been considered in this project, which was discussed above. Thus, further investigation is required.

7.3 Further work

Only the geometric imperfections are accounted for in this statistic analysis, while other uncertainties such as non-perfect boundary conditions and test machine, scatters in nonlinear material properties, stiffener imperfection and rivets pre-stressing, etc. were not considered.

Thus, to perform virtual test on the metallic stiffened panel, further investigations required in the future in addition to the current work.

Firstly, due to the limit of geometry measurement, only the imperfection on the skin side was obtained. However, there should also be imperfect on the Z section stiffeners; those uncertainties should be included in the virtual FE model in order to get a more precise prediction in terms of the ultimate load.

Furthermore, the flexibility of the Cerrobend casting was not adequately modelled, which leads to the discrepancies of the critical load. The boundary condition is very important in determining the critical load during the whole panel global buckling. The boundary condition is not absolutely rigid in reality and there can be significant deformations after test. Thus, the uncertainties of the boundary conditions should be accounted for if possible. Introducing the variation of boundary conditions can also bring higher accuracy into the prediction.

Except elastic-plastic curve, the other characters such as scatter in material properties were not considered in the virtual FE analysis. A scattering of material properties in terms of elastic modulus or yield stress widely exists, due to the variation of temperature, thickness, manufacture process and so on. This will affect the final capacity of the panel sustaining axial compression. Thus, a specimen test on the material is necessary in order to characterise the material from batch to batch.

The pre-stress in rivets is from the fabrication in reality. Such pre-stress can significantly affect the ultimate strength characteristics. For new finite element analysis, one should establish improved rivet behaviour including pre-stressed variation.

The last step, if all the considerations above being included can still not predict in a good accuracy, one should investigate on test machine, which was assumed rigid and perfect. However, since the test machine was always treated as gage and the precision was mostly ensured, the influence on test machine will be lastly considered.

REFERENCES

[1] M.C. Y. Niu (1988), *Airframe Structural Design,* Conmilit Press.

[2] Shigley. J and Mischke. C (1986), *Standard Book of Machine Design,* McGraw-Hill.

[3] M.C. Y. Niu (1997), *Airframe Stress Analysis and Sizing,* Conmilit Press.

[4] NASA space vehicle design criteria (structures), (1968), *Buckling of thin-walled structures*.

[5] J.G.Teng and J.M.Rotter (eds.) (2004), *Buckling of Thin Metal Shells,* Spon Press, London.

[6] MATTEO BROGGI, ADRIANO CALVI and GERHART I. SCHUËLLER (2011), "RELIABILITY ASSESSMENT OF AXIALLY COMPRESSED COMPOSITE CYLINDRICAL SHELLS WITH RANDOM IMPERFECTIONS", vol. 11, no. 2, pp. 215-236.

[7] J. Campbell. (2010), Lecture notes, *Structural Stability,* School of Engineering, Cranfield University.

[8] S.P. Timoshenko, J. M. G.
Theory of elastic stability (2nd edition), New York: McGraw Hill, 1961 .

[9] Laszlo Hetey. (2009), PhD thesis, "*Idealisation error control for aerospace virtual structural testing",* Cranfield University.

[10] Quinn, D., Murphy, A., McEwan, W. and Lemaitre, F. (2009), "Stiffened panel stability behaviour and performance gains with plate prismatic substiffening", *Thin-Walled Structures,* vol. 47, no. 12, pp. 1457-1468.

[11] Jen, C. and Tai, Y. (2010), "Deformation behavior of a stiffened panel subjected to underwater shock loading using the non-linear finite element method", *Materials & Design,* vol. 31, no. 1, pp. 325-335.

[12] Perret, A., Mistou, S. and Fazzini, M. (2011), "Global behaviour of a composite stiffened panel in buckling. Part 1: Numerical modelling", *Composite Structures,* vol. 93, no. 10, pp. 2610-2618.

[13] Paik, J. K., Kim, B. J. and Seo, J. K. (2008), "Methods for ultimate limit state assessment of ships and ship-shaped offshore structures: Part II stiffened panels", *Ocean Engineering,* vol. 35, no. 2, pp. 271-280.

[14] Cao, Q. and Zhao, Y. (2010), "Buckling strength of cylindrical steel tanks under harmonic settlement", *Thin-Walled Structures,* vol. 48, no. 6, pp. 391-400.

[15] Ghorbanpour Arani, A., Rahmani, R. and Arefmanesh, A. (2008), "Elastic buckling analysis of single-walled carbon nanotube under combined loading by using the ANSYS software", *Physica E: Low-dimensional Systems and Nanostructures,* vol. 40, no. 7, pp. 2390-2395.

[16] Arbocz, J. and Starnes Jr, J. H. (2002), "Future directions and challenges in shell stability analysis", *Thin-Walled Structures,* vol. 40, no. 9, pp. 729-754.

[17] Tao, Z., Uy, B., Liao, F. and Han, L. (2011), "Nonlinear analysis of concrete-filled square stainless steel stub columns under axial compression", *Journal of Constructional Steel Research,* vol. 67, no. 11, pp. 1719-1732.

[18] Tao, Z., Uy, B., Han, L. and Wang, Z. (2009), "Analysis and design of concrete-filled stiffened thin-walled steel tubular columns under axial compression", *Thin-Walled Structures,* vol. 47, no. 12, pp. 1544-1556.

[19] Murphy, A. and Price, M. (2001), "Efficient Finite Element Modelling of Buckling and Post-buckling Behaviour of Flat Stiffened Panels", *NAFEMS World Congerss 2001,* 2001, Lake Como, Italy, .

[20] Murphy, A., Price, M., Gibson, A. and Armstrong, C. G. (2004), "Efficient non-linear idealisations of aircraft fuselage panels in compression", *Finite Elements in Analysis and Design,* vol. 40, no. 13-14, pp. 1977-1993.

[21] Lynch, C., Murphy, A., Price, M. and Gibson, A. (2004), "The computational post buckling analysis of fuselage stiffened panels loaded in compression", *Thin-Walled Structures,* vol. 42, no. 10, pp. 1445-1464.

[22] Murphy, A., McCune, W., Quinn, D. and Price, M. (2007), "The characterisation of friction stir welding process effects on stiffened panel buckling performance", *Thin-Walled Structures,* vol. 45, no. 3, pp. 339-351.

[23] Koiter "THE STABILITY OF ELASTIC EQUILIBRIUM", .

[24] Josef Singer, Johann Arbocz and Tanchum Weller (2002), *Buckling Experiments: Experimental Methods in Buckling of Thin-walled Structures,* John Wiley & Sons, inc,.

[25] J.W., H. (1973), "Imperfection-sensitivity in the plastic range", *Journal of the Mechanics and Physics of Solids,* vol. 21, no. 3, pp. 191-204.

[26] E. Byskov " Imperfection sensitivity of elastic–plastic truss columns, AIAA J. 20 (2) (1982), pp. 263–267.", .

[27] Su, X. M. and Lu, W. D. (1991), "Post-bifurcation and imperfection sensitivity analysis of plastic clamped circular plates", *International Journal of Solids and Structures,* vol. 27, no. 6, pp. 769-782.

[28] Arbocz " Post-Buckling Behaviour of Structures: Numerical Techniques for More Complicated Structures, in *Lecture Notes in Physics*, Ed. H. Araki et al., Springer-Verlag, Berlin, 1987, pp. 84–142.", .

[29] Graciano, C., Casanova, E. and Martínez, J. (2011), "Imperfection sensitivity of plate girder webs subjected to patch loading", *Journal of Constructional Steel Research,* vol. 67, no. 7, pp. 1128-1133.

[30] Hu, S. Z. and Jiang, L. (1998), "A finite element simulation of the test procedure of stiffened panels", *Marine Structures,* vol. 11, no. 3, pp. 75-99.

[31] Elishakoff, I. and Arbocz, J. (1982), "Reliability of axially compressed cylindrical shells with random axisymmetric imperfections", *International Journal of Solids and Structures,* vol. 18, no. 7, pp. 563-585.

[32] Schenk, C. A. and Schuëller, G. I. (2007), "Buckling analysis of cylindrical shells with cutouts including random boundary and geometric imperfections", *Computer Methods in Applied Mechanics and Engineering,* vol. 196, no. 35-36, pp. 3424-3434.

[33] Schenk, C. A. and Schuëller, G. I. (2003), "Buckling analysis of cylindrical shells with random geometric imperfections", *International Journal of Non-Linear Mechanics,* vol. 38, no. 7, pp. 1119-1132.

[34] Kiyohiro, I. and Kazuo, M. (1991), "Random initial imperfections of structures", *International Journal of Solids and Structures,* vol. 28, no. 8, pp. 1003-1021.

[35] Peter, A. (1992), "On the buckling analysis and design of silos and tanks", *Journal of Constructional Steel Research,* vol. 23, no. 1-3, pp. 273-294.

[36] Stull, C. J., Earls, C. J. and Aquino, W. (2008), "A posteriori initial imperfection identification in shell buckling problems", *Computer Methods in Applied Mechanics and Engineering,* vol. 198, no. 2, pp. 260-268.

[37] Z.P. Bazant and L. Cedolin (1991), *Stability of Structures,* Oxford University Press.

[38] Ikeda, K., Kitada, T., Matsumura, M. and Yamakawa, Y. (2007), "Imperfection sensitivity of ultimate buckling strength of elastic–plastic square plates under compression", *International Journal of Non-Linear Mechanics,* vol. 42, no. 3, pp. 529-541.

[39] B.D., Reddy. (1980), "Buckling of elastic-plastic discretely stiffened cylinders in axial compression", *International Journal of Solids and Structures,* vol. 16, no. 4, pp. 313-328.

[40] Qiu, Z., Wang, X. and Li, Z. (2009), "Post-buckling analysis of a thin stiffened plate with uncertain initial deflection via interval analysis", *International Journal of Non-Linear Mechanics,* vol. 44, no. 10, pp. 1031-1038.

[41] Most, T., Bucher, C. and Schorling, Y. (2004), "Dynamic stability analysis of non-linear structures with geometrical imperfections under random loading", *Journal of Sound and Vibration,* vol. 276, no. 1-2, pp. 381-400.

[42] Dassault Systèmes, (2010), *Getting Started with ABAQUS: Interaction Edition*.

[43] Dassault Systèmes, (2010), *ABAQUS/CAE User's Manual*.

[44] Dassault Systèmes, (2010), *ABAQUS Analysis User's Manual*.

[45] W. Ramberg and W.R. Osgood (1943), "Description of Stress Strain Curves by Three Parameters", .

[46] Kim J.R., R. (2003), "Full-range stress–strain curves for stainless steel alloys", *Journal of Constructional Steel Research,* vol. 59, no. 1, pp. 47-61.

[47] Quach, W. M., Teng, J. G. and Chung, K. F. (2008), "Three-stage full-range stress-strain model for stainless steels", *Journal of Structural Engineering,* vol. 134, no. 9, pp. 1518-1527.

[48] "ESDU, Metallic Material Data Handbook, DEF STAN 00 932, ESDU International Ltd, 1990.", .

[49] Cranfield University "Stressing Data Sheets, AVT-AVD 9632, Cranfield College of Aeronautics, 1999", .

[50] R Degenhardt, H Klein, A. K., H Temmen and R.Zimmermann "Buckling and Post-Buckling Analysis of Shells under Quasi-Static and Dynamic Loads", .

[51] Lynch C J and Sterling S G. "A finite element study of the postbuckling behaviour of a flat stiffened panel", *21st ICAS Congress,* 1998, Melbourne Australia, .

[52] Theodore Baumeister, Eugene A. Avallone and Ali Sadegh (2006), "Marks' standard handbook for mechanical engineers, 11th edition", in McGraw-Hill, .

[53] Pavlovčič, L., Detzel, A., Kuhlmann, U. and Beg, D. (2007), "Shear resistance of longitudinally stiffened panels—Part 1: Tests and numerical analysis of imperfections", *Journal of Constructional Steel Research,* vol. 63, no. 3, pp. 337-350.

[54] Hughes, O. F., Ghosh, B. and Chen, Y. (2004), "Improved prediction of simultaneous local and overall buckling of stiffened panels", *Thin-Walled Structures,* vol. 42, no. 6, pp. 827-856.

APPENDICES

Appendix A ABAQUS input

A.1 Integrally-stiffened panel

```
*Heading
** Job name: buckling Model name: Model-1
** Generated by: Abaqus/CAE 6.10-1
*Preprint, echo=NO, model=NO, history=NO, contact=NO
**
** PARTS
**
*Part, name=panel
*Node
      1,        290.,        -40.,          0.
      2,        290.,        -40.,          0.
      3,        302.,        -40.,          0.
   ...
   9483,         76.,         -20.,          5.
*Element, type=S4R5
  1,     1,   39, 1834,  210
  2,   39,   40, 1835, 1834
  3,   40,   41, 1836, 1835
...
9288, 9483, 1832,   38, 1833
*Nset, nset=_PickedSet2, internal, generate
    1,  9483,     1
*Elset, elset=_PickedSet2, internal, generate
    1,  9288,     1
** Section: PanelSection
*Shell Section, elset=_PickedSet2, material=L165
0.91, 5
*End Part
**
**
** ASSEMBLY
**
*Assembly, name=Assembly
**
*Instance, name=panel-1, part=panel
*End Instance
**
*Nset, nset="Bottom Nodes", instance=panel-1
    1,    4,    5,    8,    9,   11,
…
  1569, 1656, 1657, 1658, 1747
*Nset, nset="Top Nodes", instance=panel-1
```

```
   2,    3,    6,    7,   10,   12,
…
1655, 1744, 1745, 1746, 1833
*End Assembly
**
** MATERIALS
**
** both skin and stringer material L165
** fn=296N/mm2, 1/en=224,m=17
*Material, name=L165
*Elastic
68000., 0.33
*Plastic
330.,     0.
340., 0.0066
350., 0.0077
360., 0.0093
B., 0.0115
380., 0.0148
390., 0.0194
400., 0.0262
410., 0.0358
420., 0.0494
L., 0.0686
440., 0.0954
450., 0.1326
460., 0.1839
470., 0.2541
480., 0.3496
490., 0.4788
500., 0.6523
510., 0.8842
520., 1.1922
530., 1.5992
540., 2.1341
** ----------------------------------------------------------------
**
** STEP: Step-1
**
*Step, name=Step-1, nlgeom=YES, inc=1200
*Static, stabilize=0.0002, allsdtol=0, continue=NO
0.05, 1., 1e-10, 0.05
**
** BOUNDARY CONDITIONS
**
** Name: Top Type: Displacement/Rotation
*Boundary
"Top Nodes", 1, 1
```

```
"Top Nodes", 2, 2
"Top Nodes", 3, 3, 5.
"Top Nodes", 4, 4
"Top Nodes", 5, 5
"Top Nodes", 6, 6
** Name: bottom Type: Displacement/Rotation
*Boundary
"Bottom Nodes", 1, 1
"Bottom Nodes", 2, 2
"Bottom Nodes", 3, 3
"Bottom Nodes", 4, 4
"Bottom Nodes", 5, 5
"Bottom Nodes", 6, 6
**
** OUTPUT REQUESTS
**
*Restart, write, frequency=0
**
** FIELD OUTPUT: F-Output-1
**
*Output, field, variable=PRESELECT
**
** HISTORY OUTPUT: H-Output-1
**
*Output, history
*Node Output, nset="Top Nodes"
RF1, RF2, RF3, RM1, RM2, RM3, U3
*End Step
```

A.2 Baseline model

```
*Heading
**increment: allsdtol=0.05, 0.001, 1., 1e-05, 0.01
** Job name: perfectpanel-static Model name: Model-1
** Generated by: Abaqus/CAE 6.10-EF1
*Preprint, echo=NO, model=NO, history=NO, contact=NO
**
** PARTS
**
*Part, name=Part-1
*Node
      1,        18.5,        -20.,        425.
      2,   23.0900002,        -20.,        425.
      3,   23.0900002,        -20.,        430.
      4,        18.5,        -20.,        430.
      5,        18.5,        -20.,       413.5
     ...
  26745,   305.860596,          0.,   417.333344
  26746,   302.422058,          0.,   417.333344
  26747,   298.983521,          0.,   417.333344
  26748,         357.,          0.,       427.5
  26749,         357.,          0.,   421.166656
  26750,         357.,          0.,   417.333344
*Element, type=S4R
1,    1,    2, 2381, 2382
2, 2382, 2381,    3,    4
3,    5,    6, 2383, 2386
4, 2386, 2383, 2384, 2385
5, 2385, 2384,    2,    1
...
25665, 13604,  2379,  2375, 13603
25666,  2375,  2379, 13610, 13607
25667, 13607, 13610, 13609, 13608
25668, 13608, 13609,  2374,  2373
*Nset, nset="Whole Panel", generate
     1,  26750,      1
*Elset, elset="Whole Panel", generate
     1,  25668,      1
** Section: shell section
*Shell Section, elset="Whole Panel", material=AluminiumL165
0.91, 5
*End Part
**
**
** ASSEMBLY
**
*Assembly, name=Assembly
```

```
**
*Instance, name=Part-1-1, part=Part-1
*End Instance
**
**
** @ABQCAE, object=discrete fastener
*Node
      1,        360.,          0.,          5.
      2,        360., -0.910000026,          5.
      3,        360.,          0.,         19.
      4,        360., -0.910000026,         19.
      5,        360.,          0.,         33.
     ...
    370,         10., -0.910000026,        411.
    371,         10.,          0.,        425.
    372,         10., -0.910000026,        425.
*Node
    373,        360.,          0.,        425.
    374,        360.,          0.,        411.
    375,        360.,          0.,        397.
    ...
    555,         10.,          0.,         47.
    556,         10.,          0.,         33.
    557,         10.,          0.,         19.
    558,         10.,          0.,          5.
**
** @ABQCAE, object=discrete fastener
*Element, type=CONN3D2
1, 311, 312
2, 313, 314
3, 315, 316
...
30, 369, 370
31, 371, 372
**
** @ABQCAE, object=discrete fastener
*Connector Section, elset="Attachment Lines-1-Set-1", behavior=RIVET_P80
Cartesian,
**
** @ABQCAE, object=discrete fastener
*Element, type=CONN3D2
32, 249, 250
33, 251, 252
...
61, 307, 308
62, 309, 310
**
…
```

```
** @ABQCAE, object=discrete fastener
*Connector Section, elset="Attachment Lines-6-Set-1", behavior=RIVET_P80
Cartesian,
*Nset, nset="Attachment Points-1-Set-1", generate
 528,  558,    1
*Nset, nset="Attachment Points-2-Set-1", generate
 497,  527,    1
*Nset, nset="Attachment Points-3-Set-1", generate
 466,  496,    1
*Nset, nset="Attachment Points-4-Set-1", generate
 435,  465,    1
*Nset, nset="Attachment Points-5-Set-1", generate
 404,  434,    1
*Nset, nset="Attachment Points-6-Set-1", generate
 373,  403,    1
*Nset, nset="Attachment Lines-1-Set-1", generate
 311,  372,    1
*Elset, elset="Attachment Lines-1-Set-1", generate
  1,  31,   1
*Nset, nset="Attachment Lines-2-Set-1", generate
 249,  310,    1
*Elset, elset="Attachment Lines-2-Set-1", generate
 32,  62,   1
*Nset, nset="Attachment Lines-3-Set-1", generate
 187,  248,    1
*Elset, elset="Attachment Lines-3-Set-1", generate
 63,  93,   1
*Nset, nset="Attachment Lines-4-Set-1", generate
 125,  186,    1
*Elset, elset="Attachment Lines-4-Set-1", generate
  94,  124,    1
*Nset, nset="Attachment Lines-5-Set-1", generate
  63,  124,    1
*Elset, elset="Attachment Lines-5-Set-1", generate
 125,  155,    1
*Nset, nset="Attachment Lines-6-Set-1", generate
  1,  62,   1
*Elset, elset="Attachment Lines-6-Set-1", generate
 156,  186,    1
*Nset, nset="BOTTOM band", instance=Part-1-1
    1,    2,   71,  106,  141,  176,  179,  246,  247,  316,  351,  386,  421,
424,  491,  492
 ...
26743, 26744, 26745, 26746, 26747, 26748, 26749, 26750
*Nset, nset="TOP edge", instance=Part-1-1
  69,   70,  105,  140,  175,  244,  245,  314,  315,  350,  385,  420,  489,  490,
559,  560
 ...
```

9106, 9107, 9108, 9109, 9226, 9596, 9597, 9598, 9599, 9600, 9601, 9602, 9603, 9604, 9605, 9606
9607, 9608, 9609, 9610, 9611, 9757
*Nset, nset="BOTTOM edge", instance=Part-1-1
3, 4, 72, 107, 142, 177, 178, 248, 249, 317, 352, 387, 422, 423, 493, 494
...
13580, 13581, 13582, 13583, 13584, 13599
*Nset, nset="TOP band", instance=Part-1-1
67, 68, 104, 139, 174, 242, 243, 312, 313, 349, 384, 419, 487, 488, 557, 558
...
20916, 20917, 20918, 20919, 20920, 20921, 20922, 20923, 20924, 20925, 20926, 20927, 20928, 20929, 20930, 20931
20932, 20933, 20934, 20935, 20936, 20937, 21145, 21146
*Elset, elset=_INT-ATTSETSURF-ASSY-1_SPOS, internal, instance=Part-1-1
11905, 11906, 11907, 11908, 11909, 11910, 11911, 11912, 11913, 11914, 11915, 11916, 11917, 11918, 11919, 11920
...
25655, 25656, 25661, 25662, 25663
*Surface, type=ELEMENT, name=_INT-ATTSETSURF-ASSY-1, internal
_INT-ATTSETSURF-ASSY-1_SPOS, SPOS
*Elset, elset=_INT-ATTSETSURF-ASSY-2_SPOS, internal, instance=Part-1-1
1, 2, 3, 4, 5, 6, 7, 8, 9, 10, 11, 12, 13, 14, 15, 16
...
1937, 1938, 1939, 1940, 1941, 1942, 1943, 1983, 1984
…
*Surface, type=ELEMENT, name=_INT-ATTSETSURF-ASSY-12, internal
_INT-ATTSETSURF-ASSY-12_SPOS, SPOS
*Elset, elset=_Surf-1-M_SPOS, internal, instance=Part-1-1
11907, 11908, 11909, 11910, 11914, 11915, 11916, 11917, 11918, 11919, 11920, 11921, 11925, 11926, 11927, 11928
...
20580, 20581, 20582, 20583, 20587, 20588, 20589, 20590, 21019, 21020, 21021, 21022, 21023, 21024, 21025, 21026
21027, 21453, 21454, 21455
*Surface, type=ELEMENT, name=Surf-1-M
_Surf-1-M_SPOS, SPOS
*Elset, elset=_Surf-1-S_SNEG, internal, instance=Part-1-1
1574, 1575, 1576, 1577, 1578, 1579, 1580, 1581, 1582, 1583, 1584, 1585, 1586, 1587, 1588, 1589
...
1926, 1927, 1928, 1929, 1930, 1931, 1932, 1933, 1934, 1935, 1936, 1937, 1938, 1939, 1940, 1941
1942, 1943, 1983, 1984
*Surface, type=ELEMENT, name=Surf-1-S
_Surf-1-S_SNEG, SNEG
*Elset, elset=_Surf-2-M_SPOS, internal, instance=Part-1-1

```
 11984, 11985, 11986, 11987, 12056, 12057, 12058, 12059, 12060, 12061,
12062, 12063, 12103, 12104, 12105, 12106
...
 22214, 22215, 22216, 22217, 22269, 22270, 22271, 22272, 22617, 22618,
22619, 22620, 22621, 22622, 22623, 22624
 22625, 22967, 22968, 22969
…
*Surface, type=ELEMENT, name=Surf-6-S
_Surf-6-S_SNEG, SNEG
**
** DISCRETE FASTENER: Fasteners-1
**
** @ABQCAE, object=discrete fastener, name=Fasteners-1
*Coupling, constraint name=_Fasteners-1_1_end1, ref node=311, sur-
face=_INT-ATTSETSURF-ASSY-1, influence radius=2.
*Distributing, weighting method=UNIFORM
**
** @ABQCAE, object=discrete fastener, name=Fasteners-1
*Coupling, constraint name=_Fasteners-1_1_end2, ref node=312, sur-
face=_INT-ATTSETSURF-ASSY-2, influence radius=2.
*Distributing, weighting method=UNIFORM
**
…
**
** @ABQCAE, object=discrete fastener, name=Fasteners-1
*Coupling, constraint name=_Fasteners-1_31_end1, ref node=371, sur-
face=_INT-ATTSETSURF-ASSY-1, influence radius=2.
*Distributing, weighting method=UNIFORM
**
** @ABQCAE, object=discrete fastener, name=Fasteners-1
*Coupling, constraint name=_Fasteners-1_31_end2, ref node=372, sur-
face=_INT-ATTSETSURF-ASSY-2, influence radius=2.
*Distributing, weighting method=UNIFORM
**
** DISCRETE FASTENER: Fasteners-2
**
…
*End Assembly
*Connector Behavior, name=RIVET_P80
*Connector Elasticity, component=1
30000.,
*Connector Elasticity, component=2
20000.,
*Connector Elasticity, component=3
30000.,
*Connector Plasticity, component=1
*Connector Hardening, definition=TABULAR
 875.,     0.,     0.
```

```
1589., 0.0262,     0.
1944., 0.0902,     0.
2100., 0.6662,     0.
*Connector Plasticity, component=3
*Connector Hardening, definition=TABULAR
 875.,     0.,     0.
1589., 0.0262,     0.
1944., 0.0902,     0.
2100., 0.6662,     0.
*Connector Plasticity, component=2
*Connector Hardening, definition=TABULAR
 215.,    0.,    0.
 445., 0.158,    0.
 667., 0.343,    0.
 870., 0.553,    0.
1012., 1.072,    0.
**
** MATERIALS
**
** to be modified with the plastic properties
*Material, name=AluminiumL165
*Elastic
68000., 0.33
*Plastic
310.,     0.
320.,  0.001
330., 0.0016
340., 0.0027
350., 0.0044
360., 0.0071
370., 0.0114
380., 0.0179
390., 0.0278
400., 0.0428
410., 0.0651
420., 0.0981
430., 0.1463
440., 0.2163
450.,  0.369
**
** INTERACTION PROPERTIES
**
*Surface Interaction, name=Contact
1.,
*Friction, slip tolerance=0.005
 1.05,
*Surface Behavior, pressure-overclosure=HARD
**
```

```
** INTERACTIONS
**
** Interaction: contact-1
*Contact Pair, interaction=Contact, type=SURFACE TO SURFACE
Surf-1-S, Surf-1-M
** Interaction: contact-2
*Contact Pair, interaction=Contact, type=SURFACE TO SURFACE
Surf-2-S, Surf-2-M
** Interaction: contact-3
*Contact Pair, interaction=Contact, type=SURFACE TO SURFACE
Surf-3-S, Surf-3-M
** Interaction: contact-4
*Contact Pair, interaction=Contact, type=SURFACE TO SURFACE
Surf-4-S, Surf-4-M
** Interaction: contact-5
*Contact Pair, interaction=Contact, type=SURFACE TO SURFACE
Surf-5-S, Surf-5-M
** Interaction: contact-6
*Contact Pair, interaction=Contact, type=SURFACE TO SURFACE
Surf-6-S, Surf-6-M
** ----------------------------------------------------------------
**
*IMPERFECTION,SYSTEM=R,INPUT=fourierfitting-imperfection-
2+2+2+2+2.inp
** STEP: static
**
*Step, name=static, nlgeom=YES,INC=150
displacement control till collapse
*Static, stabilize=0.0002, allsdtol=0.05, continue=NO
0.001, 1., 1e-05, 0.01
**
** BOUNDARY CONDITIONS
**
** Name: BOTTOM band Type: Displacement/Rotation
*Boundary
"BOTTOM band", 1, 1
"BOTTOM band", 2, 2
"BOTTOM band", 4, 4
"BOTTOM band", 5, 5
"BOTTOM band", 6, 6
** Name: BOTTOM edge Type: Displacement/Rotation
*Boundary
"BOTTOM edge", 1, 1
"BOTTOM edge", 2, 2
"BOTTOM edge", 3, 3
"BOTTOM edge", 4, 4
"BOTTOM edge", 5, 5
"BOTTOM edge", 6, 6
```

```
** Name: TOP band Type: Displacement/Rotation
*Boundary
"TOP band", 1, 1
"TOP band", 2, 2
"TOP band", 4, 4
"TOP band", 5, 5
"TOP band", 6, 6
** Name: TOP edge Type: Displacement/Rotation
*Boundary
"TOP edge", 1, 1
"TOP edge", 2, 2
"TOP edge", 3, 3, 2.
"TOP edge", 4, 4
"TOP edge", 5, 5
"TOP edge", 6, 6
**
** OUTPUT REQUESTS
**
*Restart, write, frequency=0
**
** FIELD OUTPUT: F-Output-1
**
*Output, field
**
** HISTORY OUTPUT: H-Output-1
**
*Output, history
*Node Output, nset="TOP edge"
RF3, U3
*End Step
```

A.3 Imperfections input

Part-1-1.1474,0, -0.09802,0
Part-1-1.1471,0, -0.04271692,0
Part-1-1.8263,0,-0.0031736374,0
Part-1-1.1475,0, 0.034644538,0
Part-1-1.1479,0, 0.065863884,0
Part-1-1.1484,0, 0.099819916,0
Part-1-1.8284,0, 0.13704472,0
Part-1-1.8285,0, 0.17175016,0
Part-1-1.8286,0, 0.20388297,0
…
10,0, 0.38065185,0
322,0, 0.10873997,0
260,0, 0.32318346,0
198,0, -0.14601079,0
136,0, -0.44600755,0
74,0,-0.088059069,0
12,0, 0.40089138,0
324,0, 0.13791748,0
262,0, 0.30793391,0
200,0, -0.15832495,0
138,0, -0.4459375,0
76,0, -0.08432535,0
14,0, 0.42483682,0
326,0, 0.17130564,0
264,0, 0.29048367,0
202,0, -0.1724162,0
140,0, -0.44585734,0
78,0,-0.080052811,0
16,0, 0.45223789,0
328,0, 0.20855547,0
266,0, 0.27101513,0
204,0, -0.18813722,0
142,0, -0.44576791,0
80,0,-0.075286112,0
18,0, 0.48280815,0
330,0, 0.24927759,0

Appendix B Result records of panel test

B.1 Panel2

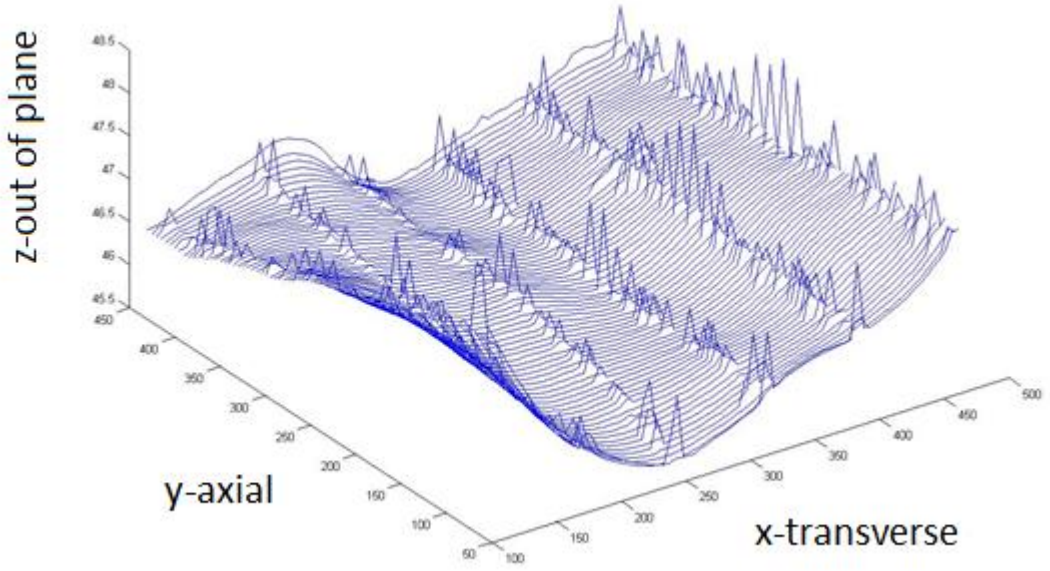

Figure B-1 Scanning lines plot along the X direction- in Panel 2

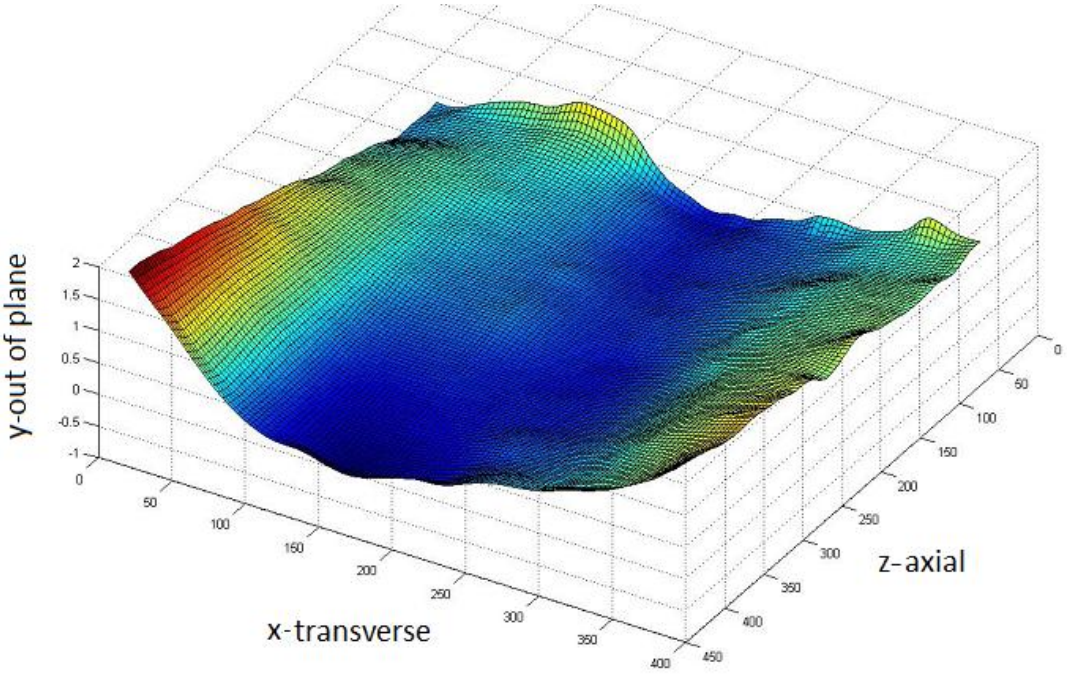

Figure B-2 Normalized geometric shape of Panel 2

B.2 Panel3

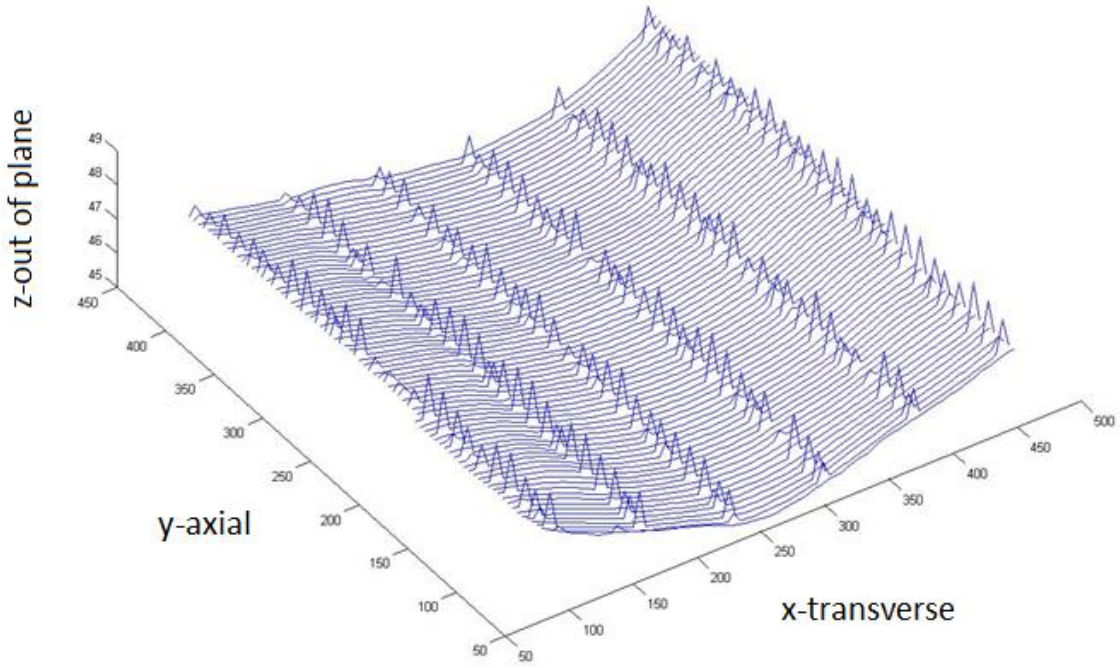

Figure B-3 Scanning lines plot along the X direction- in Panel 3

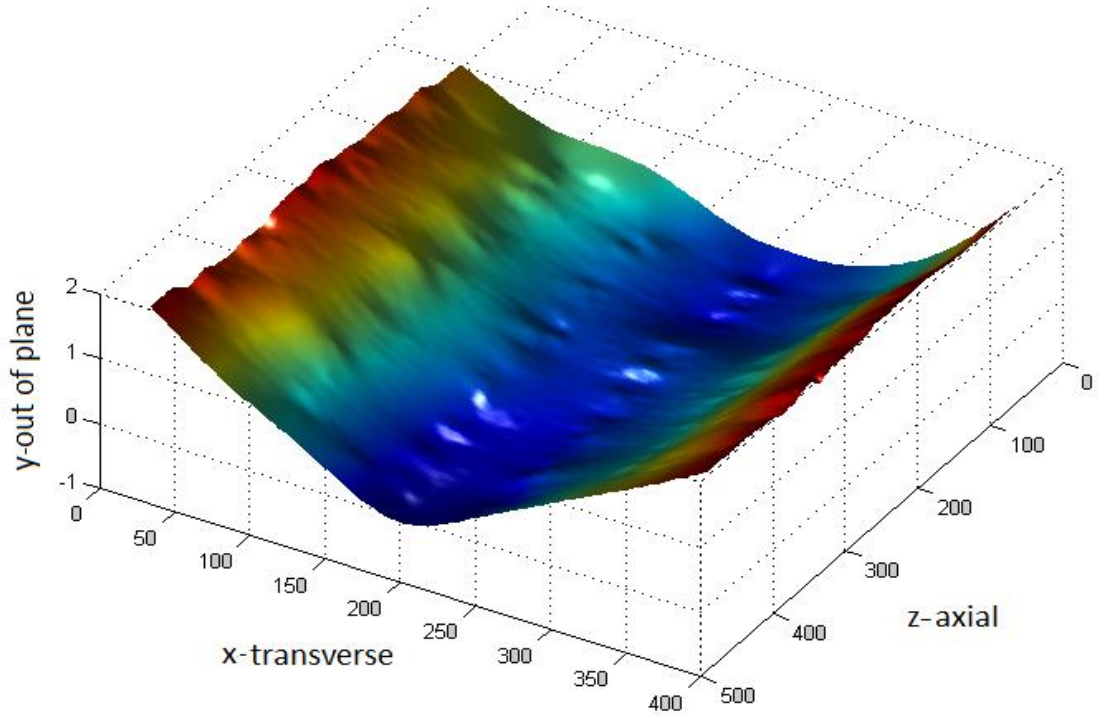

Figure B-4 Normalized geometric shape of Panel 3

B.3 Panel4

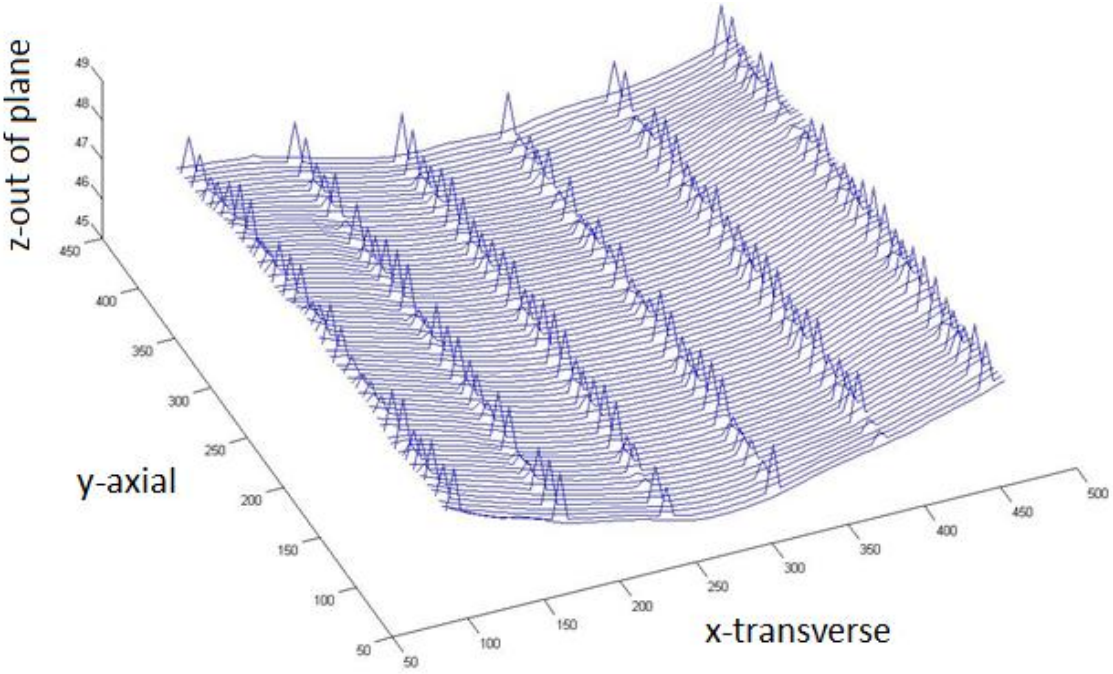

Figure B-5 Scanning lines plot along the X direction- in Panel 4

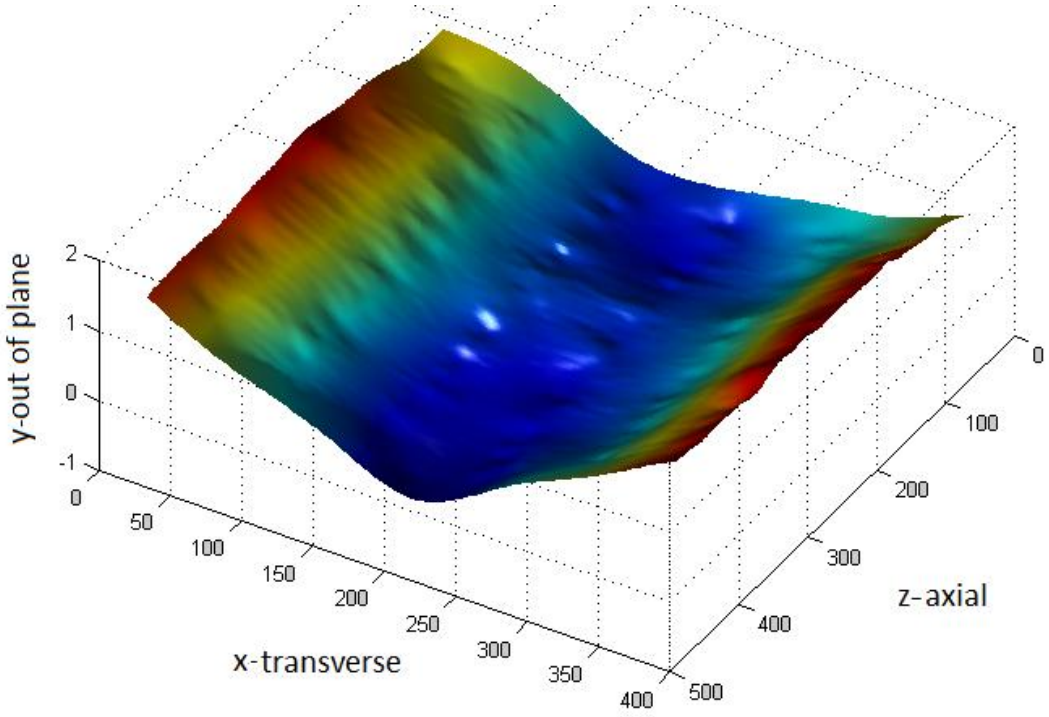

Figure B-6 Normalized geometric shape of Panel 4

B.4 Panel5

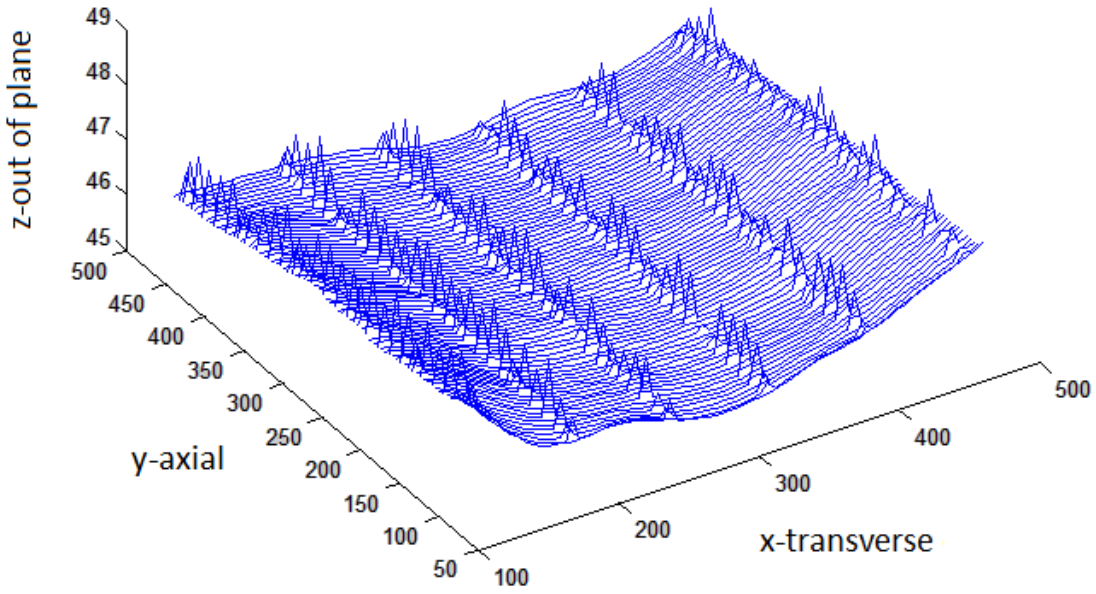

Figure B-7 Scanning lines plot along the X direction- in Panel 5

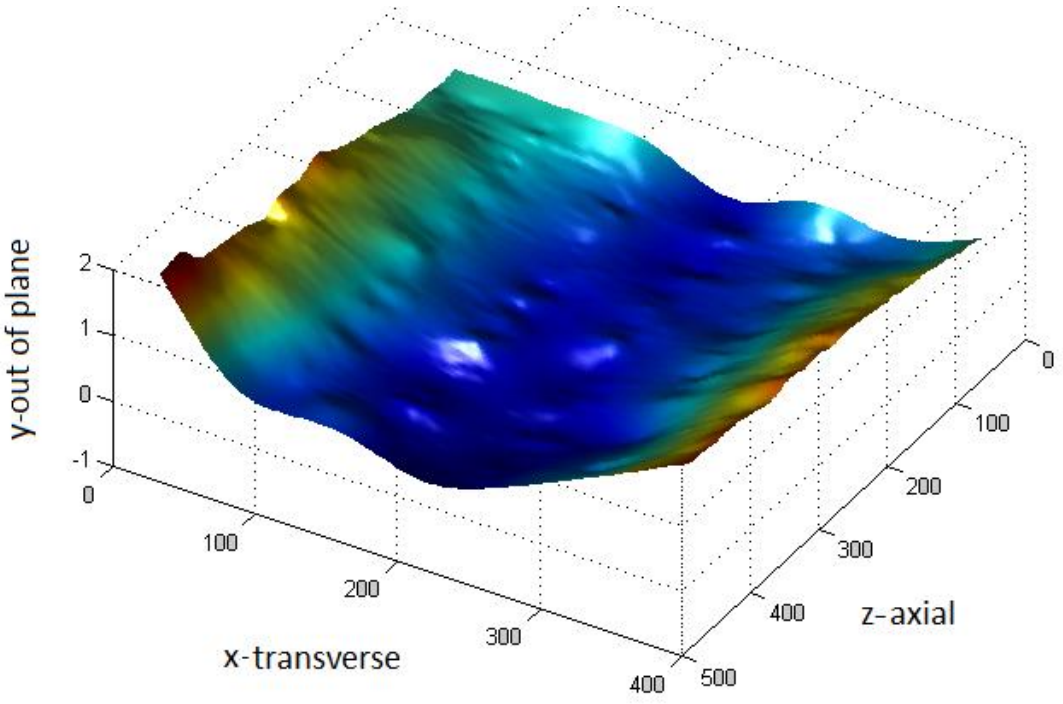

Figure B-8 Normalized geometric shape of Panel 5

B.5 Panel6

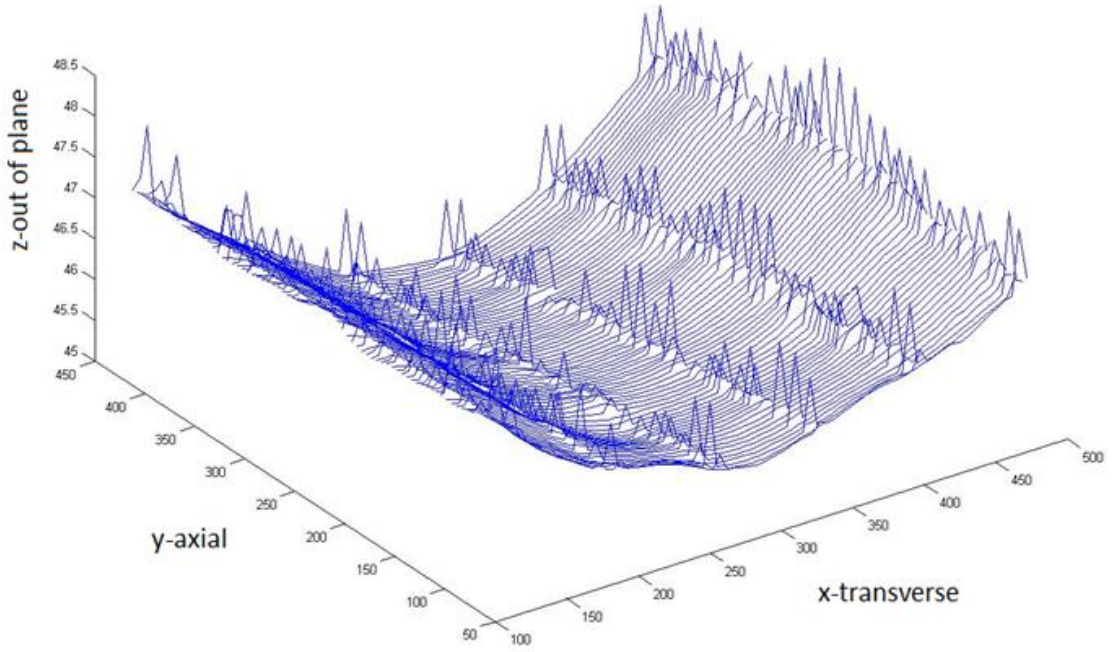

Figure B-9 Scanning lines plot along the X direction- in Panel 6

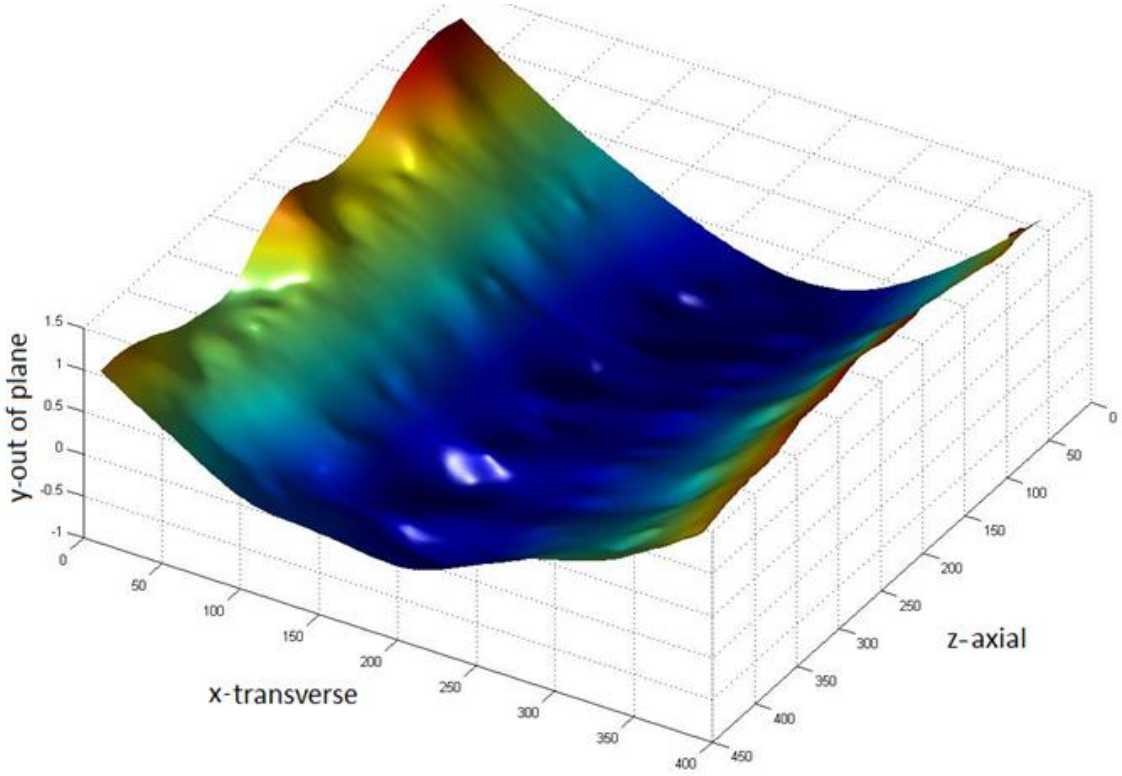

Figure B-10 Normalized geometric shape of Panel 6

Appendix C MATLAB source code

C.1 Data reduction programme of real scanning

Interchange data between perfect model and measured imperfections

```
%% input and mesh the data.
input = xlsread('panel4_input');
n = 76;
for i = 1 : n
   x(i,:)=input(74*(i-1)+1:74*i,1);
   y(i,:)=input(74*(i-1)+1:74*i,3);
   z(i,:)=input(74*(i-1)+1:74*i,5);
end
figure()
hold on
view(-35,48)
title 'Scanning lines plot along the x direction'
for i = 1 : n
   plot3(x(i,:),y(i,:),z(i,:))
end
figure()
mesh(x,y,z)
title 'Orignal mesh from the geometry scanning'
clear input n i;

%% noise point processing by deleting outliers.
% outliers are data value that are significantly different from patterns in the rest
of the data.
x2=[x(:,1),x(:,4:15),x(:,18:29),x(:,32:43),x(:,46:57),x(:,60:71),x(:,74)];
y2=[y(:,1),y(:,4:15),y(:,18:29),y(:,32:43),y(:,46:57),y(:,60:71),y(:,74)];
z2=[z(:,1),z(:,4:15),z(:,18:29),z(:,32:43),z(:,46:57),z(:,60:71),z(:,74)];
figure()
mesh(x2,y2,z2)
title 'first noise point processing'
for j=1:62
   for i=2:75
      if z2(i,j)>z2(i-1,j)+0.06;
         z2(i,j)=NaN;
      end
   end
end

for j=1:62
   for i=1:75
      if z2(i,j)>z2(i+1,j)+0.06;
         z2(i,j)=NaN;
```

```
        end;
    end;
end;
z2(76,9)=NaN;
z2(:,1)=NaN;
figure()
mesh(x2,y2,z2)
title 'final noise point processing'
clear x y z i j;
```

%% tranform the Coordinates system from xyz(in measurement) to XZY(in FE model)

```
X0=x2-89;
Y0=z2;
Z0=465-y2;
figure()
mesh(X0,Z0,Y0)
view(-28,-56)
title 'Coordinates system tranform'
clear x2 y2 z2;
```

%% read the coordinate from perfect FE model.

```
[ndata,text,alldata]=xlsread('perfectpanel.xls'); %read alldata include text from excel.
Xdata=ndata(1:112,3);%size=112.
Zdata=ndata(1:14000,7);%size=14000.
X=Xdata';
for i=1:125
    Z(i,1)=Zdata((i-1)*112+1);
end;
clear Xdata Zdata i;

% for y=-0.91: get values of X&Z.
Xdata_1=ndata(14001:14024,3); %sizeX=24.
Zdata_1=ndata(14001:17000,7); %sizeZ=125. <125*24=3000>
X1=Xdata_1';
for i=1:125
    Z1(i,1)=Zdata_1((i-1)*24+1);
end;
clear Xdata_1 Zdata_1 i;

% for y=0: get values of X&Z of assembly node.
Xdata_2=ndata(17001:17006,3); %sizeX=6.
Zdata_2=ndata(17001:17186,7); %sizeZ=31. <31*6=186>
X2=Xdata_2';
for i=1:31
    Z2(i,1)=Zdata_2((i-1)*6+1);
end;
```

```
clear Xdata_2 Zdata_2 i;

% for y=-0.91: get values of X&Z of assembly node.
Xdata_3=ndata(17187:17192,3); %sizeX=6.
Zdata_3=ndata(17187:17372,7); %sizeZ=31. <31*6=186>
X3=Xdata_3';
for i=1:31
   Z3(i,1)=Zdata_3((i-1)*6+1);
end;
clear Xdata_3 Zdata_3 i;

%% interpolation and extrapolation, using function "gridfit".
% thanks to John D'Errico, Model 2-d surfaces from scattered data. %
Ygrid = gridfit(X0,Z0,Y0,X,Z,'autoscale','on');
figure()
surf(X,Z,Ygrid)
view(-12,-80)
title 'Surface grid-fitting after system tranform'
clear X0 Z0 Y0;
%%
% Linear model Poly11:
%     f(x,y) = p00 + p10*x + p01*y
% Coefficients (with 95% confidence bounds):
%       p00 =       46.18  (46.16, 46.2)
%       p10 =  -0.0009626  (-0.001033, -0.000892)
%       p01 =   0.0009625  (0.0009022, 0.001023)
%
% Goodness of fit:
%   SSE: 2953
%   R-square: 0.1079
%   Adjusted R-square: 0.1078
%   RMSE: 0.4593

p00 = 46.18;p10 = -0.0009626; p01 = 0.0009625; %obtained from surface fitting
toolbox.
[XX,ZZ]=meshgrid(X,Z);
Yfit= p00 + p10*XX + p01*ZZ; %acquire the best fit plane.
YY=Ygrid-Yfit; %D-value, difference from the curve and best-fit plane.

figure()
surf(XX,ZZ,YY)
view(-31,-62)
shading interp
colormap(jet(256))
camlight right
lighting phong
title 'Deviaton out of the bestfit plane'
```

```
clear p00 p01 p10 Yfit Ygrid;

%%
% aquire YY1: the deformation in the inner flange of all stiifeners(at y=-0.91);
% when X1=X, and Z1=Z,the value of YY1 can be acquired same as that of the
point in Y.
for i=1:24
   for m=1:112
      if X1(i)==X(m)
         for j=1:125
            for n=1:125
               if Z1(j)==Z(n)
                  YY1(j,i)=YY(n,m);
               end
            end
         end
      end
   end
end; clear i m j n;
for i=1:6
   for m=1:112
      if X2(i)==X(m)
         for j=1:31
            for n=1:125
               if Z2(j)==Z(n)
                  YY2(j,i)=YY(n,m);
               end
            end
         end
      end
   end
end; clear i m j n;
for i=1:6
   for m=1:112
      if X3(i)==X(m)
         for j=1:31
            for n=1:125
               if Z3(j)==Z(n)
                  YY3(j,i)=YY(n,m);
               end
            end
         end
      end
   end
end; clear i m j n;

%%
```

```
% aquire X Y Z value lined up in a colum from XX YY ZZ.(YY=the deformation of skin at y=0)
for i=1:125;
   X_colum((i-1)*112+1:i*112,1)=X(:);
   Y_colum((i-1)*112+1:i*112,1)=YY(i,:);
   Z_colum((i-1)*112+1:i*112,1)=Z(i,:);
end; clear i;
% U_colum=[X_colum,Y_colum,Z_colum];  %U_colum is 3 colums of data that demostrate the coordinates in X Y Z direction, respectively.
for i=1:125
   X1_colum((i-1)*24+1:i*24,1)=X1(:);
   Y1_colum((i-1)*24+1:i*24,1)=YY1(i,:);
   Z1_colum((i-1)*24+1:i*24,1)=Z1(i,:);
end; clear i;
% U2=[XU2,YU2,ZU2];    %U2 is 3 colums of data that demostrate the coordinates in X Y Z direction, respectively.
for i=1:31
   X2_colum((i-1)*6+1:i*6,1)=X2(:);
   Y2_colum((i-1)*6+1:i*6,1)=YY2(i,:);
   Z2_colum((i-1)*6+1:i*6,1)=Z2(i,:);
end; clear i;
for i=1:31
   X3_colum((i-1)*6+1:i*6,1)=X3(:);
   Y3_colum((i-1)*6+1:i*6,1)=YY3(i,:);
   Z3_colum((i-1)*6+1:i*6,1)=Z3(i,:);
end; clear i;

B=ndata(:,1);
save panel4_output.dat X Z XX YY ZZ X1 Z1 X2 Z2 X3 Z3 B;
% clear X Z XX YY ZZ;
% clear X1 YY1 Z1;

%% rewrite the new values of the 3rd,5th,7th colum into'ndata'.

D=[X_colum;X1_colum;X2_colum;X3_colum];
F=[Y_colum;Y1_colum;Y2_colum;Y3_colum];
H=[Z_colum;Z1_colum;Z2_colum;Z3_colum];

% Write the new values into 'ndata_new'.
ndata_new(:,1)=B;
ndata_new(:,2)=D-D;
ndata_new(:,3)=F;
ndata_new(:,4)=H-H;
clear B D F H
%%
%write all the data out to a .inp file.
 s=['imperfection-panel4.inp'];
for i=1:17000
```

```
    str1{i,1}='Part-1-1';
end,clear i;
for i=17001:17372
    str1{i,1}='';
end,clear i;
totaldata=[str1,num2cell(ndata_new)];

filename = s;
fid = fopen(filename, 'w');

for i=1:17000
    fprintf(fid, '%s.%g,%g,%12.8g,%g\n', totaldata{i,:});
end
for i=17001:17372
    fprintf(fid, '%s %g,%g,%12.8g,%g\n', totaldata{i,:});
end
fclose(fid);
%%
stringer_data=xlsread('perfectpanel-stringerdata.xls');
Xsdata=stringer_data(1:9750,2);
for j=1:78
    Xs(1,j)=Xsdata((j-1)*125+1);
end;clear j Xsdata;
Zs=stringer_data(1:125,4);
for j=1:13          %if Xs<=23.09
    for i=1:125
        Ys(i,j)=YY(i,5);
    end
end

for j=14:26     %if Xs<=93.09 && Xs>23.09
    for i=1:125
        Ys(i,j)=YY(i,26);
    end
end
for j=27:39  %if Xs<=163.1 && Xs>93.09
    for i=1:125
        Ys(i,j)=YY(i,47);
    end
end
for j=40:52  %if Xs<=233.1 && Xs>163.1
    for i=1:125
        Ys(i,j)=YY(i,68);
    end
end
for j=53:65  %if Xs<=303.1 && Xs>233.1
    for i=1:125
        Ys(i,j)=YY(i,89);
```

```
    end
end
for j=66:78  %if Xs>303.1
    for i=1:125
        Ys(i,j)=YY(i,110);
    end
end
clear j i;
for j=1:78;
    Xs_colum((j-1)*125+1:j*125,1)=0;
    Ys_colum((j-1)*125+1:j*125,1)=Ys(:,j);
    Zs_colum((j-1)*125+1:j*125,1)=0;
end; clear j;
S=[stringer_data(:,1),Xs_colum,Ys_colum,Zs_colum];
for i=1:9750
    str2{i,1}='Part-1-1';
end,clear i;

totaldata=[str2,num2cell(S)];
fid = fopen(filename, 'a');
for i=1:9750
fprintf(fid, '%s.%g,%g,%12.8g,%g\n',totaldata{i,:});
end
fclose(fid);

clear all;
```

C.2 Surface fitting

```
clc;
l=430;w1=pi/l;
b=370;w2=pi/b;

int=3;q=1;
A00=linspace(0.6525,1.014,int)';
A01=mean([0.002309,-0.1376,-0.06298]);
A02=mean([0.0137,0.08285,0.02309]);
A10=linspace(-1.191,0.2949,int)';
A11=linspace(-0.2564,0.0477,int)';
A12=linspace(0.5809,-0.3154,int)';
B01=linspace(-1.015,-1.61,int)';
B02=mean([-0.01308,0.1761,0.07956]);
B11=linspace(1.86,-0.4612,int)';
B12=linspace(0.02205,0.2366,int)';

for p1=1:int
   for p2=1:int
      for p3=1:int
         for p4=1:int
            for p5=1:int
               for p6=1:int
                  for p7=1:int
for j=1:112
   for i=1:125
      YY_fit(i,j) = A00(p1)*cos(0*w1*ZZ(i,j) )*cos(0*w2*XX(i,j) )+...
                A10(p2)*cos(1*w1*ZZ(i,j) )*cos(0*w2*XX(i,j) )+...

A01(q)*cos(0*w1*ZZ(i,j) )*cos(1*w2*XX(i,j) )+B01(p3)*cos(0*w1*ZZ(i,j) )*sin(1*w
2*XX(i,j) )+...

A11(p4)*cos(1*w1*ZZ(i,j) )*cos(1*w2*XX(i,j) )+B11(p5)*cos(1*w1*ZZ(i,j) )*sin(1*
w2*XX(i,j) )+...

A02(q)*cos(0*w1*ZZ(i,j) )*cos(2*w2*XX(i,j) )+B02(q)*cos(0*w1*ZZ(i,j) )*sin(2*w2
*XX(i,j) )+...

A12(p6)*cos(1*w1*ZZ(i,j) )*cos(2*w2*XX(i,j) )+B12(p7)*cos(1*w1*ZZ(i,j) )*sin(2*
w2*XX(i,j) );
   end
end; clear i j;

M=max(abs(YY_fit));MM=max(M);
if MM<1.72
   figure()
   surf(XX,ZZ,YY_fit)
```

```
    set(gcf,'color',[1 1 1])
    shading interp
    colormap(jet(256))
    view(-36,36)

text1=['A00=',num2str(A00(p1)),',A10=',num2str(A10(p2)),',B01=',num2str(B01(
p3)),',A11=',num2str(A11(p4))];

text2=['B11=',num2str(B11(p5)),',A12=',num2str(A12(p6)),',B12=',num2str(B12(
p7))];
    text={text1;text2};
    title(text)
    colorbar

name=['Z:\MATLAB\DFS\figure',num2str(p1),num2str(p2),num2str(p3),num2str(
p4),num2str(p5),num2str(p6),num2str(p7),'.jpg'];
    print(gcf,'-dpng',name);

for i=1:125;
    X_colum((i-1)*112+1:i*112,1)=X(:);
    Y_colum((i-1)*112+1:i*112,1)=YY_fit(i,:);
    Z_colum((i-1)*112+1:i*112,1)=Z(i,:);
end; clear i;

for i=1:24
    for m=1:112
        if X1(i)==X(m)
            for j=1:125
                for n=1:125
                    if Z1(j)==Z(n)
                        YY1_fit(j,i)=YY_fit(n,m);
                    end
                end
            end
        end
    end
end; clear i m j n;

for i=1:6
    for m=1:112
        if X2(i)==X(m)
            for j=1:31
                for n=1:125
                    if Z2(j)==Z(n)
                        YY2_fit(j,i)=YY_fit(n,m);
                    end
                end
            end
```

```
        end
    end
end; clear i m j n;

for i=1:6
    for m=1:112
        if X3(i)==X(m)
            for j=1:31
                for n=1:125
                    if Z3(j)==Z(n)
                        YY3_fit(j,i)=YY_fit(n,m);
                    end
                end
            end
        end
    end
end; clear i m j n;

for i=1:125
    X1_colum((i-1)*24+1:i*24,1)=X1(:);
    Y1_colum((i-1)*24+1:i*24,1)=YY1_fit(i,:);
    Z1_colum((i-1)*24+1:i*24,1)=Z1(i,:);
end; clear i;
for i=1:31
    X2_colum((i-1)*6+1:i*6,1)=X2(:);
    Y2_colum((i-1)*6+1:i*6,1)=YY2_fit(i,:);
    Z2_colum((i-1)*6+1:i*6,1)=Z2(i,:);
end; clear i;
for i=1:31
    X3_colum((i-1)*6+1:i*6,1)=X3(:);
    Y3_colum((i-1)*6+1:i*6,1)=YY3_fit(i,:);
    Z3_colum((i-1)*6+1:i*6,1)=Z3(i,:);
end; clear i;
D=[X_colum;X1_colum;X2_colum;X3_colum];
F=[Y_colum;Y1_colum;Y2_colum;Y3_colum];
H=[Z_colum;Z1_colum;Z2_colum;Z3_colum];
ndata_new(:,1)=B;
ndata_new(:,2)=D-D;
ndata_new(:,3)=F;
ndata_new(:,4)=H-H;
s=['fourierfitting-imperfection-
',num2str(p1),num2str(p2),num2str(p3),num2str(p4),num2str(p5),num2str(p6),n
um2str(p7),'.inp'];
for i=1:17000
    str1{i,1}='Part-1-1';
end,clear i;
for i=17001:17372
    str1{i,1}='';
```

```
end,clear i;
totaldata=[str1,num2cell(ndata_new)];
filename = s;
fid = fopen(filename, 'w');

for i=1:17000
   fprintf(fid, '%s.%g,%g,%12.8g,%g\n', totaldata{i,:});
end
for i=17001:17372
   fprintf(fid, '%s %g,%g,%12.8g,%g\n', totaldata{i,:});
end
fclose(fid);
%%
stringer_data=xlsread('perfectpanel-stringerdata.xls');
Xsdata=stringer_data(1:9750,2);
for j=1:78
   Xs(1,j)=Xsdata((j-1)*125+1);
end;clear j Xsdata;
Zs=stringer_data(1:125,4);
for j=1:13         %if Xs<=23.09
   for i=1:125
      Ys(i,j)=YY_fit(i,5);
   end
end
for j=14:26    %if Xs<=93.09 && Xs>23.09
   for i=1:125
      Ys(i,j)=YY_fit(i,26);
   end
end
for j=27:39  %if Xs<=163.1 && Xs>93.09
   for i=1:125
      Ys(i,j)=YY_fit(i,47);
   end
end
for j=40:52  %if Xs<=233.1 && Xs>163.1
   for i=1:125
      Ys(i,j)=YY_fit(i,68);
   end
end
for j=53:65  %if Xs<=303.1 && Xs>233.1
   for i=1:125
      Ys(i,j)=YY_fit(i,89);
   end
end
for j=66:78  %if Xs>303.1
   for i=1:125
      Ys(i,j)=YY_fit(i,110);
   end
```

```
end
clear j i;
for j=1:78;
    Xs_colum((j-1)*125+1:j*125,1)=0;
    Ys_colum((j-1)*125+1:j*125,1)=Ys(:,j);
    Zs_colum((j-1)*125+1:j*125,1)=0;
end; clear j;
S=[stringer_data(:,1),Xs_colum,Ys_colum,Zs_colum];
for i=1:9750
    str2{i,1}='Part-1-1';
end,clear i;

totaldata=[str2,num2cell(S)];
fid = fopen(filename, 'a');
for i=1:9750
fprintf(fid, '%s.%g,%g,%12.8g,%g\n',totaldata{i,:});
end
fclose(fid);

end
                    end
                end
            end
        end
    end
end
```